INVESTIGATIONS OF RADIO JETS IN M87, 3C273, AND 3C345

Thesis by

John Anthony Biretta

In Partial Fulfillment of the Requirements

for the Degree of Doctor of Philosophy

California Institute of Technology

Pasadena, California

1986

(Submitted 6 June 1985)

To Barbara

ACKNOWLEDGEMENTS

There are many people to whom I wish to offer my thanks and gratitude. No doubt some will be left out, but their contributions are appreciated no less than the others.

A large debt of gratitude is due to Professor Marshall H. Cohen, my advisor, for his constant supervision and interest in my work, for many useful discussions and suggestions, and for reading all drafts and returning them in five days with useful comments.

To Professor A. C. S. (Tony) Readhead for his contagious enthusiasm and stimulating discussions on the properties of radio sources.

To Professor Roger D. Blandford for invaluable discussions on the physics of radio jets, for always having a free minute to talk, and for words of wisdom.

To Professor James E. Gunn who introduced me to the wonders of the universe at optical frequencies and the Hale 5 meter telescope. Many thanks are due for his infinite enthusiasm and patience during our collaboration in stellar populations and other topics.

His lessons on how to solve difficult problems quickly will always be an inspiration.

To Dr. Petter J. Young, my first advisor, who provided inspiration, kindness, and patience. I only wish I had understood the problem and could have been more helpful; your absence is often felt.

To Dr. K. Y. Lo for his friendly advice, words of wisdom, and collaboration on several papers.

To Drs. W. L. W. Sargent, J. B. Oke, A. T. Moffet, J. R. Mould, and J. L. Cohen for useful advice, optical data, and discussions.

To Dr. Frazer N. Owen who introduced me to extra-galactic radio astronomy (and Magdelena green chili), and who gave me the opportunity to spend two exciting and valuable summers at NRAO.

To Dr. Frank O. Clark for supporting my first efforts in radio astronomy, for his southern hospitality, and most of all for suggesting I go to Caltech.

To Dr. Joseph E. Lang, my undergraduate advisor, for spending much time learning the basics of astrophysics with me, for

teaching the value of integrity and dedication, and for insisting that I work faster. Also to Dr. David Boyle for introducing me to the right people and for permitting construction of the Thomas More College Radio Observatory (a.k.a. Arecibo North).

To Mom and Dad who eagerly supported my first explorations of the stars and distant galaxies.

To the Radio Astronomy staff - Leona Kershaw, Gloria Morales, Judith Wallrich, and JoAnn Wolpert who were always pleasant, cheerful, and helpful whether I need a paper clip, a big travel check, or the OVRO cottage. Also to Jill King who was very pleasant and helpful.

To Lilo Hauck for cookies and friendly advice at 6:30 a.m.

To Helen Knudsen who produced a copy of Izvestiia. Krymskaya A. O. 64 91 in five seconds flat, and many other miracles of library science.

To the VLBI correlator staff, without whom much of this work would have been quite impossible - George Dvorak, Allen Hubbard, Wei Sung Ho, P. S. Lee, Narina Sumbraric, Bill Whitehurst, and Jerry Zandle. Also to the VAX system managers Peter Parnicky,

Keith Shortridge, and Michael Lesser.

To the post-docs and staff who were helpful and answered many questions - Peter Bartel, Charles Lawrence (who also introduced me to Stax Lambda headphones), Tim Pearson, Steve Unwin, Joan Wrobel, and Tony Zensus.

To my fellow students who provided much comraderie, friendship, and entertainment - Abi, Alain (who had better send me two dozen chocolate glazed donuts in March 1987 - brightly colored sprinkles are optional, for the music to VAX by, and many useful discussions), Alex (for an infinite number of interesting and entertaining discussions), Alex's Grandmother (for all those delicious cookies), Ann, Big D (for his optimism and delightful Nebraskan humor), Chuck (for answering the telephone, etc.), Crazy Roger, Dave, Dean (who was a great office mate), Deborah, Fernando, Hiamin (for maintaining the water supply), James, Jim, Karl, Keith (for helpful discussions), Kevin, Kirk, Kwok, Matt, Michael (for an envigorating trek through the high Sierra), Mike (for introducing me to the local restaurants), Pawan, Radvendra, Rick, Russel, Steve L., and Steve M. (for sometimes not answering the phone).

And especially to the friends who greatly enriched my life during

recent years - Alces, Ann, Annie, Diana, Doug, Jeff, John Ventre, Nancy, Toni B., Toni 'n Bill, and WBCM.

ABSTRACT

We present observational studies of extra-galactic radio jets in M87, 3C273, and 3C345.

Observations of the M87 jet were made at 15 GHz with 0.12" resolution. All of the knots are clearly resolved both along and across the jet. Most of the knots are found to be smooth in appearance with no evidence of shocklike discontinuities. The brightest knot and the innermost knot are exceptions to this. The brightest knot (knot A) seems consistent with a shock caused by unsteady flow in the jet. Models for this feature are discussed. Combining our data with X-ray data suggests that the jet is neither freely expanding, thermally confined, nor ram pressure confined. The jet may, however, be magnetically confined.

We present 10.7 GHz VLBI observations of 3C273 with high north-south resolution. A strong, non-monotonic curvature is found in the jet at projected radii $\lesssim$5 pc. It is unlikely that this curvature can be caused by precession. Measurements of the core size show that bulk relativistic motion in the the core is not required for consistency with the observed x-ray flux.

For 3C345 we present a systematic analysis of VLBI observations at 2.3, 5.0, 10.7, 22.2, and 89 GHz. Epochs are from 1979.25 through 1984.11. A newly ejected superluminal component (C4) is observed to accelerate, change position angle, undergo a large flux outburst, and have a flat spectrum. Older components C2 and C3 have different speeds, different position angles, and show little or no acceleration. The spectrum of C3 steepens as its flux decays. There are spectral index gradients such that both C4 and C3 are farther from the "core" at higher frequencies. The moving components define an opening angle of ~27° and also show direct evidence for expansion. The counter-jet to jet flux ratio is extremely small, -0.007 ± 0.007.

These data for 3C345 are interpreted in terms of simple models involving spherical components or shocks in a relativistic jet. All of the emission regions show evidence for bulk relativistic motion with $\delta > 3$. The particle energies and pressures dominate those of the magnetic fields, unless $\delta \geq 20$. If the emission regions consist of an electron - proton plasma, then the density of thermal electrons is much less than the density of relativistic electrons. The fluxes decay with time much more rapidly than the synchrotron half-life, but much more slowly than predicted by adiabatic expansion. An attractive model for the observed kinematics identifies the emitting regions as shocks in

an apparently broad and curved jet; a curvature of $\geq 3^{\circ}$ and $\gamma \geq 10$ is required.

TABLE OF CONTENTS

INTRODUCTION

The existence of extragalactc radio jets or energy carrying beams was first suggested by Rees in 1971. These were proposed to power the doubled lobed structure found by early radio interferometer observations (Jennison and Das Gupta, 1953; Maltby and Moffet, 1963). As interferometers improved, jets became visible and many have been discovered (Bridle and Perley, 1984). This thesis investigates the structure and evolution of three of these jets in M87, 3C273, and 3C345.

The first chapter presents high resolution observations of the jet in the giant elliptical galaxy M87. This is the closest jet accessible from the northern hemisphere, and is perhaps our best opportunity to study their internal structure.

Chapters II through V investigate the superluminal radio structure in the quasars 3C273 and 3C345. There is now considerable evidence that these structures are relativistic jets (Blandford and Konigl, 1979; Cohen and Unwin, 1984). Because of the relativistic Doppler shift, it is possible to directly observe the kinematic and internal evolution of these jets. Chapter II

describes the first VLBI observations of 3C273 with high north-south resolution and examines the kinematics of this jet. Chapter III reports early 10.7 GHz observations of a new emission region in 3C345 with interesting kinematics. The last two chapters (IV and V) study the evolution of 3C345 between 1979 and 1984.

Each chapter in this thesis is a self-contained paper prepared for publication. Chapter I and II are published in the Astrophysical Journal (vol. 274, p. L27; vol. 292, p. L5). Chapter III is published in Nature (vol. 306, p. 42). Chapters IV and V will be submitted to the Astrophysical Journal.

REFERENCES

Blandford, R. D. and Konigl, A. 1983, Ap.J. 232, 34.

Bridle, A. H. and Perley, R. A. 1984, Ann.Rev.A.A. 22.

Cohen, M. H. and Unwin, S. C. 1984, in VLBI and Compact Radio Sources (IAU Symposium 110, eds. R. Fanti, K. Kellermann, and G. Setti) p. 95.

Jennison, R. C. and Das Gupta, M. S. 1953, Nature 172, 996.

Maltby, P. and Moffet, A. T. 1963, Ap.J.Supp. 7, 141.

Rees, M. J. 1971, Nature 229, 312.

CHAPTER I

Observations of the M87 Jet at 15 GHz with 0.12 Arcsecond Resolution

Published in The Astrophysical Journal

Volume 274, Pages L27-L30 (1983).

THE ASTROPHYSICAL JOURNAL, 274:L27–L30, 1983 November 1

OBSERVATIONS OF THE M87 JET AT 15 GHz WITH 0".12 RESOLUTION

J. A. BIRETTA
California Institute of Technology
FRAZER N. OWEN
National Radio Astronomy Observatory[1]
AND
PHILIP E. HARDEE
University of Alabama
Received 1983 March 1; accepted 1983 June 17

ABSTRACT

We present observations of the M87 jet made at 15 GHz with 0".12 resolution. At this resolution, all of the knots are clearly resolved both along and across the jet. Most of the knots are smooth in appearance and show no evidence of shocklike discontinuities. The brightest knot and the innermost knot are exceptions to this. The brightest knot (knot A) seems consistent with a shock caused by unsteady flow in the jet. Models for this feature are discussed.

Combining our data with X-ray data suggests that the jet is neither freely expanding, thermally confined, nor ram pressure confined. The jet may be magnetically confined.

Subject headings: galaxies: jets — interferometry — radio sources: extended

I. INTRODUCTION

Ever since its identification with the radio source Virgo A (Bolton, Stanley, and Slee 1949), the study of M87 (NGC 4486, 3C 274) and its jet have yielded one of our most interesting insights into extragalactic nonthermal phenomena. Owen, Hardee, and Bignell (1980, hereafter OHB) in 1980 published 5 and 15 GHz maps of the jet at 1".0 and 0".6 resolution respectively. These maps showed the striking similarity between the radio and optical images of the jet. Recently Nieto and Lelievre (1982) have published optical pictures with approximately 0".8 resolution confirming the similarity. X-ray and infrared observations are consistent with the same brightness distribution (Schreier, Gorenstein, and Fiegelson 1982; Stocke, Rieke, and Lebofsky 1981). In this *Letter* we present new observations made at 15 GHz with 0".12 resolution which reveal further structural details in the jet.

II. OBSERVATIONS AND REDUCTIONS

Observations of M87 were made with the VLA in the A configuration (Thompson *et al.* 1980) at 15 Ghz on 1982 March 4 UT. About 4 hr of integration was obtained with a bandwidth of 50 MHz and a center position R.A.(1950) = $12^h28^m17^s.0$, decl.(1950) = 12°40'0".0. An external calibrator was observed every 15 minutes, and 3C 286 was observed once to calibrate phase.

[1]Operated by Associated Universities, Inc., under contract with the National Science Foundation.

After standard calibration, the corrected visibility data were Fourier transformed, CLEANed, and self-calibrated in the standard way (Schwab 1980). After six iterations of self-calibration, the ratio of the peak intensity to the rms noise far away from the source was about 6000:1 on the CLEAN map. The peak intensity is 2.1 Jy per CLEAN beam area at the nucleus. The CLEAN restoring beam is a 0".12 FWHM circular Gaussian function.

III. RESULTS

A contour plot of the CLEAN map is presented in Figure 1. Figure 2 (Plate L1) shows a gray-scale display of the same map, Figure 3 (Plates L2 and L3) shows a detail of knots A and B. For an assumed distance of 16 Mpc (Mould, Aaronson, and Huchra 1980), the linear scale is 78 pc per arc second.

Important features in this map are summarized below:

1. All of the knots are resolved both across and along the jet.

2. The jet appears to expand at a roughly constant opening angle between the nucleus and knot A. At knot A, the jet broadens abruptly. Between knots A and B, the width of the jet remains constant or decreases slightly.

3. Most of the knots do not show sharp discontinuities in surface brightness. The brightness distribution along the jet is fairly smooth in a knot and is roughly symmetric about the brightest point in the knot. Knots A and D are exceptions to this.

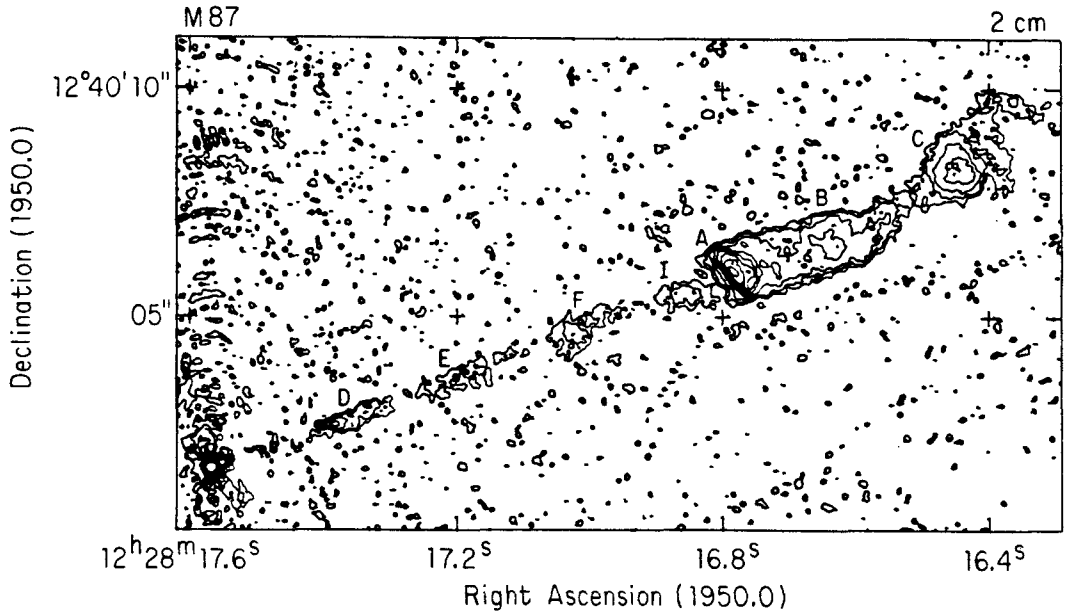

FIG. 1.—Contour plot of CLEAN map. Contour levels are at −0.8, 0.8, 1.6, 3.2, 5.6, 8.0, 10.4, 12.8, 15.2, 17.6, 20.0, 22.4, 24.8, 27.2, 29.6, 32.0, 64.0, 128.0, and 256.0 mJy per CLEAN beam area. The CLEAN beam is a 0".12 FWHM Gaussian function. The peak flux is 2.1 Jy per beam at the nucleus. The knots have been labeled with their usual letter identifications.

4. Knot A has a sharp discontinuity on the side toward the nucleus. The surface brightness rises from half the maximum to the maximum in 0".16 (after beam deconvolution) indicating the discontinuity is resolved. The discontinuity appears quite linear transverse to the jet and is at a projected angle of approximately 73° to the axis of the inner jet. On the side away from the nucleus, the surface brightness falls off more slowly and the jet has a roughly constant width. The local jet axis bends by approximately 3° to the south at knot A.

5. The four inner knots (D, E, F, and I) have roughly equal spacings. This spacing may decrease slightly with distance from the nucleus.

6. Quasi-sinusoidal oscillation is present in the region of the jet more than 12" from the nucleus.

IV. DISCUSSION

a) Confinement of the Jet

Most discussions of jets in the literature have considered either free jets or thermally confined jets. The M87 jet presents problems for both of these confinement schemes.

A free jet would expand at a constant angle which is defined by the Mach number at the nozzle. While the M87 jet appears to expand at a constant angle between the nucleus and knot A, it does not expand between knots A and B. The jet appears to have a well-defined edge between knots A and B, so it is almost certain that we are detecting the true width of the jet. Thus, at least part of the M87 jet does not appear to be freely expanding.

If the jet is to be thermally confined, it must be in pressure balance with the external medium. Consider knot B. This region is well resolved and fairly smooth, suggesting it is not a shock or some very transient phenomenon. A minimum pressure calculation (Burns and Owen 1979; Hardee 1982) with upper and lower frequency cutoffs of 10^8 and 10^{14} Hz, a spectral index $\alpha = -0.6$ ($S_\nu \propto \nu^\alpha$), and equal electron and proton energies yields $P_{\min} \sim 4 \times 10^{-9}$ dynes cm^{-2}. From *Einstein Observatory* X-ray data, Schreier, Gorenstein, and Feigelson (1982) and Lea, Mushotzky, and Holt (1982) calculate external pressures of 3×10^{-10} and 6×10^{-10} dynes cm^{-2}, respectively, at this distance from the nucleus. Hence, it seems unlikely that knot B is thermally confined. Similar internal pressures are found for the other knots. Only the two knots adjacent to the nucleus experience external pressures sufficient to give thermal confinement. We conclude that most of the

knots cannot be thermally confined. In the X-ray models, the interstellar medium pressure is expected to fall off at least as fast as r^{-1}, where r is the distance from the center of the galaxy. If projection effects are important, the knots will be farther from the nucleus than we have assumed and would experience even lower external pressures. The jet could be thermally confined if it were highly relativistic ($\gamma > 50$) and aligned within 1° of the line of sight (OHB), but such an alignment seems improbable. It appears unlikely that the jet is thermally confined, even when projection and relativistic effects are considered.

Dynamic ram-pressure confinement (Christiansen, Rolison, and Scott 1979) is an alternate possibility. In this model, confinement results from the supersonic motion of discrete plasma clouds through the surrounding medium. Each plasma cloud will possess a stationary bow shock at the leading edge and an expansion region at the trailing edge. As a result, we expect the surface brightness of the knots to be asymmetric with the brightest region away from the nucleus. Only two of the knots are observed to have an asymmetric surface brightness distribution, and in both cases the brightest region is toward the nucleus. For this reason, ram-pressure confinement also seems unlikely.

An additional possibility is that the jet carries an electric current and is magnetically confined (Benford 1978). Since the magnetic field lies primarily along the jet (OHB), except in knots A and C, the confining magnetic field must lie primarily outside the observed jet. Such a magnetic field might be produced by a surface current in the jet and a return current well outside the jet. In this case, the sinusoidal oscillations reported by OHB and Laing (1980) could be the result of a dynamically driven Kelvin-Helmhotz instability, as discussed by Hardee (1982), with pressure confinement produced by the confining magnetic field coupled to the external medium. The structure of knot A could, however, pose difficulties for magnetic confinement.

b) Structure of the Jet

Knot A suggests a shock. Its surface brightness distribution exhibits a sharp discontinuity on the upstream side and a slow falloff on the downstream side. Knot D has a similar, asymmetric appearance which is brightest on the upstream side. The other knots appear symmetric and do not resemble shocks. This seems to argue against the ram-pressure–confined jet already discussed.

Blandford and Königl (1979) have suggested that the knots are ram-pressure–confined interstellar cloud remnants in a plasma beam. This would produce the appropriate asymmetries in knots A and D. However, the expected curved bow shocks are unlike the discontinuity at knot A which appears linear transverse to the jet. Also, the regular spacing of the inner knots seems inconsistent with randomly located interstellar clouds.

It seems more likely that the knots are caused by unsteady flow or by pinching of the jet. In particular, knot A is probably a shock caused by faster material overtaking slower material (Rees 1978). Conceivably, knot D is also consistent with this hypothesis. The uniform spacing of the inner knots (D, E, F, and I) suggests some quasi-periodic behavior with E, F, and I being a more evolved state compared with knot D. If the knots were caused by pinching, we might expect some change in jet width, and our observations present no evidence of this. This would seem to rule out active pinches, although these knots could be evolved from quasi-periodic pinching upstream of knot D.

c) Knot A

Knot A appears to be a shock caused by high-velocity material overtaking slower material. The sudden change at knot A in the magnetic field direction from parallel to perpendicular to the jet (OHB) also suggests this conclusion. Suppose knot A is a strong adiabatic shock in which the thermal pressure dominates. For this type of shock, the flow velocity relative to the shock decreases from v_1 to $v_2 = v_1/4$ (westward velocity into and out of shock respectively), and the density increases from ρ_1 to $\rho_2 = 4\rho_1$ across the shock (see Landau and Lifshitz 1959).

A minimum velocity for the jet may be estimated by requiring that bulk kinetic energy supply the luminosity of the shock. The rate of bulk kinetic energy flow into the shock is

$$\dot{E}_{\rm shock} \sim \tfrac{1}{2}\rho_1 v_1^3 \sigma,$$

where σ is the cross sectional area of the inner jet and $\rho_1 \leq \rho_2 \leq 2 \times 10^{-25}$ g cm^{-3} is the density inferred from polarization observations (OHB). The observed luminosity of knot A is $L_{\rm knot\ A} \sim 2 \times 10^{41}$ ergs s^{-1}, where we have assumed upper and lower frequency cutoffs of 10^3 and 10^{14} Hz and a spectral index $\alpha = -0.6$. If thermalization of bulk kinetic energy at the shock is to supply the shock's luminosity, then

$$v_1 \geq (2L_{\rm knot\ A}/\rho_1\sigma)^{1/3} \geq 3 \times 10^8 \text{ cm s}^{-1}.$$

The velocity of the inner jet, $v = v_1 + v_s$, where $v_s \equiv$ shock velocity, must be at least this large.

We can attempt to estimate the downstream velocity, v_2, from an observed cooling length and a synchrotron half-life:

$$v_2 = l/t_{1/2} = 9.6 \times 10^{-13} l \nu^{1/2} B^{3/2} \text{ (cgs)},$$

where l is the observed cooling length in which the postshock intensity decreases to half the maximum and $t_{1/2}$ is the synchrotron half-life (Moffet 1975). Mea-

sured cooling lengths at 1.7 and 15 GHz are $l = 1''.0$ (Charlesworth and Spencer 1982) and $l = 0''.4$ (OHB) respectively. Both of these observations have an approximately $0''.5$ FWHM beam. Comparison of these observations provides evidence that l decreases with frequency as expected in this picture. For our observations, $l = 0''.32$ and $v_2 \sim 5 \times 10^7$ cm s^{-1}.

We can estimate the shock Mach number, M_1, by assuming that the jet material expands adiabatically behind the shock. The jet internal pressure will increase from P_1 before the shock to P_2 immediately after the shock. The jet radius might then expand adiabatically until the pressure is reduced to a lower pressure P_{dn} downstream from the shock. This expansion appears to occur between knots I and A, and

$$P_{dn} = (R_A/R_1)^{\eta} P_2 = (R_A/R_1)^{\eta} \times \left[2\Gamma M_1^2/(\Gamma + 1) - (\Gamma - 1)/(\Gamma + 1)\right] P_1,$$

where M_1 is Mach number of the flow into the shock. Comparison of the jet radii at knots A and I gives $R_A/R_1 \sim 2$. We assume $\Gamma = 5/3$. For a magnetically confined jet, the confining field, which is produced by an approximately constant current, decreases as the jet expands. Hence the exponent $\eta = -2\Gamma + 2$ with the result that $M_1 \sim 1.5$.

The appearance of a sharp, linear feature transverse to the jet places constraints on the angle between the jet axis and the line of sight. The sharp appearance of the shock indicates that the observed photons have traveled nearly parallel to the shock front in the shock's reference frame. This requires that

$$v_s/c \sim \cos\theta,$$

where θ is the angle between the jet axis and the line of sight measured in our frame and v_s is the velocity of the shock front. For the nonrelativistic case, the jet must lie near the plane of the sky. This is the most probable geometry (largest solid angle). If the jet is highly relativistic, it must also be at a small angle to the line of sight.

V. SUMMARY

Our observations indicate the following:

1. The M87 jet is neither a simple, freely expanding jet nor a thermally confined jet. Ram-pressure confinement also seems unlikely. Magnetic confinement is a plausible method of confining the jet.

2. Except for knot A and perhaps knot D, the knots do not contain shocklike discontinuities.

3. Knot A appears to be a shock that is most simply explained by newer jet material overtaking older jet material.

4. A shock-model for knot A implies a low Mach number shock and a jet velocity greater than 3×10^8 cm s^{-1}.

It is a pleasure to acknowledge many enlightening discussions with R. Blandford, M. Cohen, W. Christiansen, J. Eilek, M. Norman, J. Scott, and P. Wilkinson. Thanks are also extended to the VLA telescope operators, the NRAO programming staff, and J. Ventre. Research in astronomy at Caltech is supported in part by the National Science Foundation.

REFERENCES

Benford, G. 1978, *M.N.R.A.S.*, **183**, 29.
Blandford, R. D., and Königl, A. 1979, *Ap. Letters*, **20**, 15.
Bolton, J. G., Stanley, G. J., and Slee, O. B. 1949, *Nature*, **164**, 101.
Burns, J. O., and Owen, F. O. 1979, *A.J.*, **84**, 1478.
Charlesworth, M., and Spencer, R. E. 1982, *M.N.R.A.S.*, **200**, 953.
Christiansen, W. A., Rolison, G. G., and Scott, J. S. 1979, *Ap. J.*, **234**, 456.
Hardee, P. E. 1982, *Ap. J.*, **261**, 457.
Laing, R. A. 1980, *M.N.R.A.S.*, **193**, 427.
Landau, L. D., and Lifshitz, E. M. 1959, *Fluid Mechanics*, trans. J. B. Sykes and W. H. Reid (London: Pergamon), p. 331.
Lea, S. M., Mushotzky, R. F., and Holt, S. S. 1982, *Ap. J.*, **261**, 42.
Moffet, A. T. 1975, in *Stars and Stellar Systems*, Vol. 9, *Galaxies and the Universe*, ed. A. Sandage, M. Sandage, and J. Kristian (Chicago: University of Chicago Press), p. 217.
Mould, J., Aaronson, M., and Huchra, J. 1980, *Ap. J.*, **238**, 458.
Nieto, J.-L., and Lelievre, G. 1982, *Astr. Ap.*, **109**, 95.
Owen, F. O., Hardee, P. E., and Bignell, R. C. 1980, *Ap. J. (Letters)*, **239**, L11 (OHB).
Rees, M. 1978, *M.N.R.A.S.*, **184**, 61P.
Schreier, E. E., Gorenstein, P., and Fiegelson, E. D. 1982, *Ap. J.*, **261**, 42.
Schwab, F. R. 1980, *Proc. Soc. Photo-Opt. Instrum. Eng.*, **231**, 18.
Stocke, J. T., Rieke, G. H., and Lebofsky, M. J. 1981, *Nature*, **294**, 319.
Thompson, A. R., Clark, B. G., Wade, C. M., and Napier, P. J. 1980, *Ap. J. Suppl.*, **44**, 151.

J. A. BIRETTA: 105-24 California Institute of Technology, Pasadena, CA 91125

PHILIP E. HARDEE: Department of Physics and Astronomy, University of Alabama, Box 1921, University, AL 35486

FRAZER N. OWEN: National Radio Astronomy Observatory, P. O. Box 0, Socorro, NM 87801

PLATE L1

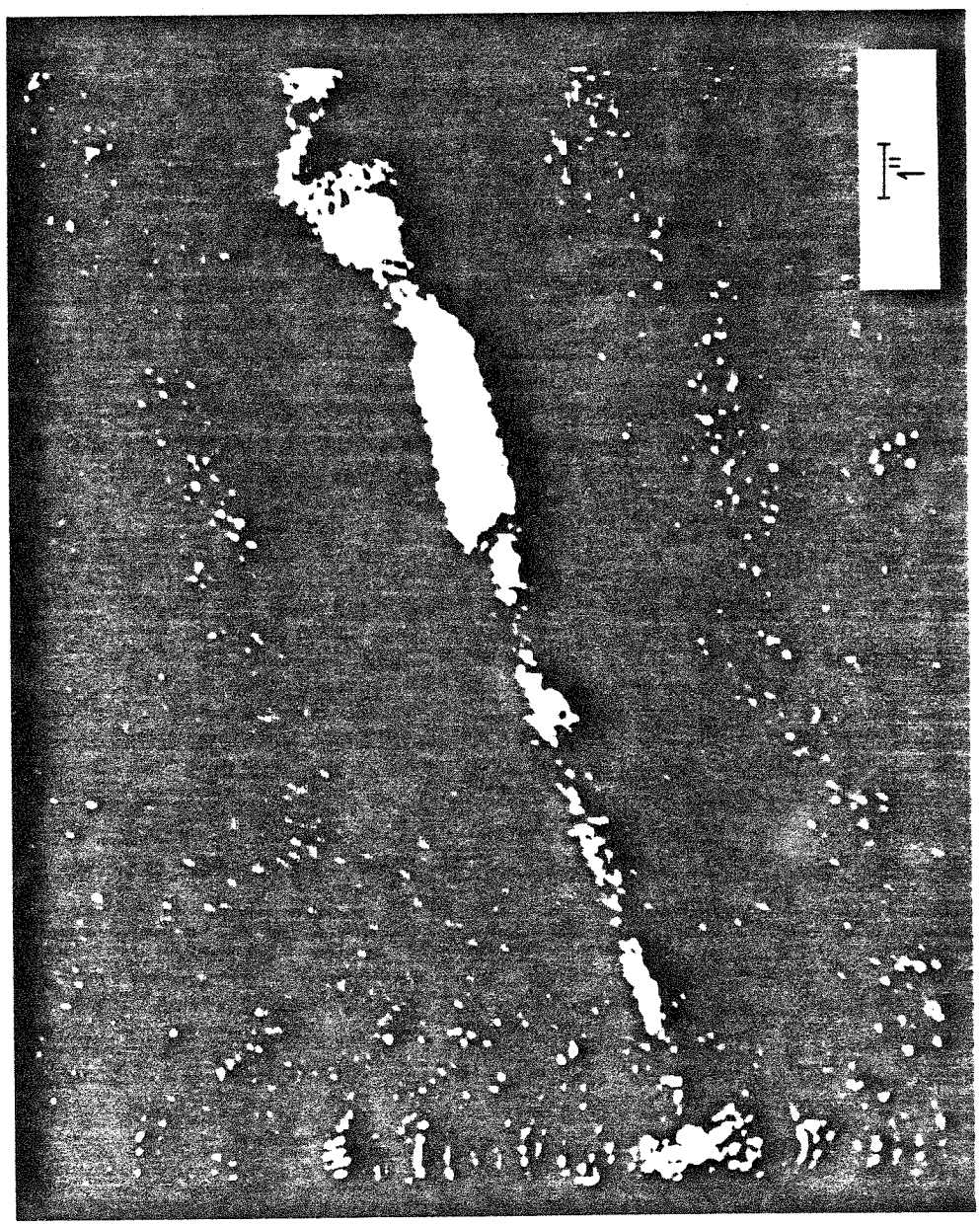

FIG. 2.—Gray-scale display of CLEAN map. Scale is approximately linear from 0 to 1.6 mJy per CLEAN beam area.

PLATE L2

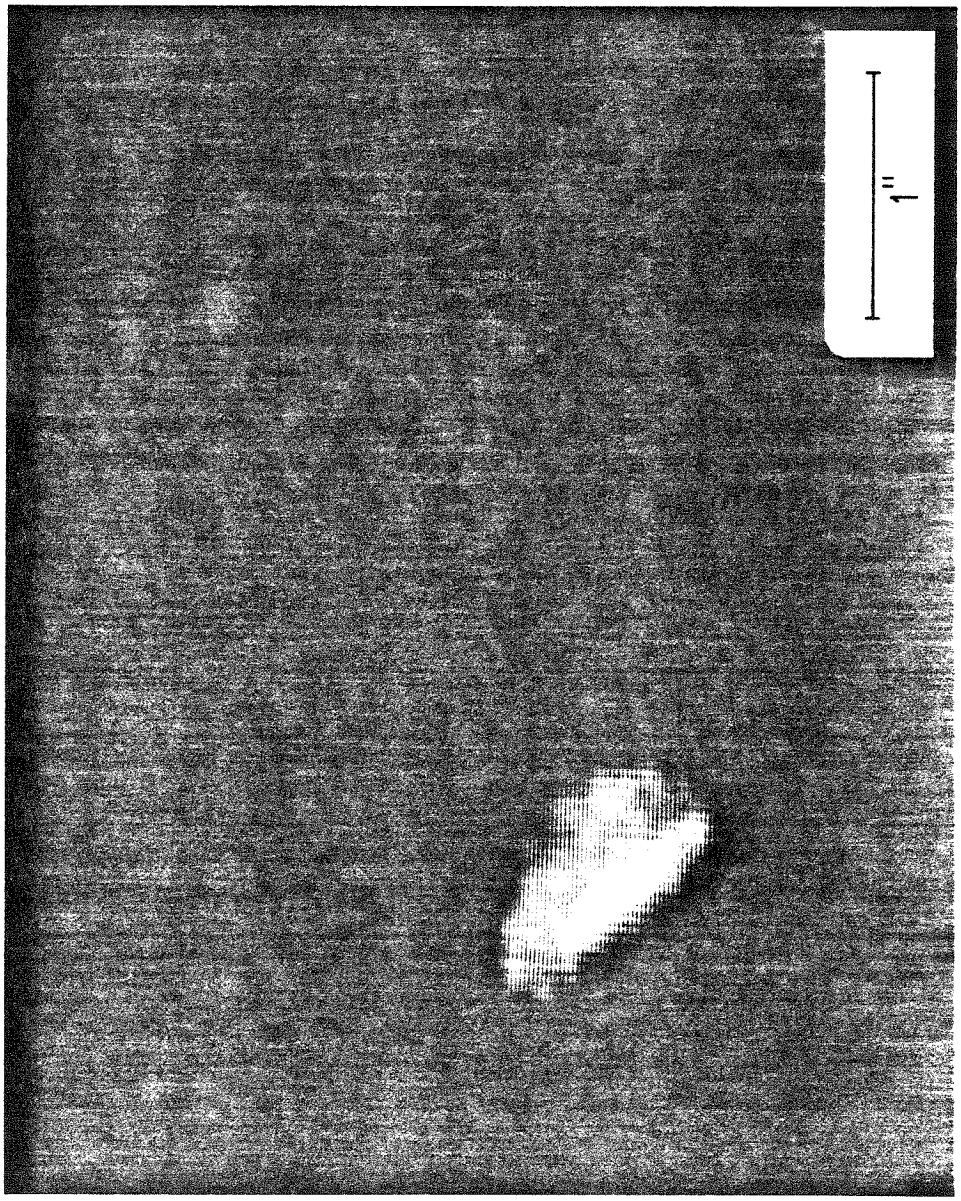

FIG. 3*a*

FIG. 3.—(*a*) and (*b*) Gray-scale display of knots A and B. The scale is approximately linear from 5 to 15 mJy per CLEAN beam in (*a*), and 1 to 6 mJy per CLEAN beam in (*b*).

PLATE L3

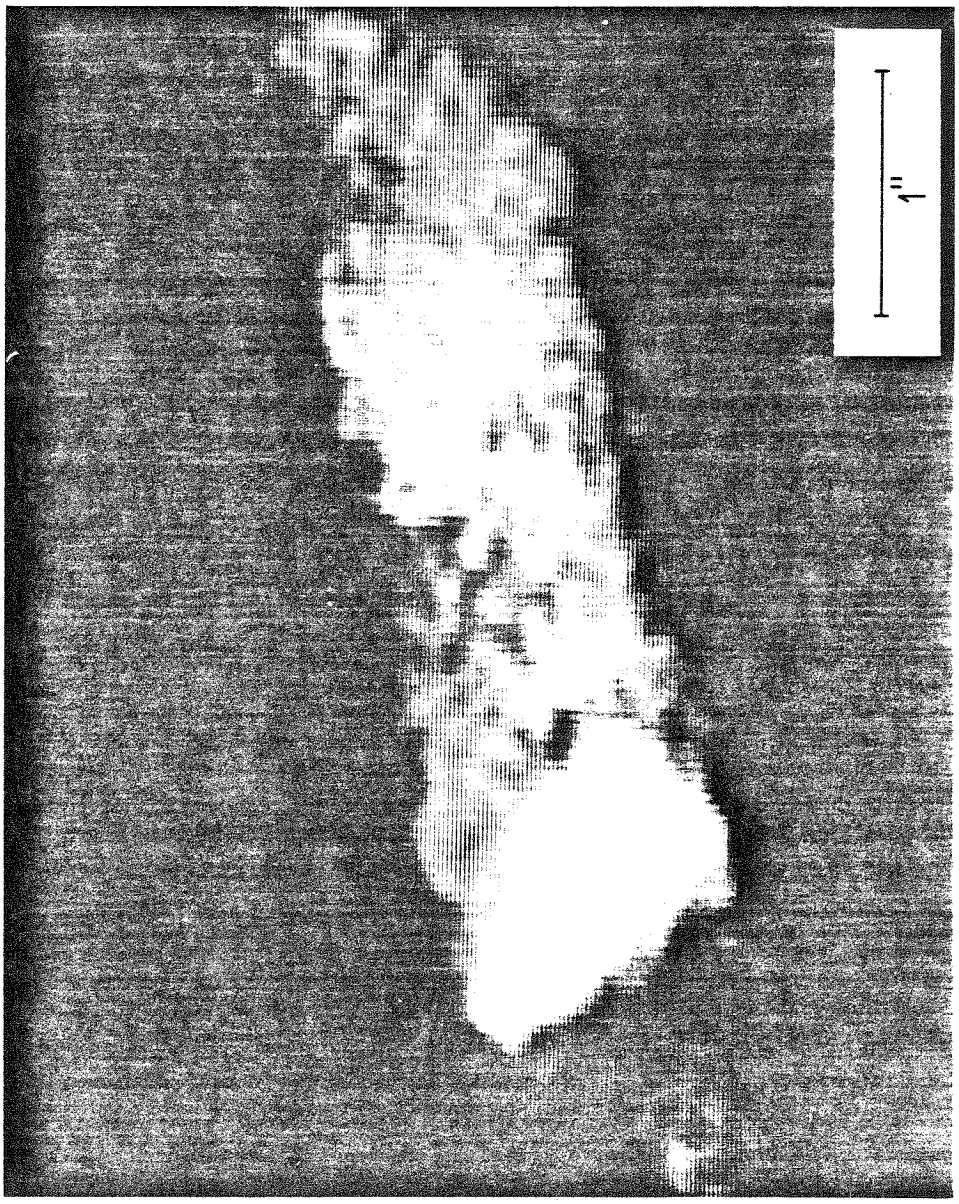

FIG. 3*b*

BIRLTA, OWEN, AND HARDIE (*see* page L27)

CHAPTER II

Observations of 3C273 with High North-South Resolution

Published in the The Astrophysical Journal

Volume 292, Pages L5-L8 (1985).

Observations of 3C273 with High North-South Resolution

J. A. Biretta, M. H. Cohen, H. E. Hardebeck

California Institute of Technology

P. Kaufmann, Z. Abraham, A. A. Perfetto,

E. Scalise, Jr., R. E. Schaal

Instituto de Pesquisas Espaciais

P. M. Silva

Observatorio Nacional

Abstract

We present the first VLBI maps of 3C273 with high north-south resolution. A strong, non-monotonic curvature is found in the jet at projected radii $\lesssim 5$ pc. Measurements of the core size show that bulk relativistic motion in the core is not required for consistency with the observed x-ray flux.

I. Introduction

The compact radio source in the quasar 3C273 (z=0.158; Schmidt, 1963) shows superluminal motion with v/c~6 (Pearson et al., 1981; Unwin et al., 1985, herein after U85). Since it lies at a declination of +2°, the northern hemisphere VLBI networks give a north-south resolution nearly an order of magnitude worse than the east-west resolution. The compact source is elongated at position angle (P.A.) ~−115° and motions along this direction are seen. However, it has not been possible to show that the compact source is narrow and jetlike, as is the case for other superluminal sources like 3C345. It is also known that 3C345 shows complex behavior near the core, with changing position angles and acceleration (Biretta et al., 1983; Moore et al. 1983). It has not been possible to test 3C273 for this behavior because of the poor north-south resolution.

To improve the north-south resolution we have instrumented the Itapetinga (Brazil) radio telescope with a 10.7 GHz receiver for VLBI. This Letter reports the first results obtained with Itapetinga arrayed with other telescopes in Europe and the USA.

Throughout this Letter we will assume H_0=100 km s^{-1} Mpc^{-1} and q_0=0.5. For z=0.158 the linear scale is 1.77 pc/milli-arcsecond (mas). The uncertainties quoted are 1.0 sigma.

II. Observations

Very Long Baseline Interferometric observations of 3C273 were made on 13 February 1984 (1984.12) with a 1.8 MHz bandwidth centered at 10650.89 MHz. The antenna array consisted of M.P.I.f.R., West Germany (100m diameter) and Itapetinga, Brazil (14m) along with four stations of the U.S. V.L.B.I. network: Haystack (37m), Green Bank (43m), Fort Davis (26m), and Owens Valley (40m). At Itapetinga the room temperature parametric amplifier receiver gave a system temperature of about 400°K. The frequency/time standard was a rubidium oscillator; its time setting relative to UTC was verified by making 22 GHz V.L.B.I. observations of the W49 H_2O maser. The characteristics of the other stations are well known.

Calibration was provided by hourly system temperature measurements along with antenna temperature measurements or a gain curve. Details of the data reduction and mapping procedures will be given elsewhere (Biretta et al., in preparation). The beam has a central component of size 0.43 x 0.65 mas (FWHM) and strong north-south side lobes; the strongest side lobes are 86 percent of the central peak. To compensate for these strong side lobes a 2 percent loop-gain was used while CLEANing the map. The side lobes are strong because of the large "Amazon Gap" in the (u,v) coverage; hence information on intermediate north-south scales is

missing. We have implicitly constrained the source structure to be simple in the north-south direction in making the maps shown below. The shortest baseline has $\lambda/2D \sim 7$ mas, and there is little information about scale sizes larger than this.

III. Results

The hybrid map is presented in Figure 1. Figure 1a shows the CLEAN components smoothed with a circular Gaussian similar in size to the beam's central component. The map in Figure 1b was derived with a larger beam which includes the strong side lobes. This larger beam is essentially that which would be obtained without the Itapetinga data. Features in these maps weaker than 3 percent of the peak intensity are thought to be unreliable. Comparison of these two figures shows the obvious advantage of using a southern hemisphere telescope on an equatorial source. Even though the side lobes are strong, the detection of a significant fraction of the total flux on baselines to Itapetinga indicates that the north-south structure must be compact. The alternate possibility is periodic north-south structure which mimics the dirty beam; this seems contrived and is therefore rejected.

Three major components are present in the map. The easternmost is bright and compact, and we will assume it to be identical with the component labeled D by U85. The brightest component in the middle is labeled C7a, following the notation of U85. This component is brightest at its southwestern edge and is extended along a line towards the western component. We have labeled the extension C7b. The western component, which is weak and extended, is labeled C5 since an extrapolation of the data presented by U85 would put their component C5 at about this position in early 1984. This identification must be tentative until maps at intervening epochs are considered (Biretta et al., in preparation). Component C6 of U85 is not seen in our map.

IV. Discussion

The high north-south resolution permits us to examine two aspects of the source which were previously obscured: the curvature of the jet near the core, and the sizes of individual components. We will interpret our data in terms of the relativistic jet model for superluminal radio sources (Blandford and Königl, 1979). The merits of this model are discussed by Scheuer (1984) and Begelman, Blandford, and Rees (1984).

Our data show that there is a substantial change in the P.A. of the jet near the core. The P.A.'s are plotted in Figure 2, as a function of distance from the core. At small radii ($r \lesssim 1$ mas) components C7a and C7b have P.A. $-127^\circ \pm 1^\circ$ and -139° $+4/-2^\circ$, respectively. The best comparable data are from U85 who find P.A. -129° and -134° for component C6 when at r~0.8 and ~1.3 mas, respectively. At $r \geq 6$ mas we find that component C5 has P.A. $-114^\circ \pm 4^\circ$. Data from the literature give similar P.A.'s for other components when near this radius. Hence there appears to be a $18^\circ \pm 5^\circ$ change in the P.A. of the jet at projected distances of ~2 pc from the core. This result is similar to that found for 3C345 by Readhead *et al.* (1983); they found a ~45° change in the P.A. of the jet at projected radii of ~2 pc.

Our observations show further that the curvature of the jet is not monotonic. The P.A. of the jet increases between r~1 and r~5 mas, but then decreases between r~5 and r~40 mas (Figure 2). Hence the direction of curvature changes at projected radii of ~10 pc. This behavior is quite different from 3C345 in which the direction of curvature is constant from projected radii of 2 pc to 4 kpc (Browne *et al.* 1982; Readhead *et al.*, 1983)

It is unlikely that the curvature of the jet can be explained as a simple precession. There is no geometry which can account for both the straightness of the jet between ~20 mas and 20" (Conway et al., 1981; Perley, 1984) and the non-monotonic curvature near the core. A more complex model might invoke both precession at $r<20$ mas and a collimation at $r\geq 20$ mas to explain the straightness of the large scale jet. For this model, our data imply a precession period $\leq 300(20^{\circ}/\theta)$ years, where θ is the angle between the jet axis and the line of sight. The proper motion of the superluminal knots requires $\theta<20^{\circ}$ (U85), and the likelihood of a certain geometry decreases as θ becomes small. For example, if $\theta\geq 5^{\circ}$ the required period is $\leq 10^{3}$ years. Such a rapid precession could be produced by a pair of orbiting super-massive objects (Begelman, Blandford, and Rees, 1980), but the orbit would decay by gravitational radiation in $\sim 10^{6}$ years. This explanation is unattractive since the required precession would occur for only a short time. Other arguments against precession are presented by Conway et al. (1981).

An alternative explanation for the curvature is bending of the jet by presssure gradients (Readhead et al., 1978; Begelman, Blandford, and Rees, 1984). Since the curvature is not monotonic, two different pressure gradients would be required at projected radii r~2 pc and r~20 pc. If the older data for component C4

which show P.A.~-99° near the core are correct, then a more complex model would be needed in which components move along different paths while near the core. Such a model might invoke ejection in a wide cone (Rees, 1980), instabilities in an accretion disk along with collimation at projected $r \geq 5$ pc, or instabilities in the jet itself (Hardee, 1979; Ferrari, Trussoni, and Zaninetti, 1981). Alternatively, components might first appear localized within or at the edges of the jet, and might subsequently evolve to fill the jet's entire width. Since both 3C273 and 3C345 show strong curvature at projected radii of ~2 pc, it is likely that the same mechanism is operating in both quasars.

Calculations of the inverse Compton X-ray flux for compact sources are very sensitive to the sizes of the radio emitting region. For other superluminal sources this calculation gives direct evidence for bulk relativistic motion towards the observer (3C345 - Unwin et al., 1983; NRAO 140 - Marscher and Broderick, 1981; Marscher and Broderick, 1982). This calculation has been worked out for 3C273 by U85 who assume a core diameter (component D) of 0.8 mas. This diameter is consistent with the upper limit we obtain with our better resolution. Hence, we confirm their finding that the inverse Compton X-ray calculation gives no evidence for bulk relativistic motion in the core of 3C273. Since accurate component spectra are needed for this calculation, a

discussion of components C5 and C7 will be presented elsewhere (Biretta *et al.*, in preparation).

Future observations with more complete north-south coverage are needed to check these results and study the position angles of new components while they are near the core. Unfortunately, there are very few high frequency VLBI antennas at low or southern latitudes.

We gratefully acknowledge the assistance of many individuals, including P. Alces, D. Foss, M. Morris, A. Rogers, S. Unwin, D. Williams, and S. H. Zisk. This work was supported in part by National Science Foundation grant AST82-10259, and by a USA-Brazil bilateral scientific agreement (NSF/CNPq).

V. References

Begelman, M. C., Blandford, R. D., and Rees, M. J. 1984, Rev. Modern Physics 56, 255.

Begelman, M. C., Blandford, R. D., and Rees, M. J. 1980, Nature 287, 307.

Biretta, J. A., Cohen, M. H., Unwin, S. C., and Pauliny-Toth, I. I. K. 1983, Nature 306, 42.

Blandford, R. D. and Königl, A. 1979, Ap.J. 232, 34.

Browne, I. W. A., et al. 1982, Nature 299, 788.

Cohen, M. H., et al. 1983, Ap.J. 272, 383.

Conway, R. G., Davis, R. J., Foley, A. R., Ray, T. P. 1981, Nature 294, 540.

Ferrari, A., Trussoni, E., and Zaninetti, L. 1981, M.N.R.A.S. 196, 1051.

Hardee, P. E. 1979, Ap.J. 234, 47.

Marscher, A. P. and Broderick, J. J. 1981, Ap.J. 249, 406.

Marscher, A. P. and Broderick, J. J. 1982, Ap.J.Lett. 255, L11.

Moore, R. L., Readhead, A. C. S., and Baath, L. L. 1983, Nature 306, 44.

Niell, A. E., Kellerman, K. I., Clark, B. G., Shaffer, D. B. 1975, Ap.J.Lett. 197, 109.

Pearson, T. J., et al. 1981, Nature 290, 365.

Perley, R. A., 1984, in VLBI and Compact Radio Sources (IAU Symposium 110), eds. R. Fanti, et al., p.153.

Readhead, A. C. S., et al. 1978, Nature 276, 768.

Readhead, A. C. S., et al. 1983, Ap.J. 265, 107.

Readhead, A. C. S., et al. 1979, Ap.J. 231, 299.

Rees, M. J. 1980, in The Origin of Cosmic Rays (IAU Symposium 94), eds. G. Setti, et al., p.139.

Scheuer, P. A. G. 1984, in VLBI and Compact Radio Sources (IAU Symposium 110), eds. R. Fanti, et al., p.197.

Schilizzi, R. T., et al., 1975, Ap.J. 201, 263.

Schmidt, M., 1963, Nature 197, 1040.

Unwin, S. C., et al., 1983, Ap.J. 271, 536.

Unwin, S. C., et al., 1985, Ap.J. 289, 109 (U85).

Figure captions.

Figure 1. Hybrid map of 3C273 at 11 GHz for 1984.12 epoch. North is at the top and east is at the left. Contours are at -2, 2, 4, 6, 10, 20, 35, 50, 70, and 90 percent of the peak intensity. The scale is 1.20 mas per tick mark. The beam is a 0.6 mas diameter circular Gaussian function in (a), and a 4.2 by 0.6 mas elliptical Gaussian function (b).

Figure 2. Position angles of components plotted against r (distance from the core component D). Data with error bars are from this paper. Other data are from: Niell, et al. (1975, early data); Schilizzi, et al. (1975, early data); Readhead, et al. (1978, early data); Readhead, et al. (1979, component C4); Perley, (1984, VLA jet); Pearson, et al. (1981, C4); Cohen, et al. (1983, C1, C2, C3); and U85 (1985, C2, C3, C4, C5, C6). Niell, et al. and Schilizzi, et al. assumed the components were colinear, so their P.A.'s are averages for the three components they detected. Niell, et al. indicate that models with colinear components gave a poor fit to the data.

Running title:

VLBI Observations of 3C273

Authors' Addresses:

J. A. Biretta and M. H. Cohen

105-24 Robinson Laboratory

California Institute of Technology

Pasadena, CA 91125

H. E. Hardebeck

Owens Valley Radio Observatory

California Institute of Technology

P.O. Box 387

Big Pine, CA 93513

P. Kaufmann, Z. Abraham, A. A. Perfetto,

E. Scalise, Jr., R. E. Schaal

Instituto de Pesquisas Espaciais, CNPq

C.P. 515, 12.000 - São José dos Campos

Sao Paulo, Brasil

P. M. Silva

Observatorio Nacional, CNPq

R. General Bruce 586

20921 - RIO de Janeiro, Brasil

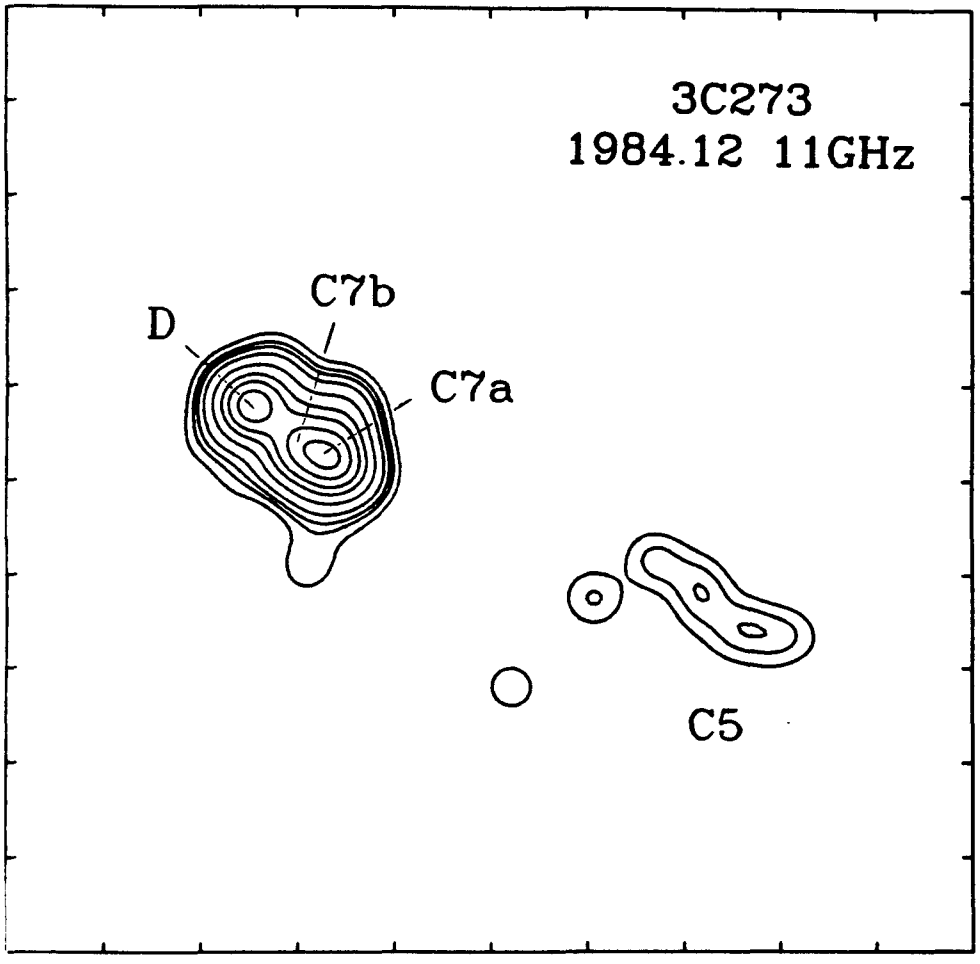

Figure 1a.

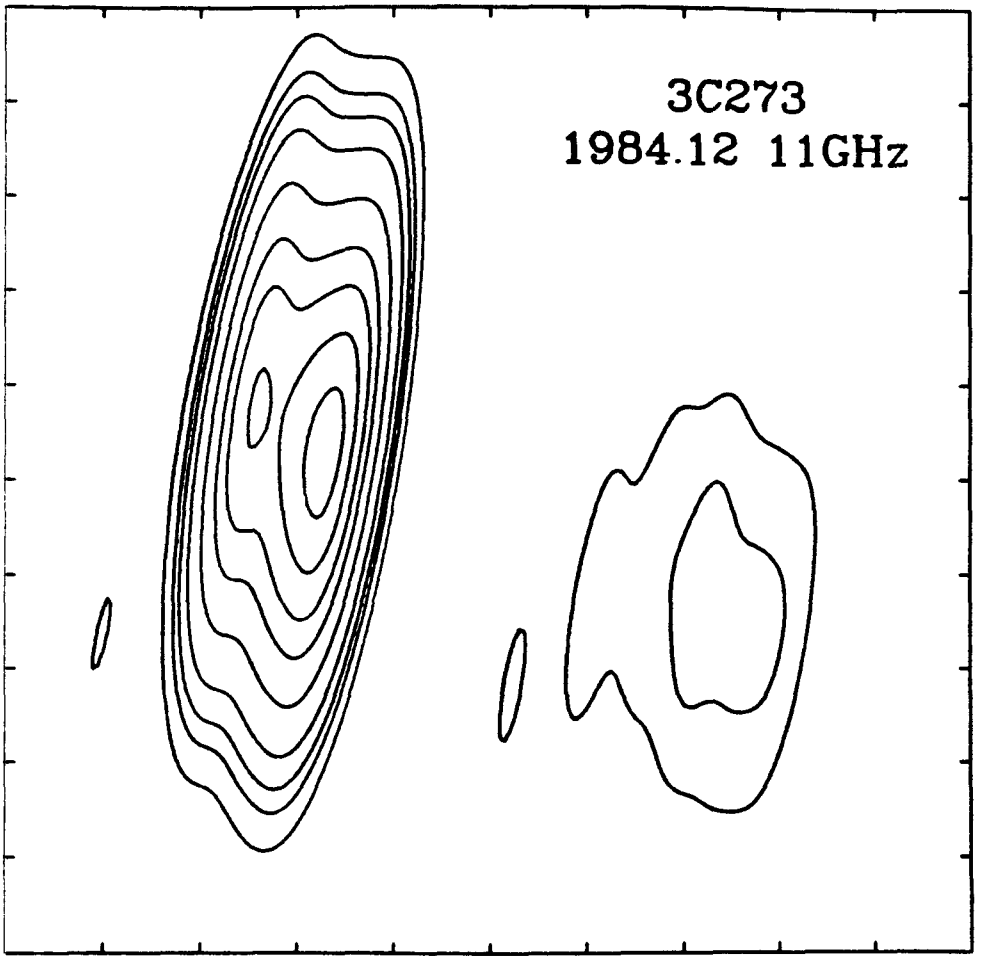

Figure 1b.

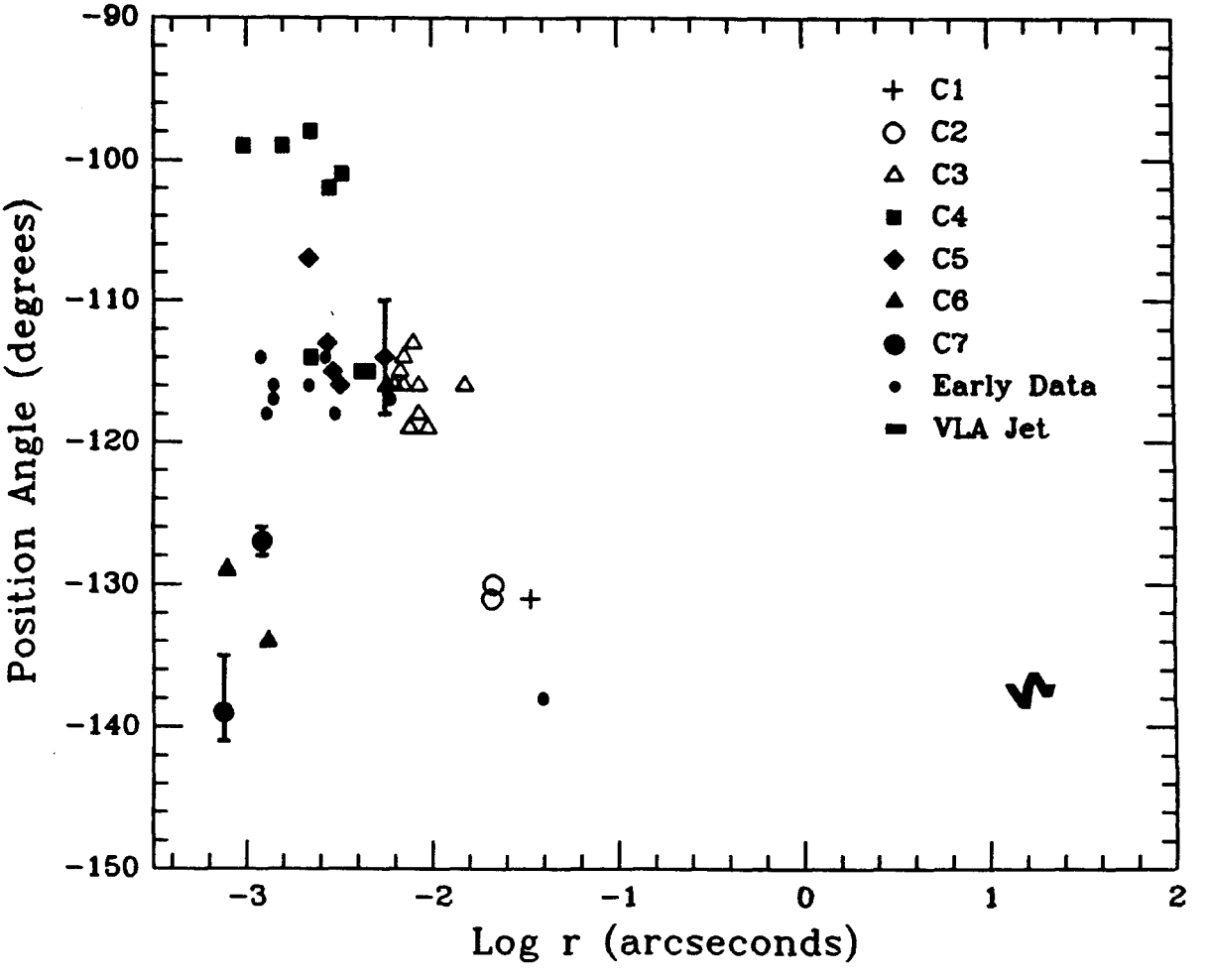
-90
-100
-110
-120
-130
-140
-150
-3
-2
-1
0
1
2
Position Angle (degrees)
Log r (arcseconds)
C1
C2
C3
C4
C5
C6
C7
Early Data
VLA Jet

Figure 2.

CHAPTER III

Non-Radial Ejection in 3C345

Published in Nature

Volume 306, Pages 42-44 (1983).

Reprinted from Nature, Vol. 306, No. 5938, pp. 42-44, 3 November, 1983

Non-radial ejection in 3C345

J. A. Biretta, M. H. Cohen & S. C. Unwin

California Institute of Technology, Pasadena, California 91125, USA

I. I. K. Pauliny-Toth

Max-Planck-Institut für Radioastronomie, 5300 Bonn 1, Auf dem Hügel 69, FRG

The radio source 3C345 is associated with a 16th magnitude quasar with $z = 0.595$ (ref. 1). At radio wavelengths it has six major components. From largest to smallest these are: a low brightness halo[2]; a 3 kpc curved jet[3]; three steep-spectrum components (C_1, C_2, and C_3) which define a curved jet[4,5]; and a compact component D which is self-absorbed at frequencies up to at least 10 GHz. Components C_2 and C_3 show proper motion relative to D at an apparent superluminal speed. We present VLBI observations at 10.7 GHz which show that a new radio component C_4 has appeared and is moving along a non-radial path. This behaviour is consistent with the hypothesis that bending causes the jet curvature. We interpret our observations in light of the relativistic beam model[6] as this is currently the most attractive explanation for both the superluminal effect and the weak X-ray emission[4].

The position angle (PA) misalignment between the small- and large-scale structures, which is seen in many radio sources, is especially large in 3C345 (ref. 7). Observations at 22 GHz show that the PA of the structure at radius (r) ~ 0.3 m arc s is about −130° (refs 7, 8) while the large scale jet (r ~ 3 arc s) has PA ~ −30° (ref. 3). Explanations of this misalignment or curvature include motion along a bent jet[9] or precession of the central engine combined with ballistic motion of the ejecta[10].

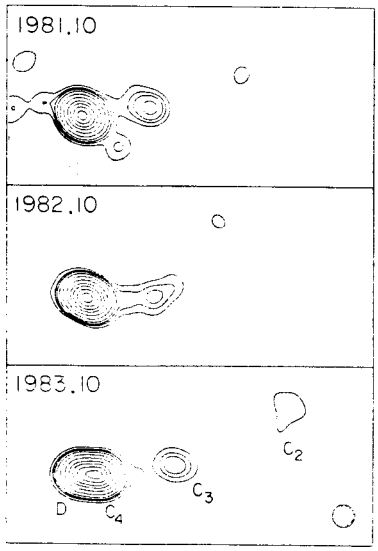

Fig. 1 Contour plot of clean map from three epochs. Contour levels are at −1, 1, 2, 3, 5, 10, 20, 35, 50, 70, and 90% of the peak intensity of 6.9, 9.4, and 7.7 Jy per beam area respectively at the 1981.1, 1982.1, and 1983.1 epochs. The hatched region indicates the clean restoring beam, which is a 0.50 m arc s circular gaussian function. North is at the top, and the width of the map is 10.00 m arc s.

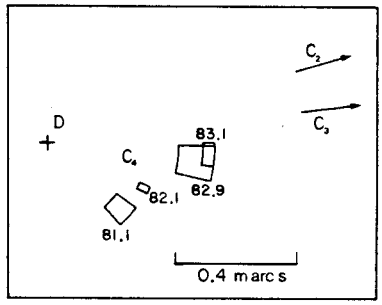

Fig. 2 Positions of component C_4 assuming core component D is stationary. North is up.

In both cases the curvature could be strongly amplified by projection, so the large observed misalignment is plausible. Cohen *et al.*[5] have recently presented evidence that component C_2 moved radially at a constant PA from $r = 1$ to 4 m arc s during the period 1971–82, which is consistent with the precession hypothesis. We now present evidence, however, that the motion of a new component C_4 is non-radial with respect to D. The new evidence is consistent with motion along a bent jet. We return to this apparent discrepancy below.

VLBI observations were made at four epochs between 1981.1 and 1983.1 at 10,651 MHz in left-circular polarization with a bandwidth of 1.8 MHz. At each epoch the longest baseline gave an angular resolution $\lambda/2D = 0.33$ m arc s. Details of the observations will be presented elsewhere.

Hybrid maps were made for all except the third epoch; the mapping technique described by Unwin *et al.*[4] was used. The maps are presented in Fig. 1. For each epoch, two-component models were fit to the bright eastern region which had a scale size <1 m arc s. These models consisted of an eastern point source and a western elliptical gaussian component. This model gave a much better fit than a pair of point sources. A least-squares algorithm was used to obtain model parameters which best fit the visibility amplitudes and closure phases. In all cases the final model was insensitive to the starting model.

Figure 1 shows that the source consists of a slightly resolved eastern region which contains most of the flux, and a faint extension ~2 m arc s to the west. Two-component models of the bright eastern region for all four epochs are presented in Table 1. For the assumed model the quoted uncertainties include the range of possible parameter values. Our results are in good agreement with those of Moore *et al.*[11] which were obtained independently at a different frequency. Minor differences between the results, as well as size and spectral evolution of the components will be described elsewhere (refs 4, 12, and J.A.B. *et al.* in preparation). For a deceleration parameter $q_0 = 0.05$ the scale is 7.9 pc m arc s^{-1} k^{-1} where $k = H_0/55$ and H_0 is the Hubble constant.

Table 1 Two component models of bright eastern region in 3C345

Epoch	1981.10	1982.10	1982.86	1983.10
No. of stations	5	6	3	6
Component flux (Jy)				
eastern	5.8	6.0	5.0	4.6
western	2.8	6.4	8.4	8.1
Radius* (m arc s)	0.32 ± 0.04	0.35 ± 0.02	0.49 ± 0.06	0.53 ± 0.02
PA (deg)*	−132 ± 6	−115 ± 2	−97 ± 6	−94 ± 4

* Vector from eastern to western component.

The results may be summarized as follows:
(1) At each epoch a minimum of two components is required to fit the bright eastern region. The models in Table 1 give a very good fit to the data.
(2) The relative PA and the separation of the two components increase monotonically with epoch.
(3) For epochs with maps, the PA and separation indicated by the map are consistent with the model.

As the structure of the source is not well resolved by our maps it must be inferred from the above models and other evidence. The structure at previous epochs consisted of an unresolved component D and discrete jet components which moved away from D (ref. 4). Unless the basic nature of the source has changed, the elongation in our maps must be due to a new jet component. Hence we identify the western component in our models with a new jet component C_4 and the eastern component with the unresolved component D. Figure 2 shows the locations of C_4 relative to D.

Our observations show that the radius vector from D to the new component has changed PA by $\sim 38°$ as the component separated from D. These and similar observations presented by Moore *et al.*[11] are the first observation of an extragalactic radio source in which a discrete component has changed PA. In the relativistic jet model of the superluminal effect[6] the unresolved, flat spectrum component D is near the central engine and the outer components are identified with plasma clouds or shock waves which move along a jet at relativistic velocities. The change in PA of this new component would then indicate that it has moved along a bent or curved jet. This is consistent with the suggestion[9] that the large misalignment or curvature seen in some sources is due to projection effects which amplify a small intrinsic bend caused by external pressures. Figure 2 shows that the trajectory of the new component is not appreciably curved between $r \sim 0.3$ and 0.5 m arc s. Hence there must be a strong curvature at $r < 0.3$ m arc s if the component is to originate in the core.

Observations at 22 GHz also give evidence for this new component. In 1977.8 and 1978.7 the core was extended along $PA = -135°$ (ref. 8) and in 1981.25 the extension was ~ 0.3 m arc s at $PA = -130° \pm 5°$ (ref. 7). These data and our own at 1981.10 (Table 1) are consistent with the hypothesis that 3C345 had a slowly moving component with proper motion $|\dot{\mu}| < 0.1$ m arc s yr^{-1} for 3 yr or more. For the data in Fig. 2, the proper motion $\dot{\mu}$ has mean directions $PA = -50° \pm 31°$ and $-62° \pm 11°$ and magnitudes 0.10 ± 0.04 and 0.24 ± 0.04 m arc s yr^{-1} during 1981 and 1982 respectively. The above estimates indicate that there has been an apparent acceleration of the component. The proper motion of C_4 is less than that of C_3 and C_2 which had $|\dot{\mu}| = 0.31$ and 0.42 m arc s yr^{-1} respectively in 1982. This difference and the above acceleration could be due to actual differences/changes in the bulk velocity or in the angle between the velocity vector and the line of sight. With $k = H_0/55$ the apparent transverse velocity of C_4 in a co-moving frame was $(9.9 \pm 1.6)k^{-1}c$ during 1982.

Cohen *et al.*[5] recently reported evidence that (1) during 1972–82 component C_2 moved radially at $PA \sim -75°$ from $r = 1$ to 4 m arc s, and (2) C_3 at similar radii had a different $PA -89°$. Their conclusion is based on high-quality maps from 1979 to 1982, and less reliable data from 1971 to 1976. This result appears to be contradicted by the direct evidence shown above, that the track is not radial. We see three possible explanations for the discrepancy: (1) a component may have different behaviour at $r < 0.6$ and > 1.0 m arc s. (2) Different components may follow different paths due to either precession or dynamical effects which move the jet. (3) The interpretation of the 1971 to 1976 data may be incorrect. Re-analysis (ref. 13, and J.A.B. *et al.*, in preparation) of the 1974.5 data of Wittels *et al.*[14] show that this possibility is unlikely.

Received 3 July; accepted 25 August 1983.

1. Burbidge, E. M. *Astrophys. J. Lett.* **142**, 1674–1676 (1965).
2. Schilizzi, R. T. & de Bruyn, A. G. *Nature* **303**, 26–31 (1983).
3. Browne, I. W. A. *et al. Nature* **299**, 788–793 (1982).
4. Unwin, S. C. *et al. Astrophys. J.* **271**, 536–550 (1983).
5. Cohen, M. H. *et al. Astrophys. J.* **269**, 1–4 (1983).
6. Blandford, R. D. & Königl, A. *Astrophys. J.* **232**, 34–48 (1979).
7. Readhead, A. C. S., Hough, D. H., Ewing, M. S., Walker, R. C., & Romney, J. D. *Astrophys. J.* **265**, 107–131 (1983).
8. Bååth, L. B. *et al. Astrophys. J. Lett.* **243**, 123–126 (1981).
9. Readhead, A. C. S., Cohen, M. H., Pearson, T. J. & Wilkinson, P. N. *Nature* **276**, 768–771 (1978).
10. Begelman, M. C., Blandford, R. D. & Rees, M. J. *Nature* **287**, 307–309 (1980).
11. Moore, R. L., Readhead, A. C. S. & Baath, L. *Nature* **306**, 44–46 (1983).
12. Moore, R. L., Biretta, J. A., Readhead, A. C. S. & Baath, L. *VLBI and Compact Radio Sources, IAU Symp. No. 110* (in the press).
13. Cotton, W. D. in *Radio Interferometry Techniques for Geodesy*, 193–197 (NASA Conf. Publ. 2115, 1980).
14. Wittels, J. J. *et al. Astr. J.* **81**, 933–949 (1976).

CHAPTER IV

The Evolution of the Compact Radio Source in 3C345: VLBI Observations

To be submitted to The Astrophysical Journal

The Evolution of the Compact Radio Source in 3C345: VLBI Observations

J. A. Biretta and R. L. Moore

California Institute of Technology

Received _____

Abstract

We present a systematic analysis of VLBI observations of 3C345 at 2.3, 5.0, 10.7, 22.2, and 89 GHz. Epochs are from 1979.25 through 1984.11. A newly ejected component (C4) accelerates, changes position angle, undergoes a large flux outburst, and has a flat spectrum. Older components C2 and C3 have different speeds, different position angles, and show little or no acceleration. The flux of C3 decays and its spectrum steepens. The distance between the "core" component (D) and "outer" components (C3 and C4) is larger at higher frequencies due to spectral index gradients in the "core" and/or "outer" components. The moving components define an opening angle of ~27° and show direct evidence of expansion. The counter-jet to jet flux ratio is -0.007 ± 0.007. Detailed physical interpretation will be presented elsewhere.

I. Introduction

The quasar 3C345 is an interesting object at many frequencies. Ku, Helfand, and Lucy (1980) have detected it as a 2 KeV x-ray source. At optical and infrared frequencies its flux varies by a factor of five, making it one of the most variable quasars (Grandi and Tifft 1974; Neugebauer et al. 1979; Pollock et al. 1979). It has a high and variable optical polarization (Moore and Stockman 1981) and there is evidence for optical nebulosity surrounding it (Hutchings, Crampton, and Campbell 1984). At radio frequencies it is one of the strongest known compact sources and its high frequency flux varies by a factor of two on a time scale of a few years.

The radio structure of 3C345 consists of a faint 20 arcsecond diameter steep spectrum halo (Schilizzi and de Bruyn 1983), a 3 arcsecond long steep spectrum jet which terminates in a bright hot spot (Browne et al. 1982b), and a milli-arcsecond (mas) scale compact region which has a flat spectrum and dominates the flux above ~100 MHz. Early evidence of superluminal motion in the mas scale structure was given by Cohen et al. (1976) and Wittels et al. (1976). Due to its brightness and high declination, it has become perhaps the best studied of the seven known superluminal sources (Cohen and Unwin 1984). Unwin et al. (1983) have presented results of VLBI monitoring at two frequencies

between 1979 and 1981. They give clear evidence for superluminal motion and for Doppler factors much larger than unity, based on the weakness of the inverse Compton X-ray flux. Recently Biretta et al. (1983) and Moore et al. (1983) have presented evidence for interesting kinematics of a newly ejected component.

In this paper we present new VLBI observations from 1982 through 1984 and a systematic re-analysis of previously reported VLBI data (Biretta et al. 1983; Cohen et al. 1983; Moore, Readhead, and Baath 1983; Readhead et al. 1983; Unwin et al. 1983; Backer 1984). A total of twenty epochs are analyzed and presented. The observational and data reduction procedures are given in Section II. Sections III and IV, respectively, describe qualitative and quantitative results. Important results are summarized in Section V. Subsequent papers will present evidence from total flux monitoring and physical interpretations.

Throughout this paper we will use a redshift $z=0.595$ (Burbidge 1965) and assume $H_0=100$ h km sec^{-1} Mpc^{-1} and $q_0=0.5$. For a standard Friedmann cosmology 1.00 mas corresponds to 3.79 h^{-1} pc. A proper motion of 1.00 mas yr^{-1} corresponds to $v/c=19.7\ h^{-1}$. Quoted uncertainties are 1.0 sigma.

II. Observations and Reductions

Very Long Baseline Interferometric (VLBI) observations were made of 3C345 at 2.3, 5.0, 10.7, and 22.2 GHz. Details of the epochs and antenna arrays are given in Table 1. About 12 hours of observation were obtained at each epoch. A bandwidth of 1.8 MHz was recorded using MkII equipment (Clark 1973; Moran 1973). System temperatures were measured every hour at 2.3, 5.0, and 10.7 GHz, and every half-hour at 22.2 GHz. Antenna temperatures were also measured wherever possible.

The recorded data were subsequently correlated at the CIT-JPL five station processor (Thomas 1981). Correlation amplitudes and phases were measured with the PHASOR fringe fitting program. For signal-to-noise ratios (S/N) between 10 and 3 the amplitudes were corrected for the positive bias introduced by the Rice distribution and truncation (Linfield 1981). For $S/N \leq 3$ the bias is difficult to correct; hence the uncertainties for these data points were increased by a factor of 3. Correlation coefficients were converted to flux densities using the technique described by Cohen (1975) and the flux scale of Baars *et al.* (1974). Data from the 1982.42 epoch were processed at the M.P.I.f.R. correlator at Bonn, F.R.G. (Baath *et al.* 1985). The 89.0 GHz visibility data (epoch 1982.38) are from Backer (1984).

Our approach to converting the visibility data to a source image differs from that used previously. Early methods involved fitting 2- or 3-component models to the visibility data to obtain the source structure (Wittels *et al.* 1976). This had the disadvantage that a detailed starting model was required, and there was no independent way of testing to see whether the assumed starting model was correct. Later hybrid mapping (Readhead and Wilkinson 1978) permitted the source structure to be derived with many more degrees of freedom. It has become the preferred method because of this ability to derive structure with few *apriori* assumptions. However, there is yet no proof that hybrid mapping yields a unique map for VLBI data where much of the (u,v) Fourier transform plane contains no data. Neither is there a simple algorithm for quantifying the uncertainty at each point in the map caused by the missing (u,v) data.

Our method attempts to use both mapping and model-fitting to their fullest advantage. These advantages are: (1) maps can reconstruct the source structure with few initial assumptions; (2) models give a simplified description of the source with few free parameters, and (3) it is easy to estimate formal uncertainties for models due to missing (u,v) coverage. In brief summary the procedure is this: We first map the data starting from a point source model. Once the basic source structure is apparent, models

are used to self-calibrate the data. Finally, maps are used to self-calibrate the data until convergence is achieved. For the purpose of quantitative analysis, models with formal uncertainties (due to (u,v) coverage, etc.) are fit to the self-calibrated data.

A. Mapping Procedure

Maps were made from the visibility data for every epoch with four or more antennas. The mapping procedure involves several "major" iterations. Each major iteration begins with the unadjusted visibilities (with no self-calibration applied), and a model; it results in a map and improved self-calibrated visibility data. For the first major iteration a point source starting model is used. Later major iterations start with a more complex model which is obtained by fitting to the adjusted visibilities produced by the previous major iteration.

Each major iteration proceeds as follows. Given the starting model, the first step is to perform several iterations of self-calibration (Cornwell and Wilkinson 1981) using only this simple model. That is, the visibilities are corrected based on this starting model; a new source model is fit to the data; then the new model is used to further correct the visibilities, and so on. This step introduces a compactness constraint which is

helpful in reconstructing the source intensity distribution from incomplete (u,v) data.* After these iterations with models have converged, the data are then self-calibrated through several more iterations using maps. The visibilities are Fourier transformed, the resulting map is CLEANed, the CLEAN components are used to further correct the visibilities, and so forth. During self-calibration, antenna gains were permitted to vary on time scales of a few hours at 2.3, 5.0, and 10.7 GHz and on time scales of a few minutes at 22.2 GHz. The major iteration is ended when

---

* This step is similar to the technique of CLEANing a small "window" during the early self-calibration iterations. "Windowing" restricts the flux to be in a certain small region of the map, while our procedure only restricts the flux to be contained in a few components. This has several advantages. First, it permits the flux to be located anywhere in the image plane, whereas windowing restricts the flux to a small specified area. Secondly, it can accommodate large, extended features without introducing many free parameters. Third, the model provides the best description of the source for the fewest free parameters. Hence it rejects spurious features not required by the visibility data during the first iterations of self-calibration. Any inconsistencies between the visibility data and model are corrected during later self-calibration with maps.

the self-calibration has converged and the fit to the (u,v) data ceases to improve.

After each major iteration the starting model is compared with the improved map and revised by adding components and re-fitting to the improved visibility data. This new model and the uncorrected visibility data (with only apriori calibration) are used to begin the next major iteration. This method constantly improves the starting model for the mapping procedure (Pearson and Readhead 1984) and improves the dynamic range of the final map. Typically four major iterations are used.

B. Calculation of Models for Use in Quantitative Analysis

We have fit models to the (u,v) data for the purpose of deriving quantitative measurements. These models permit us to quantify the uncertainty caused by incomplete (u,v) coverage.

Models consisting of several optically thin, homogeneous spherical components were fit to the final self-calibrated visibility data using a non-linear least-squares algorithm. Optically thin spheres were used since their shape is invariant under rotation and relativistic transformation, which will simplify later analyses. The starting model was chosen to

resemble the final hybrid map. A typical map and model are shown in Figure 1.

Uncertainties in the model parameters were determined by the method of Arndt and MacGregor (1966). The uncertainty in a parameter was defined as the variation in that parameter which would cause the reduced chi-square to increase by a factor 1+1/N when all other parameters were allowed to vary. For random errors with a Gaussian distribution, N is the the number of independent errors minus the number of fit parameters. For perfectly calibrated data N would be simply the number of independent (u,v) points. However, calibration errors cause a correlation of the errors for data points adjacent in time. We assumed that the most serious errors in our data were due to antenna dependent calibration problems having a one-hour time scale. Hence N~(12 hours)x(1 independent error per hour)x(m) for 1 sigma errors, where m is the number of antennas. In practice we computed 2.5 sigma errors by setting $N=12m/(2.5)^2$, and then divided the result by 2.5, since this reduces numerical instabilities. This same method was used to determine whether a component should be included in the model. Components were included only if their presence was significant at the 2.5 sigma level.

Note that this method takes into account the quality of the (u,v) coverage. If a parameter is not well constrained by the (u,v) data, the chi-square will be insensitive to variations in the parameter, and hence the estimated uncertainty in the parameter will be large. Since the statistical distribution function of the calibration errors is poorly known and may be non-Gaussian, the uncertainties we give are approximate and cannot be interpreted strictly in terms of a Gaussian distribution function.

The fluxes of the model components were adjusted so that

$$S_{total} - S_{model} = S_{res}$$

would be constant from epoch to epoch, where

S_{total} = total source flux

S_{model} = total flux of model components D, C5, C4, C3.5, C2 (using the labeling convention of Unwin et al. 1983)

S_{res} = flux of components resolved by VLBI.

The purpose of this adjustment is to remove epoch-to-epoch variations in the model fluxes which are caused by antenna and correlator calibration errors. This adjustment assumes that structures too large to be seen by VLBI have constant flux on time scales of a few years.

This constant S_{res} was set to 1.02 Jy at 5.0 GHz; this is the average value for the six epochs at 5.0 GHz. Five GHz was the frequency with the best calibration. This flux of 1.02 Jy may be broken up into a contribution of 0.55 Jy from structures resolved with MERLIN (Schilizzi and de Bruyn 1983; Browne et al. 1982a) and a contribution of 0.47 Jy which must be due to emission on scales between about 20 mas and 200 mas. For other frequencies, we assumed S_{res} had a spectral index of $\alpha = -1.0$ ($S_\nu \propto \nu^\alpha$) (Schilizzi and de Bruyn 1983; Browne et al. 1982a). At 10.7, 22.2, and 89.0 GHz, components C3 and C2 do not appear in the model for some epochs. In these cases we extrapolated the 5.0 GHz flux of C2 and C3 assuming $\alpha = -1.0$ and included this flux in S_{model}. These corrections to the model flux had a median value of 5 percent; the largest correction was 50 percent for the 1983.09 epoch 22 GHz data.

C. Reliability of the Maps and Models

The reliability of our reconstruction of the source intensity distribution is limited by incomplete (u,v) coverage, by calibration errors, and by thermal noise in the antenna systems. The most serious uncertainties are those caused by incomplete (u,v) coverage. The fractions f of the gridded (u,v) plane which

contain data are given in Table 1 for each epoch.* This fraction is essentially the ratio between the number of independent data points observed and the number of independent parameters we must solve for, in making the map. The f values are typically 0.5 or less so that simple Fourier transformation of the visibility data cannot yield a unique representation of the source.

During mapping we have used two constraints in addition to the observed (u,v) data to minimize this problem: (1) the map intensity must be positive and (2) the assumption that most of the flux is in a small region near the map center. These assumptions greatly reduce the number of possible intensity distributions consistent with the observed (u,v) data, but still do not guarantee a unique map. No simple algorithm has yet been found for quantifying the uncertainty caused by uniqueness problems and poor (u,v) coverage. Lacking such an algorithm, the intensity level of weak features thought to be spurious is usually taken as the uncertainty. These intensity levels are given in Table 1 as a fraction of the peak intensity. Uncertainties estimated this way are only a rough guideline, and probably do not apply to bright regions of the map, where the uncertainties are likely to be much

---

* For the purpose of gridding, the map size was taken to be 200mas/ (GHz) which is the size used during CLEANing.

larger.

The factors listed above also limit the reliability of the models, but all these can be taken into account when estimating uncertainties on model parameters, and we have done this. Models also have an additional uncertainty: the choice of model itself. In all cases we chose the number and locations of components to resemble the map, so the basic structure of the model is justified by the appearance of the map. This uncertainty would be important only if the gross structures in the map were incorrect, and this seems very unlikely since they are the same from epoch to epoch and at different frequencies.

It is possible that details of the model could be incorrect, such as the choice of component shape (optically thin spheres), but this has little effect on the results. If we had used optically thick spheres, instead of optically thin ones, the models would remain unchanged except for the component diameters, which would decrease by a factor of 0.84. If Gaussian components were used, FWHM values equal to 0.594(sphere diameter) would have been obtained. In the one case where a component is strongly non-circular (C4 at 1984.09 epoch), the model we use and one with an elliptical component both give the same flux and mean diameter.

One final problem which might occur is in the comparison of models at different frequencies. In some cases the model at the higher frequency has additional components which were not seen at the lower frequency. In all such cases additional fits were made, with the same model being used at both frequencies. In no case were the results significantly different from the models we present.

D. Comparison with Analysis Methods of Unwin *et al.*.

Our quantitative analysis is based on models which are fit to the visibility data, while the Unwin *et al.* (1983) analysis is based on contour plots of maps. In some cases these two methods produce systematically different results.

Our component separations are in good agreement with theirs at 10.7 GHz but they obtain systematically larger separations than ours at 5.0 GHz. This is because they used two different methods at the two frequencies. At 10.7 GHz their components D and C3 were well separated so that the centroid of C3 was taken as the center of the highest few contours. However, at 5.0 GHz components D and C3 are blended together so that the centroid of C3 was taken as the point one beam HWHM east of the western half intensity point (side away from component D). But in cases where

the components are extended along the jet, as we find them to be, the centroid will occur more than a beam HWHM away from the western half intensity point. Hence their centroids for C3 are too far west at 5.0 GHz, so that they obtain separations between D and C3 which are too large.

We measure component sizes as the diameter of the spherical model component, while Unwin et al. measure directly from the maps and allow for the size of the restoring beam. We find that C2 and C3 are resolved while Unwin et al. find that "few components are significantly resolved."

The two techniques were tested by applying them to data for an artificial source which resembled 3C345 and had known component sizes. Different sets of artificial data were generated assuming 4, 6, and 8 antennas. Thermal noise and realistic calibration errors were included. The artificial data were then hybrid mapped and self-calibrated, and component sizes were measured using the above techniques. Measurement by model fitting was found to give sizes in the range 0.9 to 1.3 times the actual size, while measurement from the maps gave sizes 0.3 to 1.0 times the actual size. Hence, the sizes determined by measurement from maps appear to be biased towards small sizes. This is probably because the maps contain too many free parameters and are poorly constrained by the (u,v) data.

Our fluxes agree with those of Unwin et al. for components much smaller than the beam size. But for extended components their fluxes are much smaller than ours. Unwin et al. measure the peak brightness on the map and then multiply this by the beam area to obtain fluxes, thereby assuming the components to be unresolved. Their assumption that the components are unresolved causes them to obtain low fluxes when converting from peak surface brightness to flux. We simply use the flux found in the model-fitting procedure.

III. Qualitative Results

The maps are presented in Figure 2 and the models are presented in Table 2. Earlier versions of many maps have been presented elsewhere (Cohen et al. 1983; Unwin et al. 1983; Readhead et al. 1983; Moore, Readhead, Baath 1983; Biretta et al. 1983; Baath et al., in preparation), but in all these cases the data have been recalibrated, remapped, and modeled in the above manner. These maps and models form the largest set of homogeneous data yet assembled for a compact radio source.

All the maps show a basic "core-jet" morphology (Readhead and Pearson 1982) with bright knots in the jet. We will use the notation of Unwin et al. (1983) for labeling the "knots" and the "core."

The 2.3 GHz map shows components C1, C2, and C3. Component C3 is the brightest component while C1 is weak and extended. Component D appears as an eastern extension from C3.

The 5.0 GHz maps clearly show components C2 and C3 separating from component D.* Component D is the brightest, with C3 and C2 being progressively weaker in surface brightess. Measurements of diameter show that D tends to be smaller than C3, and C3 tends to be smaller than C2. The 1983.57 observations involved more antennas than any other epoch and the map has a high dynamic range. The ratio of peak brightness to r.m.s. noise away from the map center is ~2700:1, which is the highest value ever attained for a VLBI map. The measured noise level in the map is 2.7 $\pm$ 0.3 mJy/beam, which is in good agreement with the noise level of 2.6 mJy/beam expected for the antennas and receivers used in the observations. This map shows only weak structures beyond

---

* Bartel et al. (1984) have given evidence that D is nearly stationary on the sky; its proper motion relative to NRA0512 is .02$\pm$.02 mas/yr on a ten-year time scale.

C2 and no evidence of a counter-jet. (See below.)

The 10.7 GHz maps show motion of C2 and C3 relative to D which is similar to that seen at 5.0 GHz. In 1981 component D begins to show an extension which is labeled C4 (Biretta *et al.* 1983, Moore *et al.* 1983). This new component then moves away from D and changes P.A. from ~-135° to ~-86°. Two of the maps (1982.09 and 1983.10) show evidence for a weak component between C3 and C4 which we have labeled C3.5. This component significantly improved the fit of the model to the visibility data, so we have included it.

At 22.2 GHz maps plainly show component C4 changing P.A. and separating from D. They also show significant evolution of C4; initially it is much weaker than D but at later epochs it is of comparable brightness. At the last epoch C4 shows elongation along P.A. ~-60°. Component D itself appears to have a weak extension after 1983, once C4 is sufficiently separated from it. Although the nature of this extension is not yet clear, we have included it in the models since it significantly improves the fit, and label it C5. The three maps after 1983 all show a weak feature 0.7 mas northeast of D, but this feature was not significant at the 2.5 sigma in any one data set and was therefore not included in the models.

IV. Quantitative Results

1. Positions and Proper Motions of Component Centroids

The positions of the centroids of knots C2, C3, C4, and C5 on the sky relative to component D are shown in Figure 3. During the period 1979 to 1984 C2 moved from a radial distance r~3.6 to ~5.9 mas, C3 moved from r~1.2 to ~2.9 mas, and C4 moved from r~0.2 to 0.9 mas. To derive proper motions for the components, functions of the form $r(t)=r(t_0)+(dr/dt)t$ were fit to the data (Figure 4). The position $r(t_0)$ for some fiducial epoch t_0 and the radial proper motion dr/dt are given in Table 3. We will treat each frequency separately so as to avoid complications caused by spectral index gradients.

Components C2 and C3 have significantly different proper motions. Component C2 has the highest proper motion of all the components, $dr/dt=.48\pm.02$ mas/yr, while C3 has $dr/dt=.30\pm.01$ mas/yr. There is no significant difference in the proper motions derived at 5.0 and 10.7 GHz for these components; for C3 the difference is 5 ± 5 percent. Both C2 and C3 have little or no acceleration; the formal values of acceleration are $.08\pm.11$ and $.01\pm.04$ mas/yr^2, respectively, at 5.0 GHz. The uncertainties allow either constant velocity or a small acceleration sufficient

to give C3 the same speed as C2, when it has moved to C2's present position. Similar results have been obtained for 3C120 (Walker et al. 1984) and 3C273 (Unwin et al. 1985) in that components well separated from the "core" appear to have little or no acceleration. For C2 and C3 the magnitude of the vector proper motion $|d\vec{r}/dt|$ is nearly equal to the radial component dr/dt.

Component C4 first appears near the core with a small proper motion dr/dt ~.04 mas/yr in 1982 and then accelerates to ~.31 mas/yr by 1983.5, which is similar to the speed of C3. The acceleration cannot be an artifact of poor resolution because: (1) If there were no acceleration, backwards extrapolation of the ~.31 mas/yr motion would put the centroid of C4 coincident with the centroid of D at 1981.1, but C4 clearly appears in maps near that epoch. (2) Both the 10.7 and 22.2 GHz data give similar velocities even though the resolution differs by a factor of 2. Early evidence for this acceleration is described by Biretta et al. (1983) and Moore et al. (1983). The proper motion we obtain for 1982 is smaller than that given by Moore et al. (1983); the discrepancy arises from their use of different analysis methods on the 1981.25 and 1982.42 data. This component changes P.A. rapidly, so that its total proper motion $|d\vec{r}/dt|$ is much larger than the radial component dr/dt alone. In 1982 dr/dt~.04 mas/yr whereas $|d\vec{r}/dt|$~.07 mas/yr.

These data for C2, C3, and C4 provide clear evidence for different components having different proper motions in a superluminal radio source. The only other clear evidence for this is given by Walker *et al.* (1984) for 3C120. The data for C4 also constitute the best evidence yet found for acceleration of a component. Cohen *et al.* (1983) have given some evidence for acceleration of C2 in this source based on early models from 1971 to 1974.

The position angles of the "outer" components vary systematically with r. As C4 moved away from D, its postion angle changed from ~-135° to ~-87°. Components C3, C2, and C1, which are progressively farther from D, are roughly at P.A. -86°, -74°, and -64°, respectively. The arcsecond scale jet curves from P.A. -38° to P.A. -32° between radii 1 and 3 arcseconds (Browne *et al.* 1982b). There is marginal but direct evidence that C3 and C2 change P.A. with time. Their d(P.A.)/dt are $.8\pm.4°$/yr and $.6\pm.3°$/yr, respectively. These values of d(P.A.)/dt are much smaller than those for C4 and have the same sign. It is interesting that the 10.7, 22.2, and 89.0 GHz observations all give about the same P.A. for C4. This is contrary to the trend seen at lower frequencies and lower resolutions (Readhead *et al.* 1983) where the P.A. of the structure rotates with frequency.

The distance between the "core" component (D) and "outer" components (C3 and C4) is larger at higher frequencies due to spectral index gradients in the "core" and/or "outer" components. This can be seen in the $r(t_0)$ values in Table 3, and also in Figures 4b and 4c. Values of $r(t_0,\nu)-r(t_0,10.7\ \mathrm{GHz})$ have been calculated from results in Table 3 and are given in Table 4. The effect in most significant for components C3 and C4. The shift between 5.0 and 10.7 GHz for component C3 at 1982.0 is different from the shift seen for C4 at 1983.5. This suggests that some of the effect is due to spectral index gradients in the C components, or time variable gradients in D. Marcaide *et al.* (1984) have found similar evidence for spectral index gradients in the quasar 1038+528.

Component C3.5 is a weak component located between C3 and C4. Its mean P.A. of $-101^\circ\pm7^\circ$ is consistent with other components at similar radii. But its proper motion dr/dt~.14 mas/yr appears to be slower than either C3 or C4 when at similar radii.

Component C5 is a weak extension from component D which is seen in 1983 and 1984. Its P.A. and distance from D average -90° and ~.25 mas at 22.2 GHz; this P.A. is quite different from that at which C4 first appeared. Its proper motion is very small, $dr/dt=.00\pm.03$ mas/yr.

2. Component Fluxes

Component fluxes are plotted against epoch in Figure 5. To estimate time scales for flux variations we have fit functions of the form

$$S(t) = S(1982.0)\ \exp(t/\tau)$$

to data for components C2, C3, C3.5, and C4. Values of S(1982.0) and τ are given in Table 5. The spectra of components are plotted in Figure 6.

The fluxes for component C2 are shown in Figure 5a. At 10.7 GHz the large positive uncertainties are due to a lack of short spacings in the (u,v) plane. At 5.0 GHz the time scale for the flux to vary by a factor (e) is at least 11 years. The spectrum is straight from 2.3 to 10.7 GHz, with $\alpha = -0.59\pm0.08$.

Figure 5b shows the data for component C3. Data for 1977.56 and 1977.92 are from Cohen *et al.* (1979) and Readhead *et al.* (1979). At epoch 1982.0 the spectral index between 2.3 and 5.0 GHz is -0.37 ± 0.14. At higher frequencies the spectral index is appreciably steeper, $\alpha = -0.81\pm0.07$ between 5.0, 10.7, and 22.2 GHz. The flux decays slightly faster at 10.7 GHz (4.3 ± 0.5 years) than at 5.0 GHz (6.6 ± 0.5 years). Hence the spectral index between these frequencies steepens at a rate $d\alpha/dt = -0.11\pm0.04$ yr^{-1}. The flux e-folding times we measure for C2 and C3

correspond to half-lives of 3 years or more. This is considerably longer than the surface brightness half-lives of ~2 years found by Unwin et al. (1983). The difference is due to component size increasing with time (see below).

Component C3.5 is a weak component and it appears to decay more rapidly than any of the other components. Its flux decays with a time scale of 2.3 $\pm$ 0.4 years while the others have time scales of 4 to 6 years at 10.7 GHz. Its spectral index between 10.7 and 22.2 GHz is -0.8 ± 0.6 which is consistent with that of C2 and C3.

Component C4 undergoes a large flux outburst as it moves away from the "core" component D. Fluxes for C4 are shown in Figure 5c. The 1977.9 and 1978.8 epoch data are from Baath et al. (1981); their data lack closure phases, so that the extension from D in their map may be at the same P.A. as C4 or approximately opposite C4. At 22.2 GHz the flux of C4 rises from $\leq$1 Jy in 1978 to a peak of ~7.5 Jy at epoch 1982.4; it then decays more slowly to ~5 Jy by 1984. Similar variations are seen at 10.7 GHz. The time scale for the rise is 1.53 ± 0.10 years at 22.2 GHz, and somewhat longer, 2.2 ± 0.3 years, at 10.7 GHz. The decay time scales are much longer, -3.8 ± 0.4 and -4.8 ± 1.2 years, respectively, at 22.2 and 10.7 GHz. Because of the infrequent sampling it is not clear whether the fluxes 10.7 and 22.2 GHz peak

at the same epoch; any delay between the peaks could not exceed 1.5 years.

The largest total flux outburst ever seen in 3C345 began about 1979 (Unwin *et al.* 1983) and peaked at 1981.6 (Feldman, MacLeod, and Andrew 1981; Biretta *et al.*, in preparation). Component C4 must be largely responsible for this outburst. A similar correlation between a total flux outburst and the appearance of a new component has been seen in BL Lac (Aller and Aller 1984; Mutel and Phillips 1984). However, C4 is the first component to show an outburst after it was appreciably separated from the "core."

Spectral indices for C4 are given in Table 6. Below 10.7 GHz the spectrum rises with $\alpha \leq 0.8$. Between 10.7 and 22.2 GHz the spectral index varies between −0.30 and −0.14. It is interesting that the index at these frequencies varies by only 0.16 ± 0.14 (between 1981.25 and 1984.09) while the flux doubles and then decreases. Above 22.2 GHz the spectral index is not well determined because the 89.0 GHz data have poor closure phases.

Component C5 is a westward extension from D which is evident after 1983.0. Its flux is near 1.5 Jy and its spectrum is flat with $\alpha = -0.10 \pm 0.09$ between 10.7 and 22.2 GHz.

Due to resolution increasing with frequency, component D is often blended with new components at low frequencies, but is seen separately at high frequencies. In order to consider the same physical region when comparing fluxes at different frequencies, we must combine the flux of D with that of C5 and C4.

Fluxes for the sum of components D and C5 are shown in Figure 5d. These are data where D is resolved from C4, but not from C5. The flux of D+C5 appears to vary between 5 and 10 Jy at 22.2 GHz, and 4.5 to 7 Jy at 10.7 GHz. At 22.2 GHz the first and highest peak occurs in 1981; and a second peak occurs near or after 1984 which is due in part to C5. The 10.7 GHz data shows peaks at the same epochs. The spectral index between 5.0 and 10.7 GHz is 0.4 $\pm$ 0.2; between 10.7 and 22.2 GHz it varies from 0.22 to 0.54 (Table 6).

At 2.3 and 5.0 GHz components D, C5, and C4 are blended together at most epochs, so in Figure 5e we show the flux for the sum D+C5+C4. The large rise seen at 10.7 GHz beginning in 1979 is caused mostly by C4; hence it seems likely that C4 also causes the rise seen at 5.0 GHz. The spectrum rises sharply between 2.3 and 5.0 GHz with $\alpha = 1.95 \pm 0.13$. Between 5.0 and 10.7 GHz the spectral index varies between 0.03 and 1.05.

At epoch 1984.1 components D and C5 are resolved apart at 10.7 and 22.2 GHz. The spectral index of D between these frequencies is 0.30 $\pm$ 0.10.

3. Counter-Jet / Jet Flux Ratio

We estimate the counter-jet/jet ratio using the 1983.57 epoch 5.0 GHz map. The region of the map between 1.2 and 20.0 mas from the core was divided into eight equal octants with one octant centered on the jet. The total flux in each octant was then calculated. The four octants closest to, but not containing, the counter jet were used to measure the background flux level of the map. The uncertainty in the flux was estimated as the dispersion about the background level for these four octants. The jet and counter-jet fluxes after background subtraction were 2.97$\pm$0.02 Jy and -0.020$\pm$0.022 Jy, respectively. Hence the counter-jet/jet flux ratio is -0.007$\pm$0.007. This is the smallest ratio yet reported for for a compact radio source.

4. Component Sizes

Component diameters for C4, C3, and C2 are plotted against r (the distance from component D) in Figure 7. We may derive an approximate opening angle for the source structure by fitting a simple cone to the data in this figure. The frequency with the most complete data is 10.7 GHz; for this frequency the opening angle (full angle) is $25.9^{\circ}\pm1.6^{\circ}$ and the apex of the cone is at $r = -0.20\pm0.09$ mas. For all data at all frequencies an angle of $27.0^{\circ}\pm0.7^{\circ}$ is obtained. These calculations assume that the components are circularly symmetric. We have also taken the epochs with the best (u,v) coverage and fit separately for the component size perpendicular to the source axis. This produces an opening angle of $26.7^{\circ}\pm2.1^{\circ}$, in good agreement with the above values. This is much broader than opening angles for arcsecond scale radio jets which are typically a few degrees (Bridle and Perley 1984).

Each component also shows direct evidence for expansion. Expansion <u>rates</u> were derived by fitting straight lines to diameter (a) vs. epoch (t). Values of da/dt and a(1982.0) are given in Table 7. Expansion rates are in the range ~0.05 to ~0.15 mas/year. The wide range of values may indicate that the expansion is somewhat erratic on short time scales. For both C3 and C4 there is marginal evidence that the expansion rate is higher at the lower frequency.

The values of a(1982.0) in Table 7 indicate that components C2 and C4 have the same size at the two frequencies. Component C3, however, appears to be significantly larger at 5.0 than at 10.7 GHz; the size ratio is 1.66 ± 0.08. Opacity effects could account for only part of this effect. If C3 had the intensity distribution of an optically thick sphere (or uniform disk) at 5.0 GHz, we would overestimate its diameter by a factor 1.19 since we are fitting optically thin spheres. Hence, if C3 were completely opaque at 5.0 GHz and completely transparent at 10.7 GHz, a size ratio of 1.19 could be obtained. This is much smaller than the observed ratio and can account for only part of the observed effect.

Mean diameters for component D are given in Table 8. At 10.7, 22.2, and 89.0 GHz the diameters are all around 0.3 mas. The dispersions at 10.7 and 22.2 GHz are large and this is probably due to evolution of the source; new components continuously appear near D and initially they are blended with D and cannot be resolved as separate components. At lower frequencies larger diameters are found. Diameters of 1.17 and 1.6 mas are found at 5.0 and 2.3 GHz, respectively. For most epochs C4 and D are blended together at 5.0 but not higher frequencies. This could account for only a small part of the size difference; for epochs prior to 1982 the 5.0 GHz size is ~0.7 mas larger than

the size at higher frequencies, but the separation between D and C4 is only ~0.3 mas.

V. Summary

Our results may be summarized as follows:

a) The newly ejected component C4 accelerates from ~0.07 to ~0.31 mas/yr, which is similar to the speed of C3. Component C2 has a larger speed of 0.48 mas/yr. Both C2 and C3 show little or no acceleration.

b) C4 changes P.A. from -135° to -87°, which is also the P.A. of C3. Component C2 has a different P.A. of -74°. After 1983 the "core" extension C5 has a P.A. of -90° which is different from that at which C4 first appeared.

c) The distance between the "core" component (D) and "outer" components (C3 and C4) is larger at higher frequencies due to spectral index gradients in the "core" and/or "outer" components.

d) C4 shows a large flux outburst, increasing from ≤ 1 to ~8 Jy with a 2 year time scale, and then begins to decay with a 4 year time scale. During this evolution the spectrum remains flat. Component C3 decays with a similar time scale and its spectrum steepens.

e) The ratio of the counter-jet to jet flux is $-.007 \pm .007$ at 5

GHz.

f) The moving components define an opening angle of ~27° and show direct evidence for expansion.

It is a pleasure to thank M. Cohen, T. Pearson, A. Readhead, and S. Unwin for many useful discussions. L. Baath and D. Backer, respectively, provided visibility data for the 1982.42 and 1982.38 epochs. This work was supported by grants from the National Science Foundation.

VI. References.

Aller, H. D. and Aller, M. F. 1984,
in VLBI and Compact Radio Sources
(IAU Symposium 110, eds. R. Fanti, K. Kellermann, and G. Setti) p.119.

Arndt, R. A. and MacGregor, M. H. 1966, in Nuclear Physics
(Methods in Computational Physics vol. 6),
p. 253, App. II.

Baars, J. W. M. et al. 1974, A.A. 61, 99.

Baath, L. B. et al. 1981, Ap.J. 243, L123.

Baath, L. B. et al. 1985, in preparation.

Backer, D. 1984, in VLBI and Compact Radio Sources
(IAU Symposium 110, eds. R. Fanti, K. Kellermann, and G. Setti) p.31. Bartel, N. et al. 1984, in VLBI and Compact Radio
Sources (IAU Symposium 110, eds. R. Fanti, K. Kellermann, and G. Setti) p. 113.

Biretta, J. A., Cohen, M. H., Unwin, S. C., and
Pauliny-Toth, I. I. K. 1983, Nature 306, 42.

Bridle, A. H. and Perley, R. A. 1984, Ann.Rev.A.A.
22 319.

Browne, I. W. A. et al. 1982a, M.N.R.A.S. 198 673.

Browne, I. W. A. et al. 1982b, Nature 299 788.

Burbidge, E. M. 1965, Ap.J.Lett. 142 1674.

Clark, B. G. 1973, Proc.I.E.E.E. 61, 1242.

Cohen, M. H. et al. 1975, Ap.J. 201, 249.

Cohen, M. H. et al. 1976, Ap.J. 206, L1.

Cohen, M. H. et al. 1979, Ap.J. 231, 293.

Cohen, M. H. et al. 1983, Ap.J. 272, 383.

Cohen, M. H. and Unwin, S. C. 1984, in VLBI and Compact Radio Sources (IAU Symposium 110, eds. R. Fanti, K. Kellermann, and G. Setti) p. 95.

Cornwell, T. J. and Wilkinson, P. N. 1981, M.N.R.A.S. 196, 1067.

Feldman, P. A., MacLeod, J. M., and Andrew, B. H. 1981, IAU Circular No. 3637.

Grandi, S. A. and Tifft, W. G. 1974, P.A.S.P. 86, 873.

Hutchings, J. B., Crampton, D., and Campbell, B. 1984, Ap.J. 280, 41.

Ku, W. H.-M., Helfand, D. J., and Lucy, L. B. 1980, Nature 288, 323.

Linfield, R. 1981, Ap.J. 244, 436.

Marcaide, J. et al. 1984, in VLBI and Compact Radio Sources (IAU Symposium 110, eds. R. Fanti, K. Kellermann, and G. Setti) p.247.

Moran, J. M. 1973, Proc.I.E.E.E. 61, 1236.

Moore, R. L. and Stockman, H. S. 1981, Ap.J. 243, 60.

Moore, R. L., Readhead, A. C. S., and Baath, L. L. 1983, Nature 306.

Mutel, R. L. and Phillips, R. B. 1984, in VLBI and Compact Radio Sources (IAU Symposium 110, eds. R. Fanti, K. Kellermann, and G. Setti) p.117.

Neugebauer, G. et al. 1979, Ap.J. 230, 79.

Pearson, T. J. and Readhead, A. C. S. 1984, Ann.Rev.A.A., 22 in press.

Pollock, J. T. et al. 1979, A.J. 84, 1658.

Readhead, A. C. S. and Wilkinson, P. N. 1978, Ap.J. 233, 25.

Readhead, A. C. S. et al. 1979, Ap.J. 231, 299.

Readhead, A. C. S. and Pearson, T. J. 1982, in Extragalactic Radio Sources (IAU Symposium 97, eds. D. S. Heeschen and C. M. Wade) p.279.

Readhead, A. C. S. et al. 1983, Ap.J. 265, 107.

Schilizzi, R. T. and de Bruyn, A. G. 1983, Nature 303, 26.

Thomas, J. B. 1981, J.P.L. Publication 81-49.

Unwin, S. C. et al. 1983, Ap.J. 271, 536.

Unwin, S. C. et al. 1985, Ap.J. 289, 109.

Walker R. C. et al. 1984, in VLBI and Compact Radio Sources (IAU Symposium 110, eds. R. Fanti, K. Kellermann, and G. Setti) p.121.

Wittels, J. J. et al. 1976, A.J. 81, 933.

Table 1. Details of antenna arrays used in observations.

Epoch	Frequency (GHz)	Antennas (1)	Beam Shape (2,mas)	λ/2D(min) (3,mas)	f (4)	p (5)
1979.25	4.996	BGFOH	0.9x1.7	14	.23	3
1979.44	10.651	BKGFO	0.4x0.8	11	.28	3
1979.92	5.009	BKGFO	0.9x1.7	22	.30	2
1980.52	10.651	BKGFO	0.4x0.8	4	.32	1
1980.73	5.009	BKFO	0.9x1.7	8	.28	2
1981.09	10.651	BKGFO	0.4x0.8	8	.34	1
1981.25	22.231	BKGCYO	0.25x0.40	5	.42	2
1981.63	4.989	BKGFO	0.9x1.7	22	.37	3
1981.89	2.292	SJMGFAOH	2.6x2.1	45	.55	1
1982.09	10.651	BKGCFO	0.4x0.8	16	.43	1
1982.38	89.026	PLD	-------	.7	.01	—
1982.42	22.231	RSKGYO	0.25x0.40	4	.53	3
1982.56	4.990	BKGFO	0.9x1.7	14	.41	.5
1982.86	10.651	BFO	-------	2	.11	—
1983.09	22.231	BSKGYO	0.25x0.40	3	.59	1
1983.10	10.651	BKGFOH	0.4x0.8	12	.45	.5
1983.57	4.990	BKGIFYOH	0.9x1.7	25	.50	.1
1983.76	22.231	BSKGYO	0.25x0.40	4	.58	1
1984.09	22.231	BSKGNO	0.25x0.40	13	.47	1
1984.11	10.651	BKGFOH	0.4x0.8	10	.50	.5

Table 1 (continued).

(1) Antenna definitions:
B=Bonn 100m
C=Algonquin 50m
D=Hat Creek 6m (millimeter dish)
F=Fort Davis 26m
G=NRAO Greenbank 43m
H=Hat Creek 26m
I=Iowa 18m
J=Jodrell Bank 76m
K=Haystack 37m
L=OVRO 10m
M=Madrid 64m
N=NRL Maryland Point 26m
O=OVRO 40m
P=Kitt Peak 11m
R=Crimea 22m
S=Onsala 20m
Y=VLA 25m

(2) Shape of central component of dirty beam assuming uniform weighting of data points in (u,v) plane. Note that a circular beam was actually used for the maps we display.

(3) $\lambda/2D$ for shortest baseline.

(4) f=fraction of cells in gridded (u,v) plane which contain data. A filled aperture would have f=1. See text.

(5) p=percent of peak intensity level at which weak features in the map become unreliable.

Table 2. Results of fitting optically thin spheres to data. Quoted uncertainties are 1.0 sigma.

Epoch	ν (GHz)	Component Name	Flux (Jy)	r (MAS)	P.A. (degrees)	Diameter (MAS)
1979.25	5.0	D	4.3 +/-.3	0	---	1.5 +/-.2
		C3	2.3 +/-.2	1.19 +/-.04	-80 +/-3	0.9 +.2 -.4
		C2	0.9 +/-.2	3.64 +/-.15	-72 +/-2	1.4 +.2 -.6
1979.44	10.7	D	4.45 +.18 -.45	0	---	0.52 +.04 -.07
		C3.5	1.43 +.65 -.13	0.54 +/-.02	-104 +/-3	0.64 +.26 -.12
		C3	1.95 +/-.13	1.40 +/-.02	-89.1 +/-.9	0.85 +/-.05
		C2	0.7 +1.0 -.1	4.2 +/-.3	-76 +/-6	1.4 +1.2 -.2
1979.92	5.0	D	2.66 +/-.14	0	---	1.14 +/-.16
		C3	2.62 +/-.14	1.24 +/-.02	-85.7 +/-1.2	0.99 +/-.14
		C2	1.20 +/-.12	3.98 +/-.10	-74.3 +/-1.1	1.72 +/-.17

1980.52	10.7	D	4.4 +.4 -1.4	0	---	0.24 +.23 -0.09
		C4	3.4 +1.3 -.4	0.25 +/-.02	-135 +/-4	0.32 +.04 -.13
		C3.5	0.86 +.15 -.10	1.04 +/-.06	-97 +/-4	0.98 +/-.12
		C3	1.02 +/-.11	1.80 +/-.04	-87.4 +/-.8	0.79 +.06 -.09
		C2	0.80 +.18 -.13	4.28 +/-.10	-74 +/-2	2.0 +1.2 -.2
1980.73	5.0	D	4.28 +/-.08	0	---	1.10 +/-.05
		C3	2.25 +/-.10	1.59 +/-.02	-81.6 +/-.7	1.30 +/-.08
		C2	0.87 +/-.08	4.37 +/-.07	-73.0 +/-.8	1.7 +/-.2
1981.09	10.7	D	6.6 +.5 -.4	0	---	0.06 +.06 -.02
		C4	3.6 +.3 -.4	0.325 +/-.014	-131 +/-2	0.20 +/-.09
		C3.5	0.52 +.23 -.13	1.15 +/-.11	-108 +/-9	0.8 +/-.4
		C3	1.11 +/-.26	2.00 +/-.11	-84 +/-2	1.17 +.36 -.16
		C2	1.0 +1.0 -.2	4.6 +/-.4	-72 +/-4	2.8 +1.9 -.3

1981.25	22.2	D	9.8 +/-.2	0	---	0.14 +/-.02
		C4	3.22 +/-.16	0.377 +/-.004	-126.5 +/-1.2	0.26 +/-.03
		C3.5	0.3 +/-.1	1.11 +/-.10	-99 +/-5	0.3 +.2 -.1
		C3	0.55 +/-.13	1.95 +/-.16	-86 +/-4	0.8 +/-.2
1981.63	5.0	D	6.57 +/-.08	0	---	1.08 +/-.05
		C3	1.99 +/-.07	1.76 +/-.02	-82.9 +/-.8	1.63 +/-.08
		C2	1.33 +/-.13	4.61 +/-.05	-71.3 +/-.7	2.8 +/-.2
1981.89	2.3	D	1.54 +.25 -.15	0	---	1.6 +.3 -.6
		C3	2.42 +.17 -.25	1.70 +/-.04	-78.9 +/-1.4	1.9 +.2 -.5
		C2	1.75 +.10 -.15	4.71 +/-.10	-70.4 +/-.9	2.7 +/-.2
		C1	.56 +.55 -.16	15.5 +1.3 -2.5	-64. +/-18	13. +6 -3

1982.09	10.7	D	6.6 +/-.3	0	---	0.16 +/-.06
		C4	6.4 +/-.3	0.352 +/-.002	-115.3 +/-.6	0.10 +/-.05
		C3.5	0.40 +/-.06	0.92 +/-.02	-106 +/-4	0.0 +.3
		C3	1.00 +.10 -.17	2.18 +/-.06	-88.3 +/-1.8	1.12 +/-.13
		C2	0.79 +.27 -.12	5.12 +/-.31	-74 +/-3	2.3 +.9 -.3
1982.38	89.0	D	6 +/-5	0	---	0.28 +.14 -.28
		C4	6 +/-4	0.48 +.12 -.47	-110 +/-5	0.46 +.17 -.46
1982.42	22.2	D	6.8 +.2 -.4	0	---	0.52 +/-.02
		C4	7.5 +.4 -.1	0.410 +/-.008	-107.1 +/-.8	0.35 +/-.02
1982.56	5.0	D	8.00 +/-.15	0	---	0.90 +/-.05
		C3	1.59 +/-.16	2.00 +/-.08	-81 +/-2	1.6 +/-.2
		C2	1.08 +/-.20	5.09 +/-.16	-73 +/-2	2.2 +/-.4

1982.86	10.7	D	4.6 +.7 -.5	0	---	0.20 +.14 -.08
		C4	8.1 +1.0 -.7	0.47 +/-.01	-100 +/-2	0.30 +.08 -.12
1983.09	22.2	D	5.6 +.2 -.6	0	---	0.35 +.01 -.04
		C5	1.7 +.6 -.2	0.25 +/-.02	-79 +/-4	0.28 +/-.10
		C4	5.9 +/-.3	0.618 +/-.006	-93.8 +/-.7	0.31 +/-.02
1983.10	10.7	D	5.46 +.22 -.41	0	---	0.42 +.04 -.17
		C4	6.95 +/-.28	0.528 +/-.004	-94.5 +/-.7	0.41 +.04 -.16
		C3.5	0.38 +.18 -.14	1.3 +/-.3	-84 +/-8	1.0 +.3 -.4
		C3	0.67 +/-.17	2.53 +/-.09	-87 +/-2	0.85 +.16 -.34
		C2	1.2 +.9 -.2	5.3 +/-.5	-75 +/-5	2.9 +1.5 -.5

1983.57	5.0	D	4.55 +.19 -.71	0	---	0.71 +.06 -.12
		C4	3.6 +.5 -.2	0.544 +/-.008	-85.5 +/-1.6	0.0 +.2
		C3	1.37 +/-.06	2.43 +/-.04	-81.6 +/-.9	1.63 +/-.09
		C2	1.09 +/-.07	5.71 +/-.06	-71.2 +/-.7	2.28 +/-.14
1983.76	22.2	D	5.4 +.3 -.6	0	---	0.36 +.02 -.03
		C5	2.8 +/-.4	0.239 +/-.012	-91 +/-3	0.36 +.03 -.05
		C4	5.0 +/-.2	0.858 +/-.008	-87.6 +/-.6	0.33 +/-.01
1984.09	22.2	D	6.7 +/-.4	0	---	0.41 +/-.02
		C5	1.3 +/-.4	0.27 +/-.03	-94 +/-6	0.36 +.06 -.14
		C4	5.2 +/-.3	0.864 +/-.016	-86.7 +/-.8	0.48 +/-.02

1984.11	10.7	D	5.4 +/-.2	0	---	0.53 +.03 -.06
		C5	1.40 +.28 -.12	0.44 +/-.04	-96 +/-4	0.0 +.2
		C4	5.75 +.18 -.52	0.810 +/-.008	-86.6 +/-.4	0.51 +.02 -.07
		C3	0.54 +/-.08	2.86 +/-.08	-84 +/-2	1.1 +/-.2
		C2	0.65 +.56 -.16	5.9 +/-.4	-72 +/-4	2.8 +4.0 -.5

Table 3. Parameters describing positions and proper motions of C1, C2, C3, and C4 relative to D. Values in () are extrapolations based on dr/dt at a different frequency.

Component	ν (GHz)	Epochs Used	t_o	$r(t_o)$ (mas)	dr/dt (mas/yr)	$d\vec{r}/dt$ Magnitude (mas/yr)	$d\vec{r}/dt$ Direction P.A. (deg)	d^2r/dt^2 (mas/yr^2)	P.A.(t_o) (deg)	d(P.A.)/dt (deg/yr)
C1	2.3	1981.89	1981.89	15.5±1.9	---	---	---	---	-64±18	---
C2	2.3	1981.89	1982	(4.76±.10)	---	---	---	---	-70.4±.9	---
	5.0	all	1982	4.89±.03	.48±.02	.48±.02	-66.7±2.5	.08±.11	-71.9±.4	.59±.28
	10.7	all	1982	4.94±.13	.41±.09	.41±.09	-68 ±7	.23±.36	-73.5±1.5	.4±1.0
C3	2.3	1981.89	1982	(1.73±.04)	---	---	---	---	-78.9±1.4	---
	5.0	all	1982	1.91±.02	.297±.010	.298±.010	-78.7±2.3	.01±.04	-82.2±.4	.45±.33
	10.7	all	1982	2.21±.03	.311±.013	.312±.013	-81.5±2.8	-.03±.06	-86.5±.7	.82±.38
C4	5.0	1983.57	1983.5	(.524±.009)	---	---	---	---	-86.1±1.6	---
	10.7	1982.86-1984.11	1983.5	.640±.004	.277±.008	.295±.009	-71.7±1.5	---	-91.6±.4	8.3±.7
	22.2	1983.09-1984.09	1983.5	.751±.005	.312±.012	.330±.013	-71.3±2.2	---	-90.3±.4	7.7±.1.0
C4	10.7	1981.09,1982.09	1982	.350±.002	.027±.014	.096±.018	-49 ±7	---	-116.7±.6	15.7±2.1
	22.2	1981.25,1982.42	1982	.398±.005	.028±.008	.066±.012	-49.4±3.2	---	-114.1±.7	16.6±1.2

Table 4. Frequency dependent shifts in component positions $r(t, \nu) - r(t, 10.7\ \text{GHz})$ in mas.

Component	t	Frequency (GHz) 2.3	5.0	10.7	22.2
C2	1982	$-.18 \pm .16$	$-.05 \pm .13$	0	---
C3	1982	$-.48 \pm .05$	$-.30 \pm .04$	0	---
C4	1982	---	---	0	$+.048 \pm .005$
	1983.5	---	$-.12 \pm .01$	0	$+.111 \pm .007$

Table 5. Results of fitting exponential light curves to observed component fluxes. Fluxes for epoch 1982.0 and time scales for variation by factor e are given. All quantities are in the observer's frame of reference.

Component	Epochs Used	Frequency (GHz)	S(1982.0) (Jy)	τ (years)
C2	79.25-83.57	5.0	1.09±0.04	<-15 >11
	79.44-84.11	10.7	0.83±0.14	<-3 >3
C3	77.95-83.57	5.0	1.82±0.04	-6.6±0.5
	77.60-84.11	10.7	0.93±0.06	-4.3±0.5
C3.5	79.44-83.10	10.7	0.44±0.05	-2.3±0.4
C4	80.52-82.86	10.7	5.96±0.24	2.2±0.3
	77.9 -82.42	22.2	5.59±0.16	1.53±0.10
	82.86-84.11	10.7	8.90±0.91	-4.8±1.2
	82.42-84.09	22.2	8.22±0.36	-3.8±0.4

Table 6. Spectral indices of componets C4, D+C5, and D+C5+C4. Spectral index is defined as $\alpha = d(\ln S)/d(\ln \nu)$. Values for frequencies at or above 10.7 GHz are for epochs with near simultaneous observations. Below 10.7 GHz linear interpolation was used for the higher of the two frequencies. For components where spectral index variations were seen, the range of variation is given.

Component	Frequecies (GHz)	Epoch	α
C4	2.3, 10.7	1981.99	>0.93+0.08
	5.0, 10.7	1983.57	0.75+0.19
	10.7, 22.2	1981.17 to 1984.10	-0.30+0.04 to -0.14+0.13
	22.2, 89.0	1982.40	-0.2 +0.4/-0.8
D+C5+C4	2.3, 5.0	1981.89	1.95+0.13
	5.0, 10.7	1977.90 to 1983.57	0.03+0.18 1.05+0.12
D+C5	5.0, 10.7	1983.57	0.39+0.15
	10.7, 22.2	1981.25 to 1984.10	0.54+0.10 to 0.22+0.11
	22.2, 89.0	1982.40	-0.1 +0.4
D	10.7, 22.2	1984.10	0.30+0.10

Table 7. Expansion rates da/dt for components, and sizes a(1982.0) for epoch 1982.0. All measurements are in the observer's frame of reference.

Component	Frequecy (GHz)	da/dt (mas/year)	a(1982.0) (mas)
C2	5.0	0.17±0.05	2.15±0.08
	10.7	0.34±0.26	2.4 ±0.4
C3	5.0	0.15±0.03	1.50±0.05
	10.7	0.06±0.03	0.97±0.07
C4	10.7	0.10±0.02	0.25±0.03
	22.2	0.04±0.01	0.29±0.02

Table 8. Mean diameters of component D. Values in () are for a single epoch.

Frequecy (GHz)	Mean Diameter (mas)	Dispersion About Mean (mas)
2.3	(1.6)	---
5.0	1.07	0.26
10.7	0.30	0.19
22.2	0.36	0.14
89.0	(0.28)	---

Figure Captions.

Figure 1. Contour plot model and map for 1984.11 epoch at 10.7 GHz. Contours are at ±.1, ±.2, ±.5, ±1, ±2, ±3, ±5, ±10, ±20, ±35, ±50, ±70, and ±90 percent of the peak intensity. Shaded regions show FWHM of Gaussian convolving beam.
(a.) Model with no beam convolution.
(b.) Model convolved with 0.6 mas FWHM Gaussian function.
(c.) Map with 0.6 mas FWHM Gaussian CLEAN restoring beam.

Figure 2. Contour plots of hybrid maps. North is at top and East is at left. Contours are at ±.05, ±.1, ±.2, ±.3, ±.5, ±1, ±2, ±3, ±5, ±10, ±20, ±35, ±50, ±70, and ±90 percent of the peak intensity. In most cases some of the lower contours have been omitted for clarity. Shaded areas represent FWHM of Gaussain CLEAN restoring beam.

(a.) 2.3 GHz map. Tick marks are at 4.8 mas spacing. Lowest contour is ±1 percent. Beam FWHM is 2.4 mas.

(b.) 5.0 GHz maps. Tick marks are at 2.4 mas spacing. Lowest contours are ±1 percent except for: 1979.25 which is ±2 percent, 1982.57 which is ±0.3 percent, and 1983.57 which is ±0.05 percent. Beam FWHM is 1.2 mas.

(c.) 10.7 GHz maps. Tick marks are at 1.2 mas spacing. Lowest contours are ±0.5 percent except for 1979.44 which is ±1 percent. Beam FWHM is 0.6 mas.

(d.) 22.2 GHz maps. Tick marks are at 0.6 mas spacing. Lowest contours are ±0.5 percent except for: 1981.25 which is ±1 percent, and. 1982.42 which is ±2 percent. Beam FWHM is 0.3 mas.

Figure 3. Positions of the centroids of components C5, C4, C3, and C2 relative to component D. Approximate epochs are shown for a few 10.7 GHz data points.
(a.) Data for all components.
(b.) Enlargement of region near D.

Figure 4. Distance (r) of component centroid from component D vs. epoch.

(a.) Component C2. Lines fit to 5.0 and 10.7 GHz data have slopes of .48±.02 and .41±.09 mas/year, respectively.

(b.) Component C3. Lines fit to 5.0 and 10.7 GHz data have slopes of .297±.010 and .311±.013 mas/year respectively.

(c.) Component C4. Lines fit to 1981-1982 data have slopes of .027±.014 and .028±.008 mas/year respectively at 10.7 and 22.2 GHz. For 1983-1984 data the slopes are .277±.008 and .312±.012 mas/year respectively.

Figure 5. Fluxes of components vs. epoch. Lines have been drawn connecting data at the same frequency.
(a.) Component C2
(b.) Component C3
(c.) Component C4
(d.) Components D+C5
(e.) Components D+C5+C4

Figure 6. Fluxes components and total fluxes for epoch 1982.0.

Figure 7. Component diameters (a) plotted against distance from component D (r). The line is a fit to the 11 GHz data only, and has a slope 0.46 ± 0.03 which corresponds to a jet opening angle of 25.9° ± 1.6°.

Running title: Evolution of 3C345.

Author's address:
J. A. Biretta and R. L. Moore
105-24 Caltech
Pasadena, CA 91125

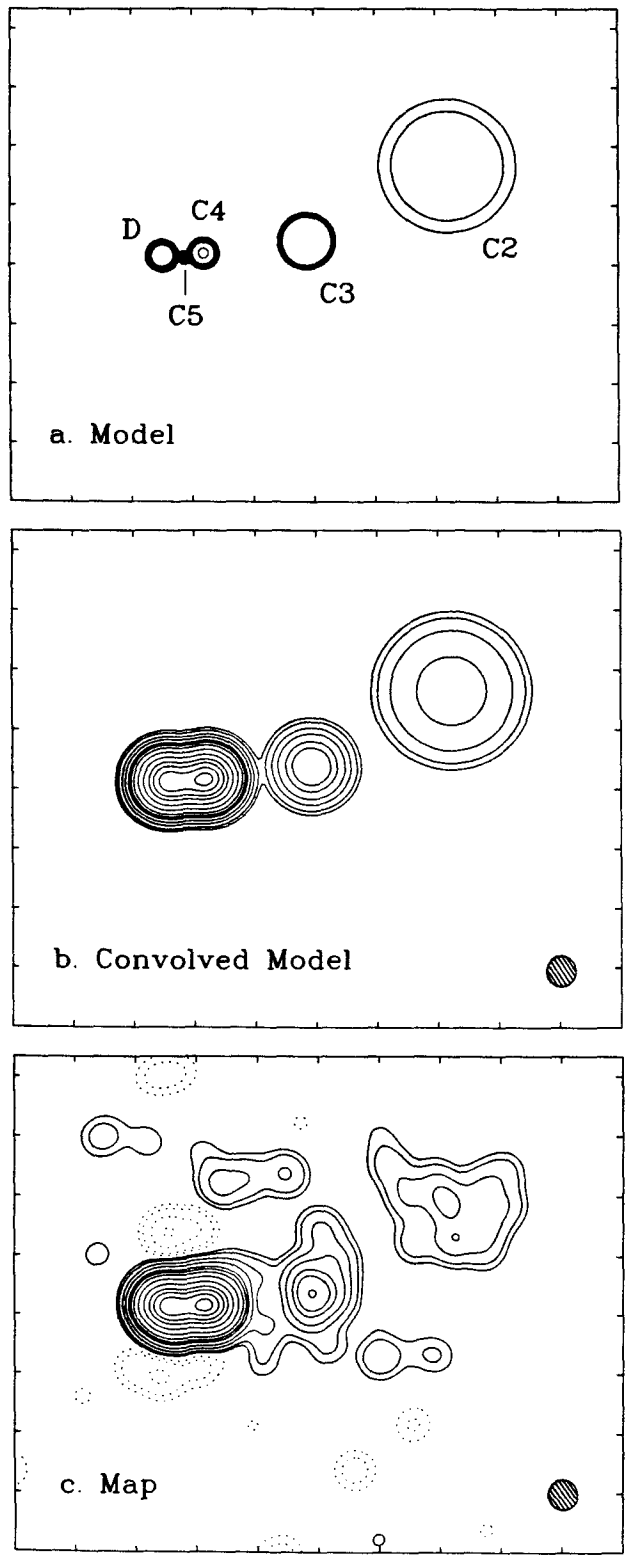

Figure 1.

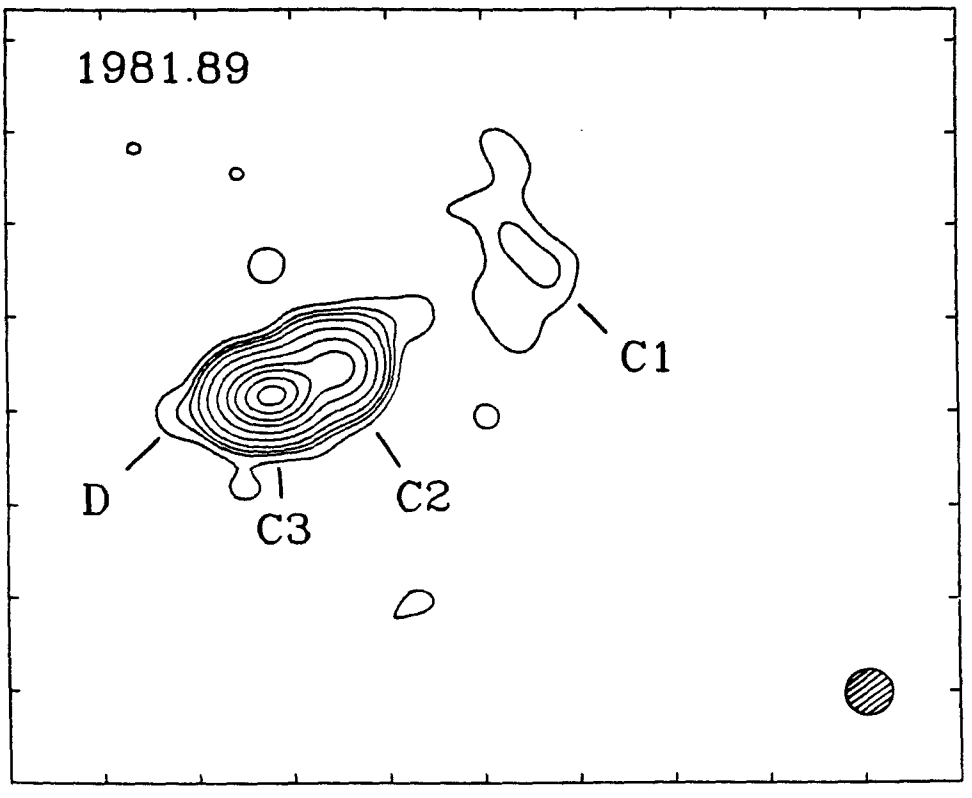

Figure 2a.

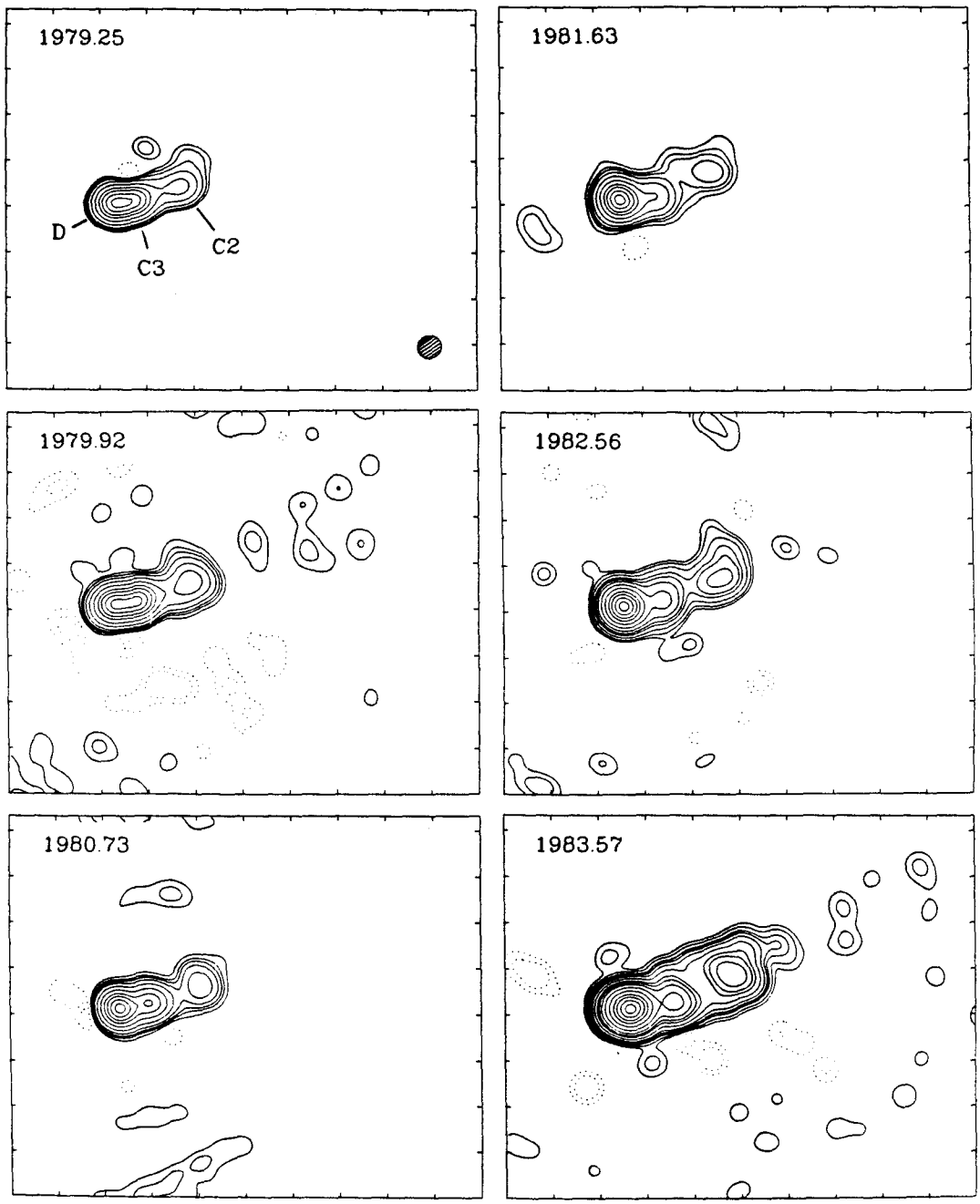

Figure 2b.

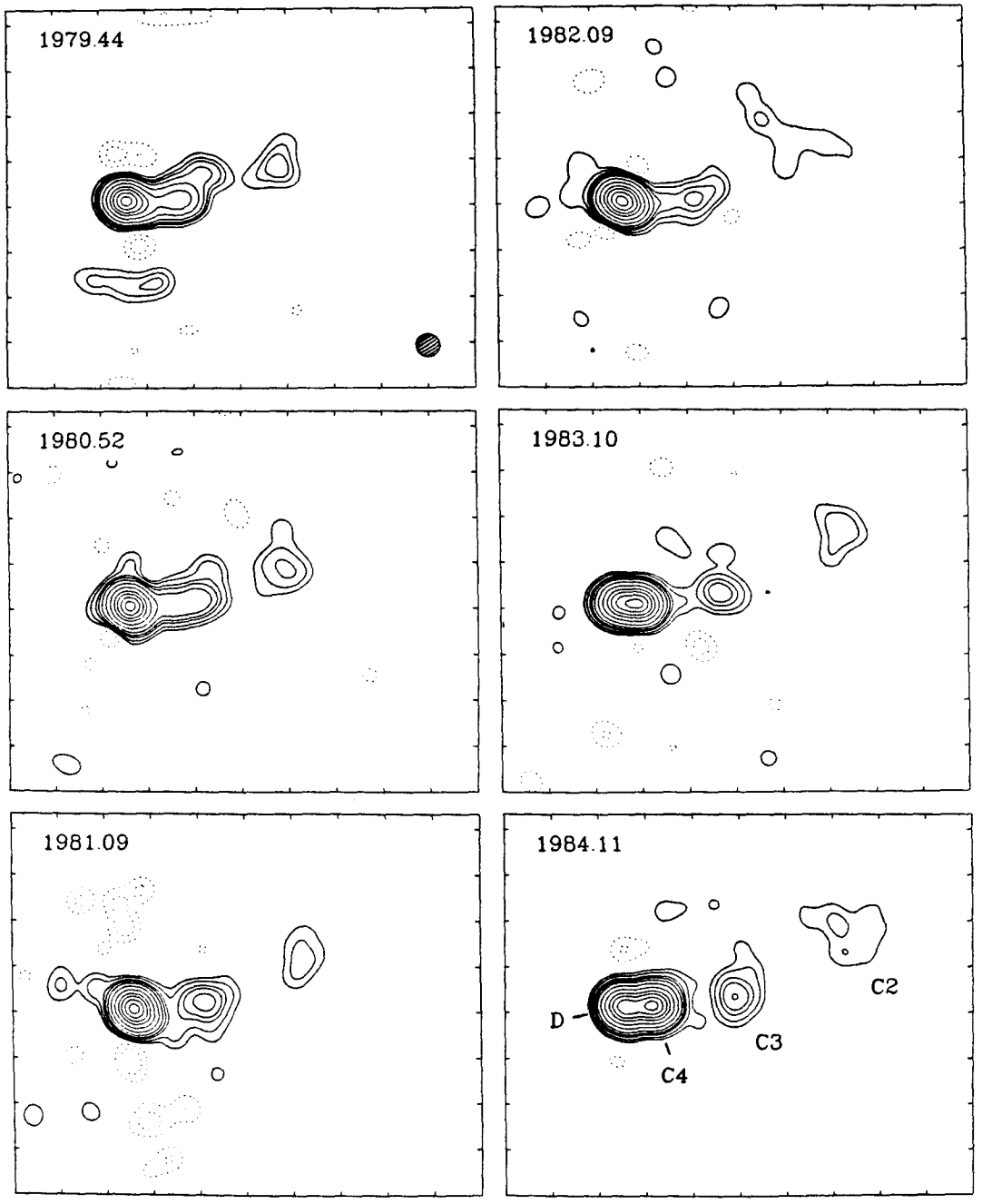

Figure 2c.

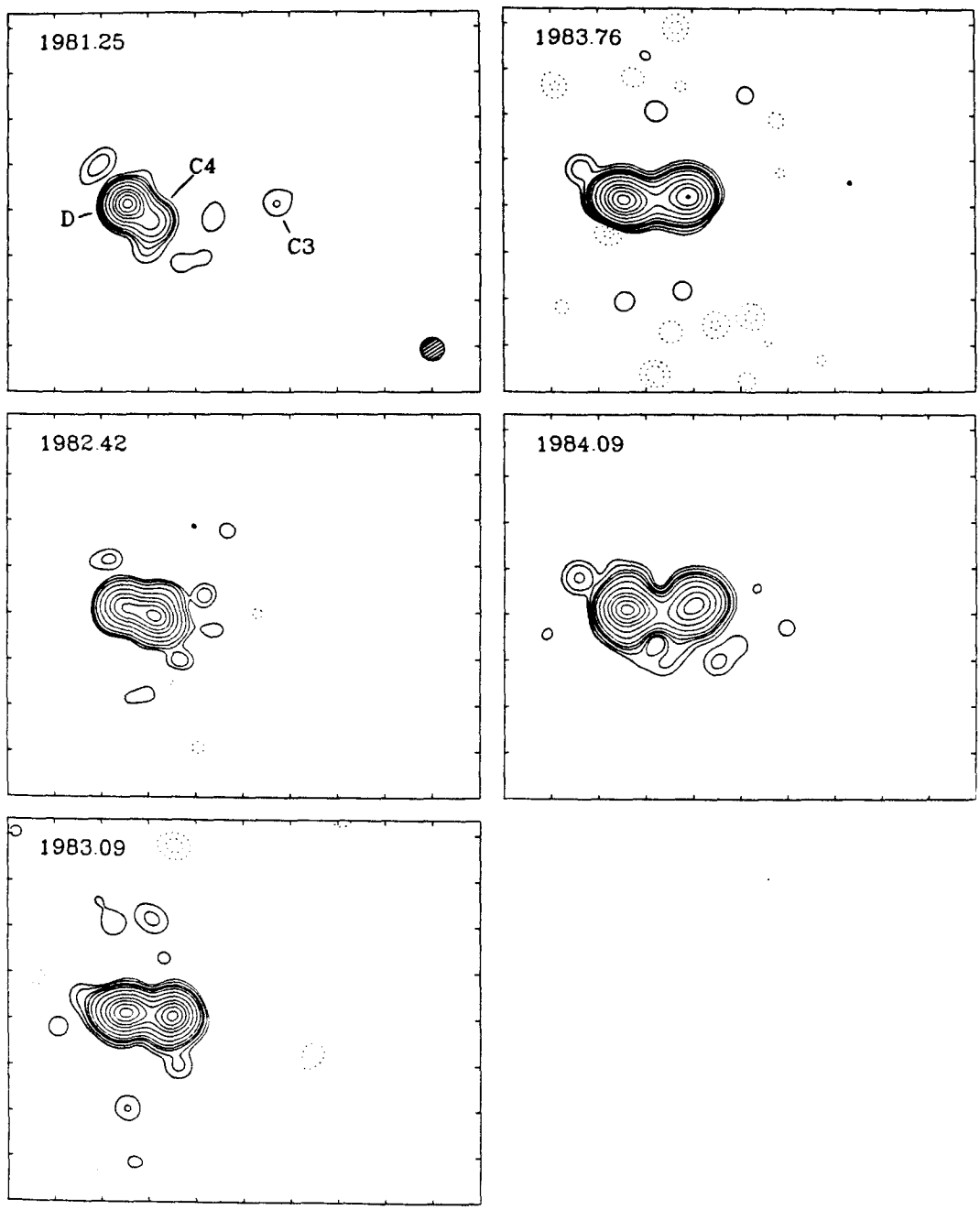

Figure 2d.

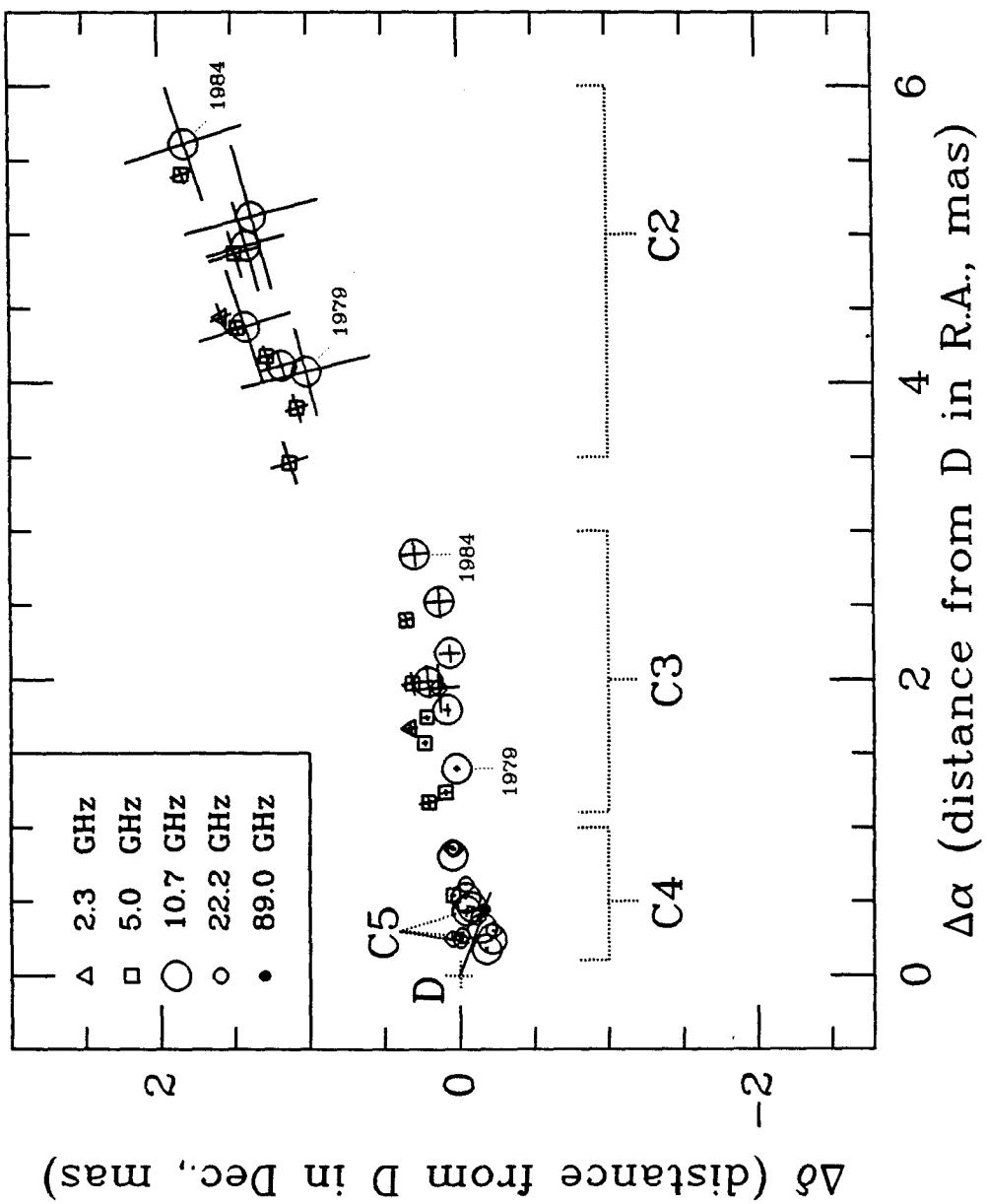
2.3 GHz
5.0 GHz
10.7 GHz
22.2 GHz
89.0 GHz
1984
1979
1984
1979
C5
D
C4
C3
C2
Δδ (distance from D in Dec., mas)
Δα (distance from D in R.A., mas)
2
0
−2
0
2
4
6

Figure 3a.

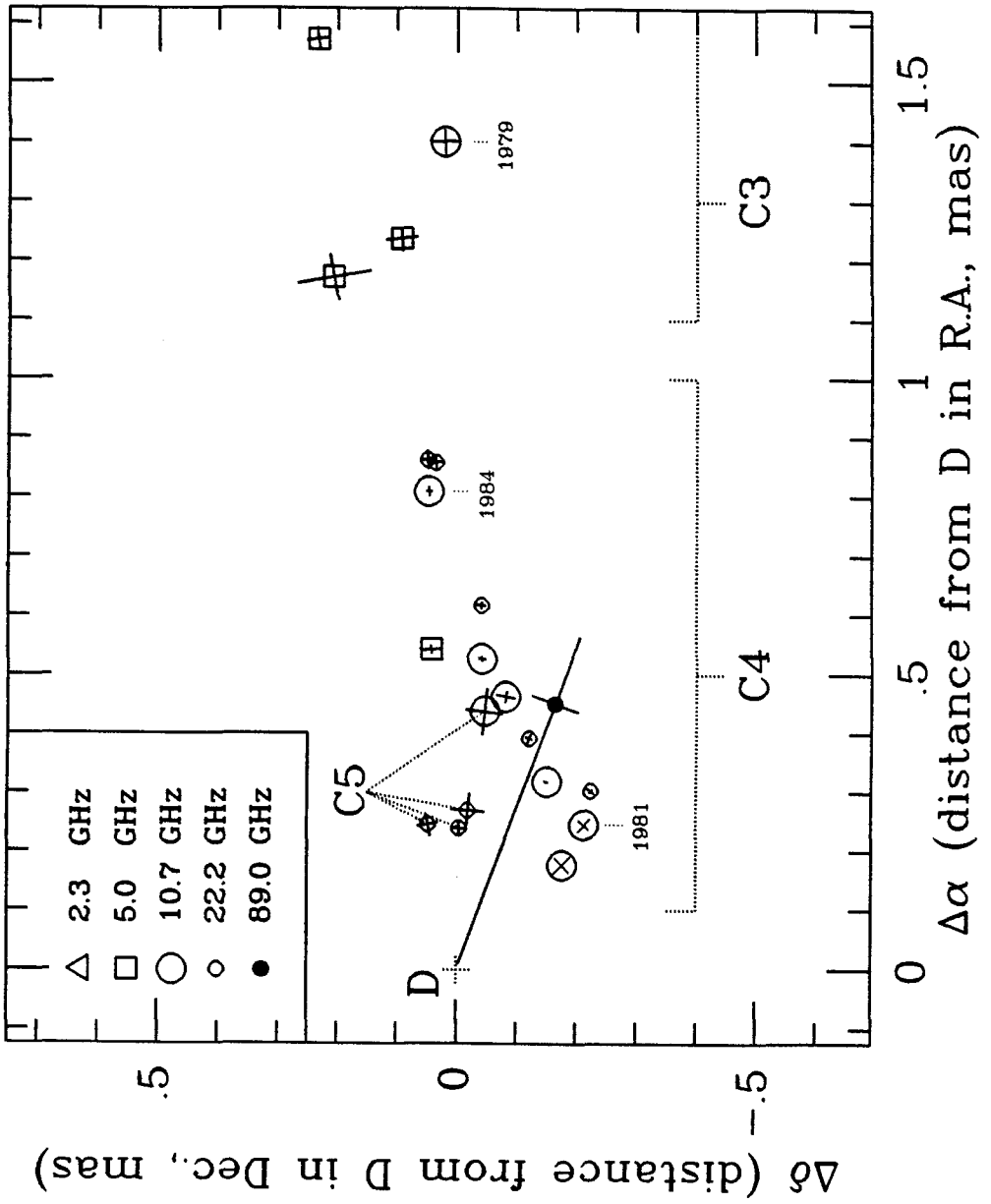
2.3 GHz
5.0 GHz
10.7 GHz
22.2 GHz
89.0 GHz
C5
D
1979
1984
1981
C3
C4
Δδ (distance from D in Dec., mas)
Δα (distance from D in R.A., mas)
.5
0
-.5
1
1.5

Figure 3b.

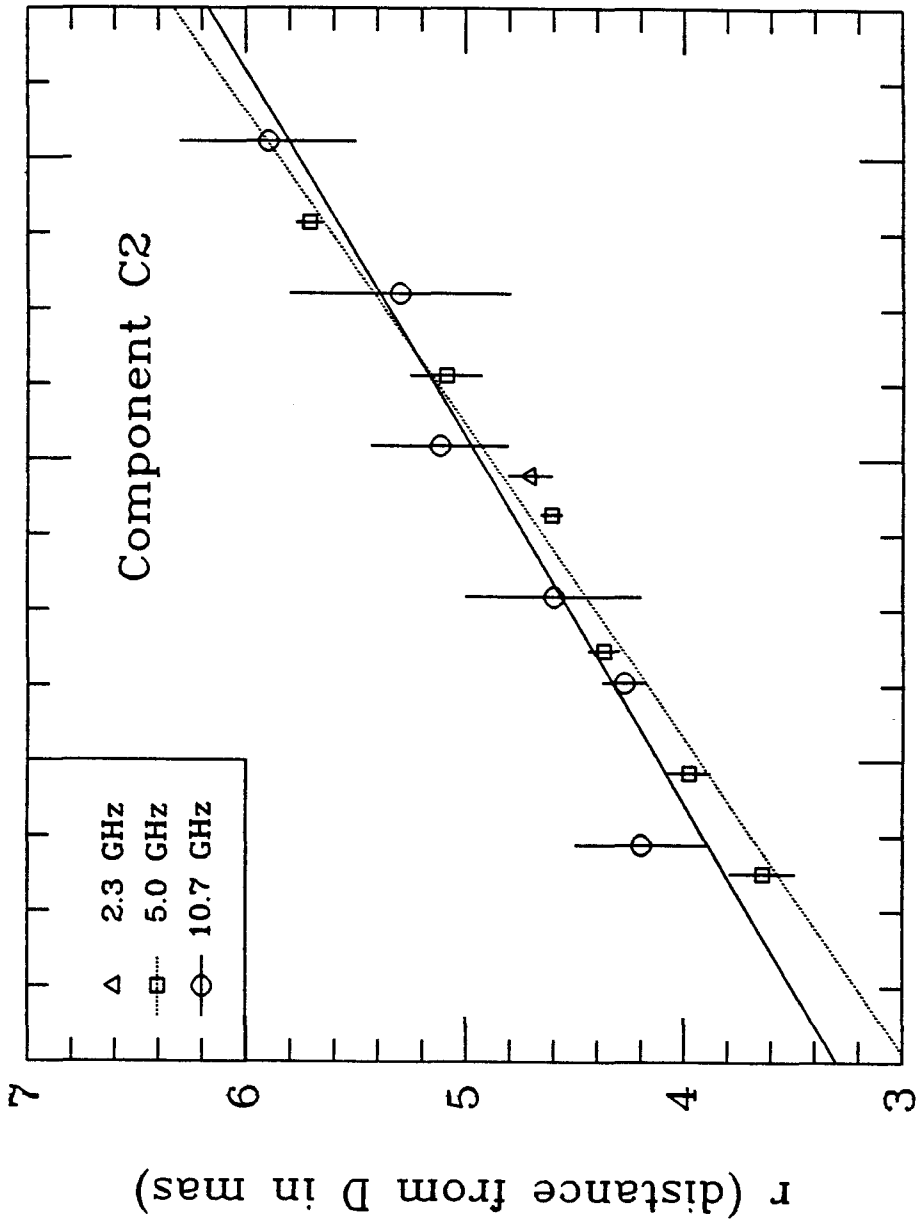
Component C2
2.3 GHz
5.0 GHz
10.7 GHz
r (distance from D in mas)
Epoch
1978
1980
1982
1984
3
4
5
6
7

Figure 4a.

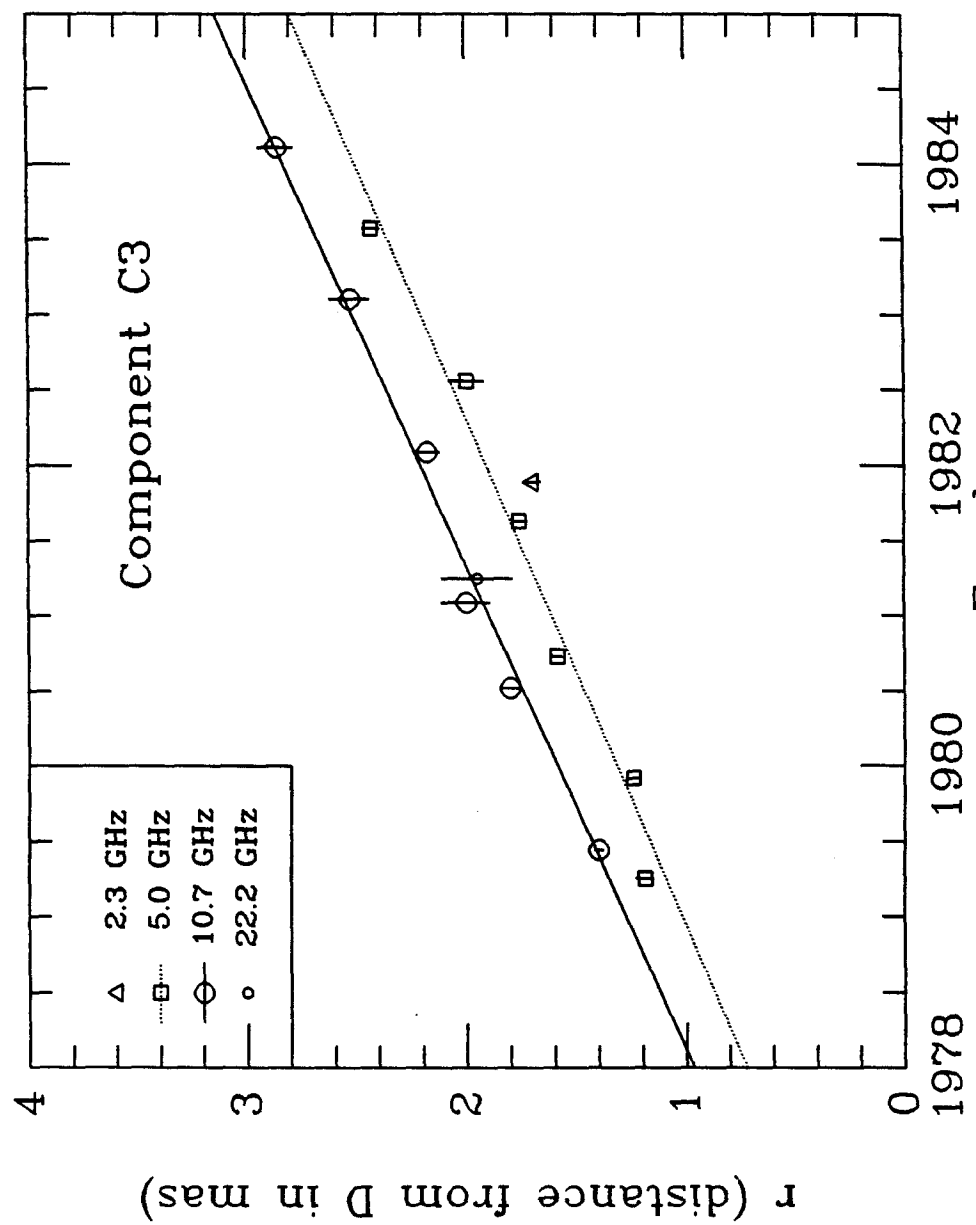
Component C3
2.3 GHz
5.0 GHz
10.7 GHz
22.2 GHz
r (distance from D in mas)
Epoch
1978
1980
1982
1984
0
1
2
3
4

Figure 4b.

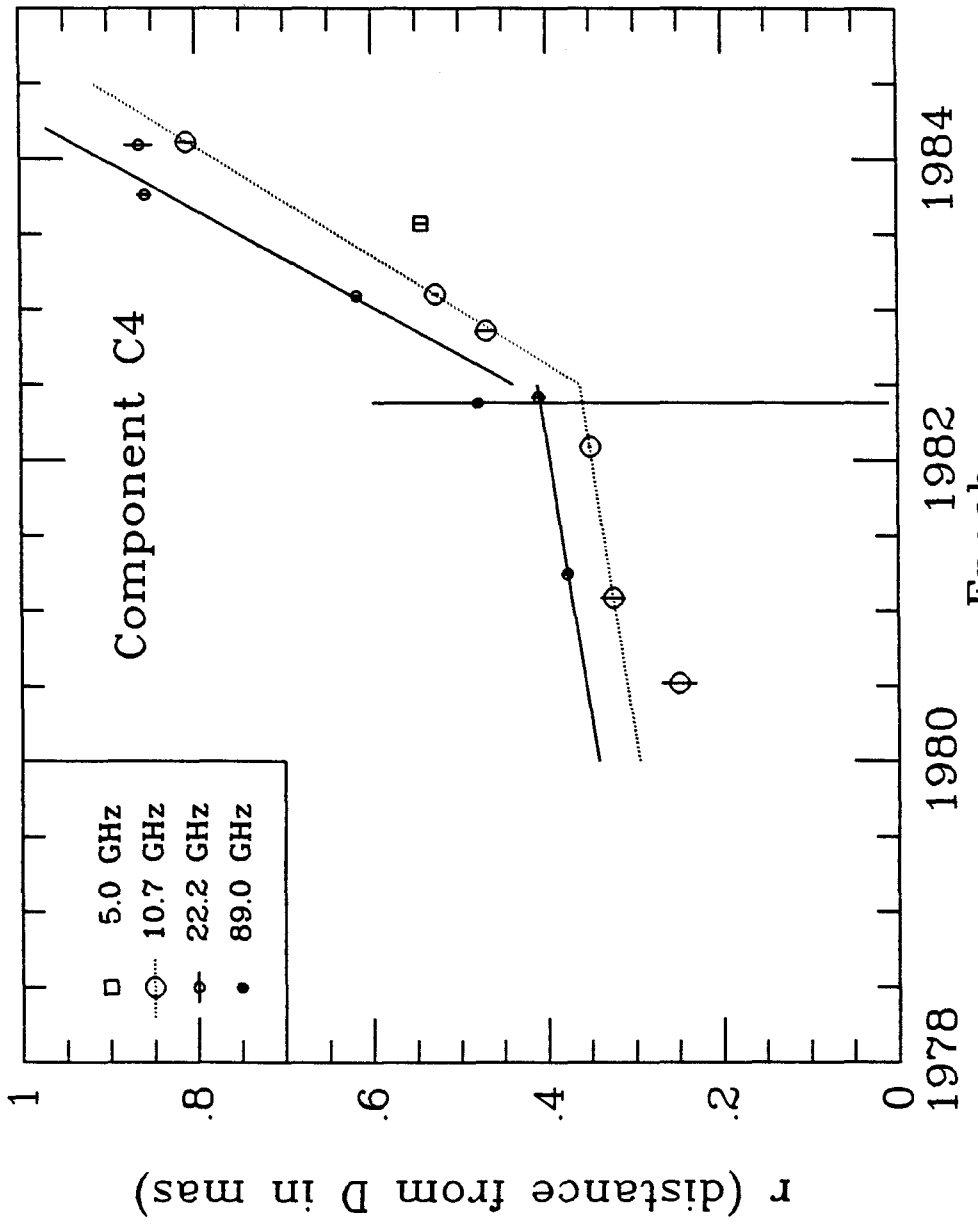
Component C4
5.0 GHz
10.7 GHz
22.2 GHz
89.0 GHz
r (distance from D in mas)
Epoch
0
.2
.4
.6
.8
1
1978
1980
1982
1984

Figure 4c.

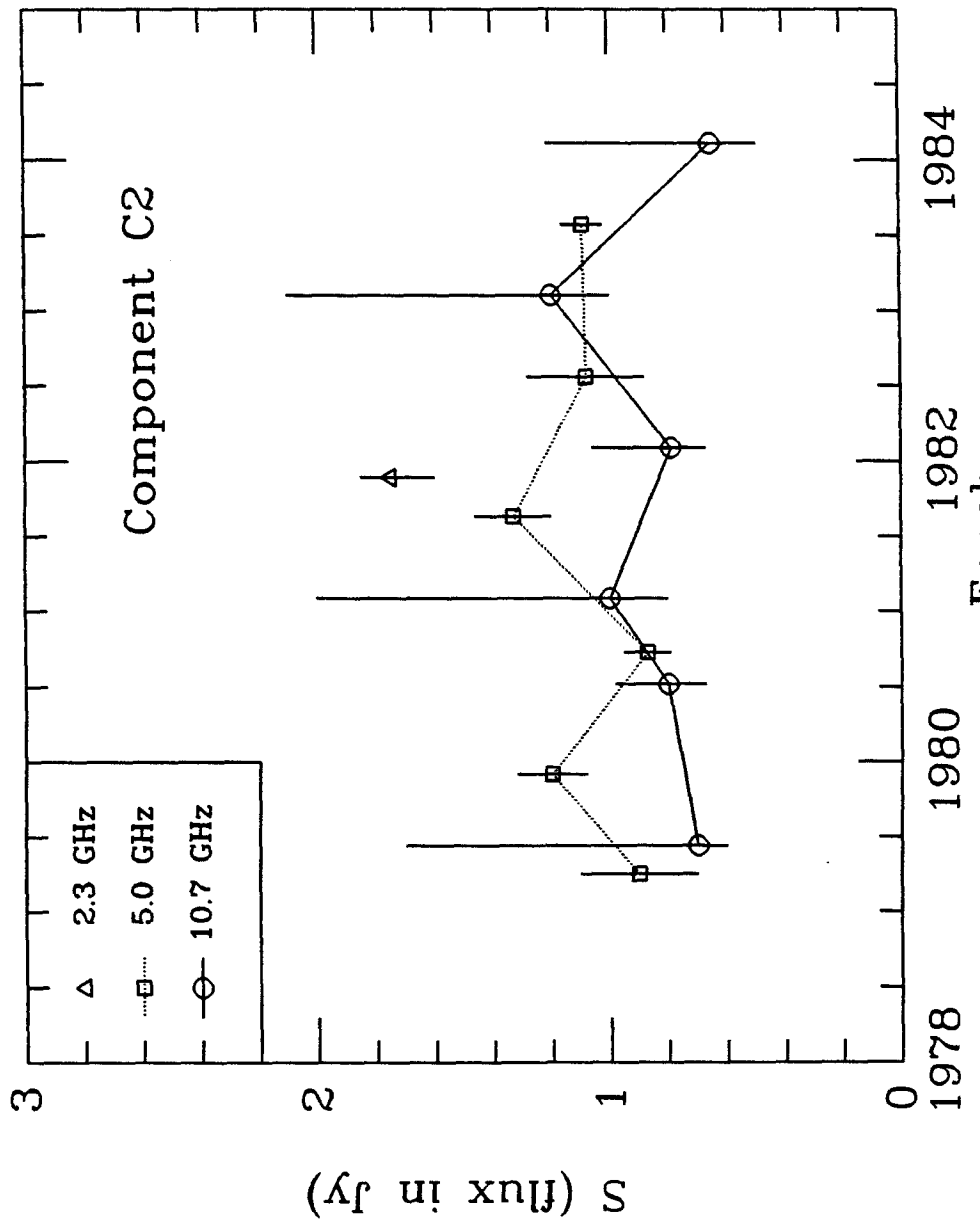
Component C2
2.3 GHz
5.0 GHz
10.7 GHz
S (flux in Jy)
Epoch
0
1
2
3
1978
1980
1982
1984

Figure 5a.

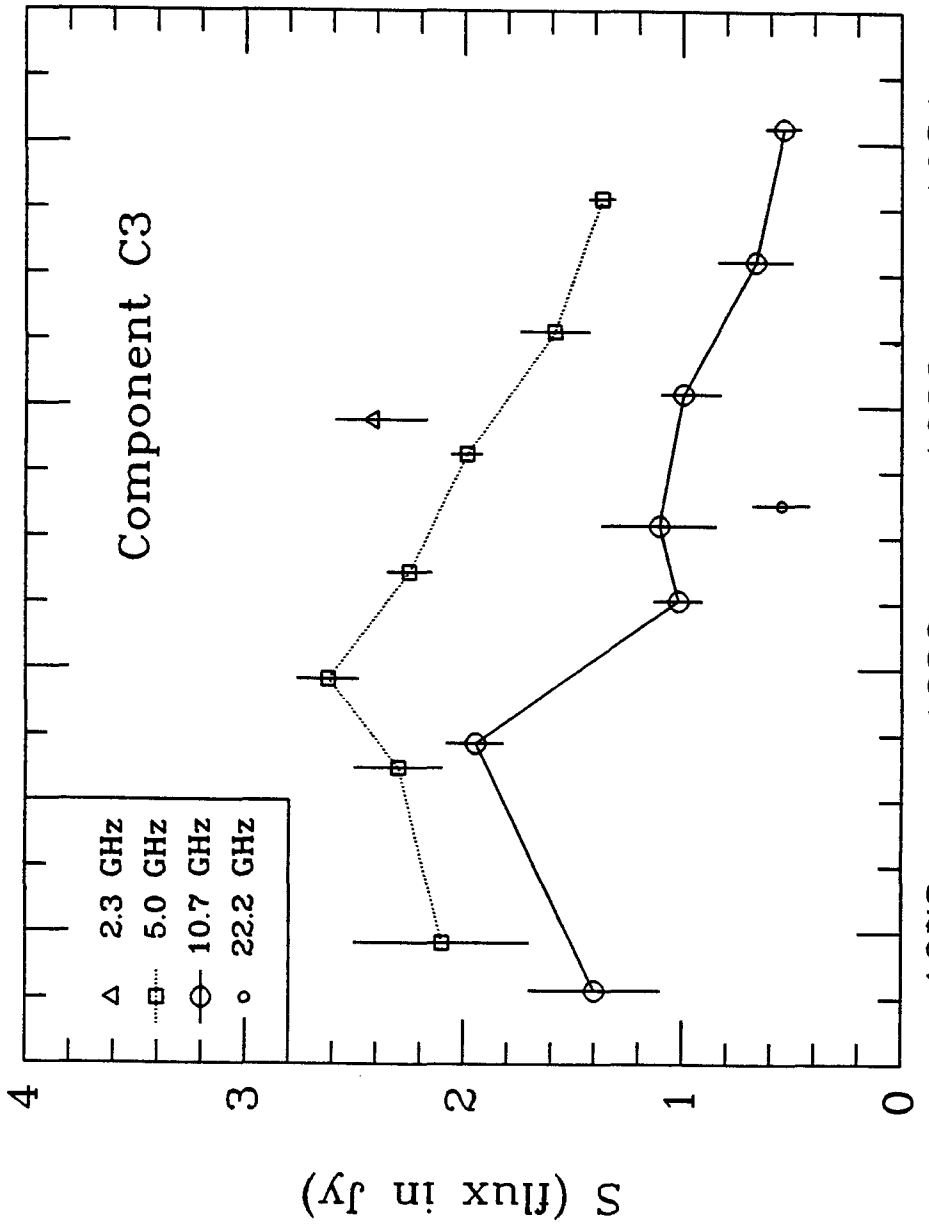
Component C3
2.3 GHz
5.0 GHz
10.7 GHz
22.2 GHz
S (flux in Jy)
Epoch
0
1
2
3
4
1978
1980
1982
1984

Figure 5b.

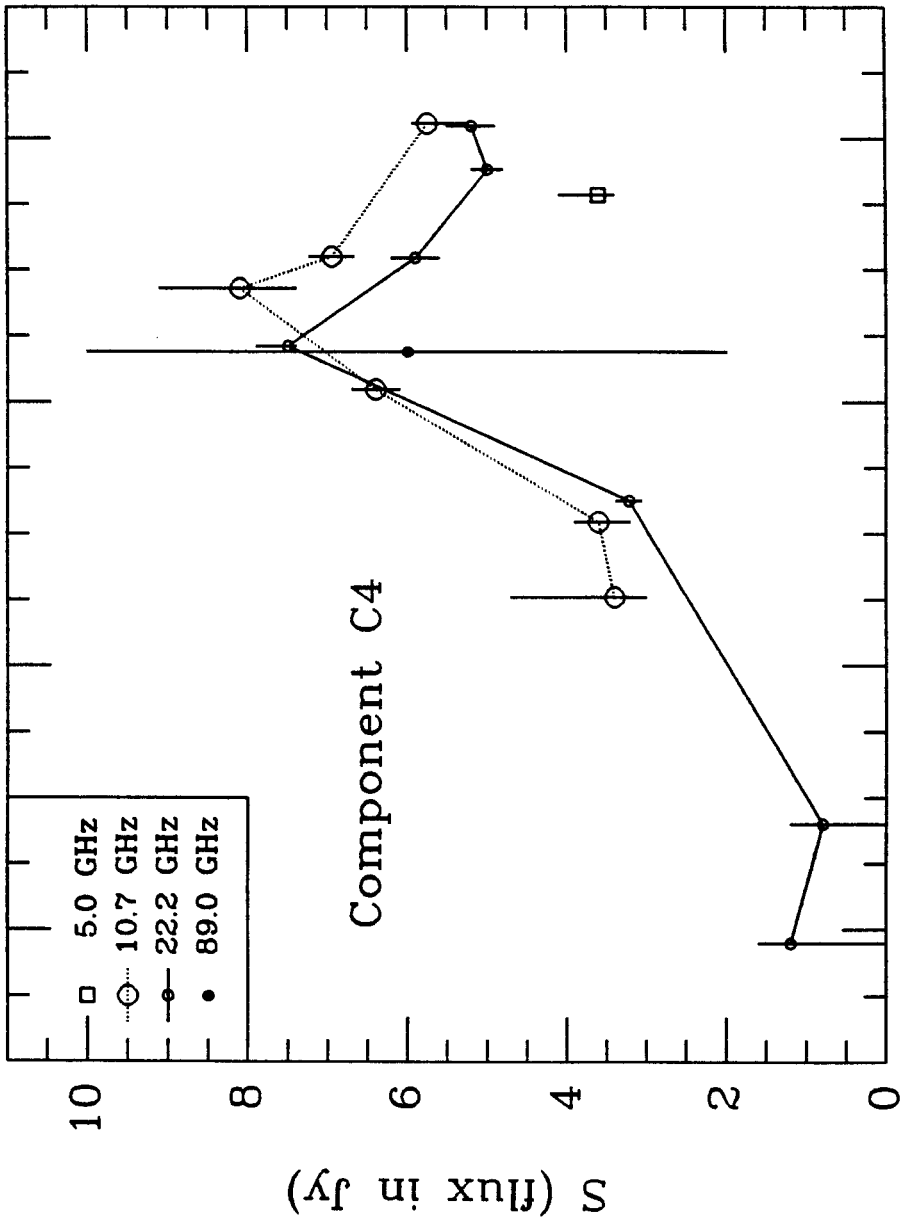
Component C4
5.0 GHz
10.7 GHz
22.2 GHz
89.0 GHz
S (flux in Jy)
Epoch
0
2
4
6
8
10
1978
1980
1982
1984

Figure 5c.

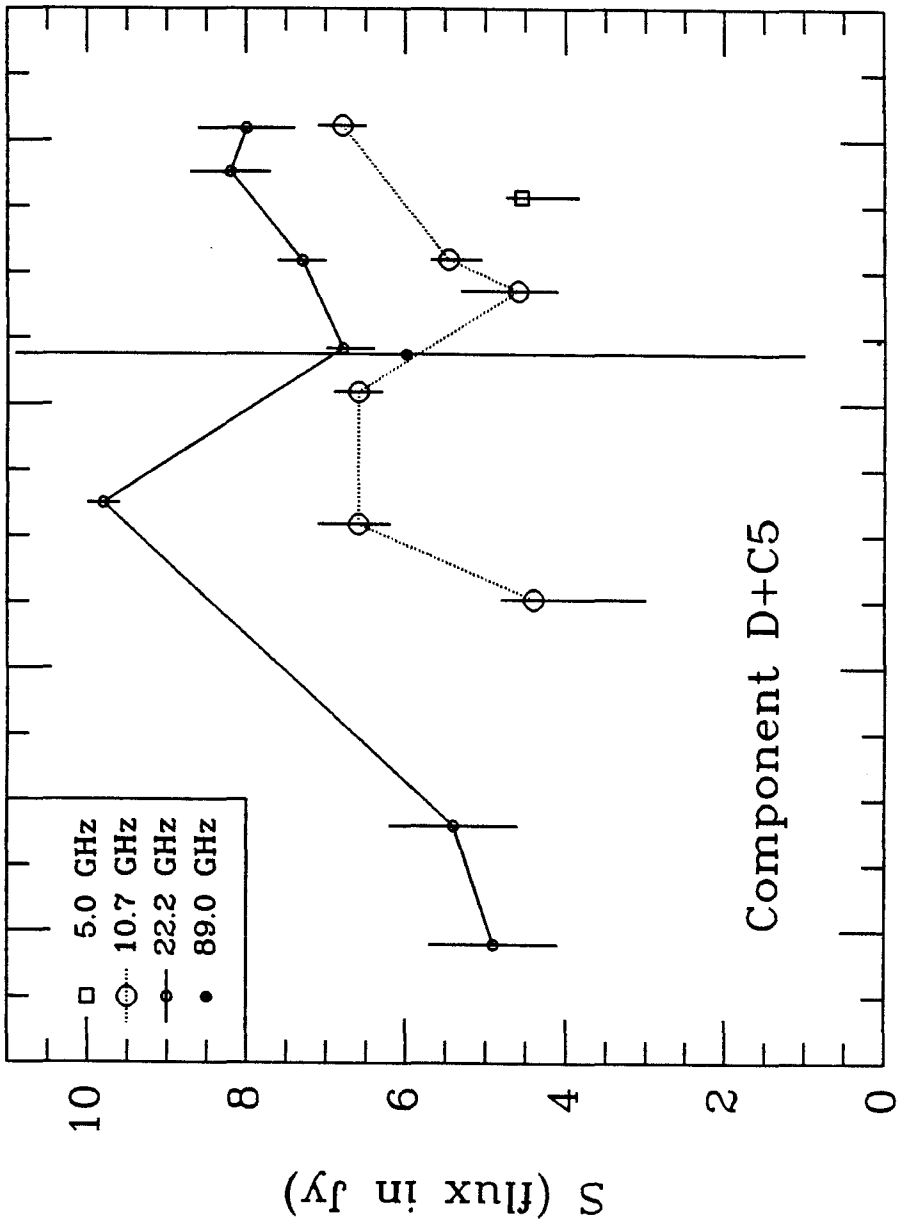
S (flux in Jy)
0
2
4
6
8
10
1978
1980
1982
1984
Epoch
Component D+C5
5.0 GHz
10.7 GHz
22.2 GHz
89.0 GHz

Figure 5d.

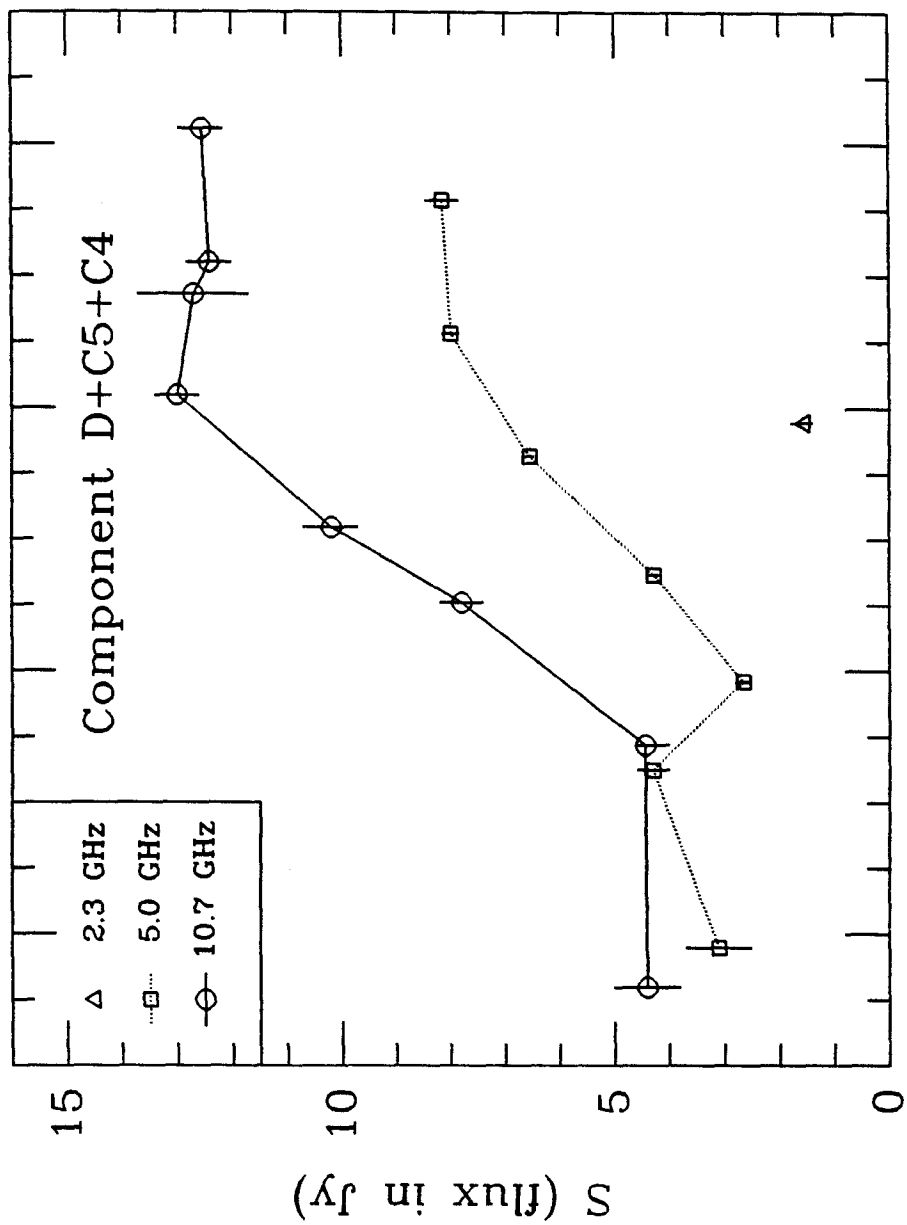
Component D+C5+C4
2.3 GHz
5.0 GHz
10.7 GHz
S (flux in Jy)
Epoch
0
5
10
15
1978
1980
1982
1984

Figure 5e.

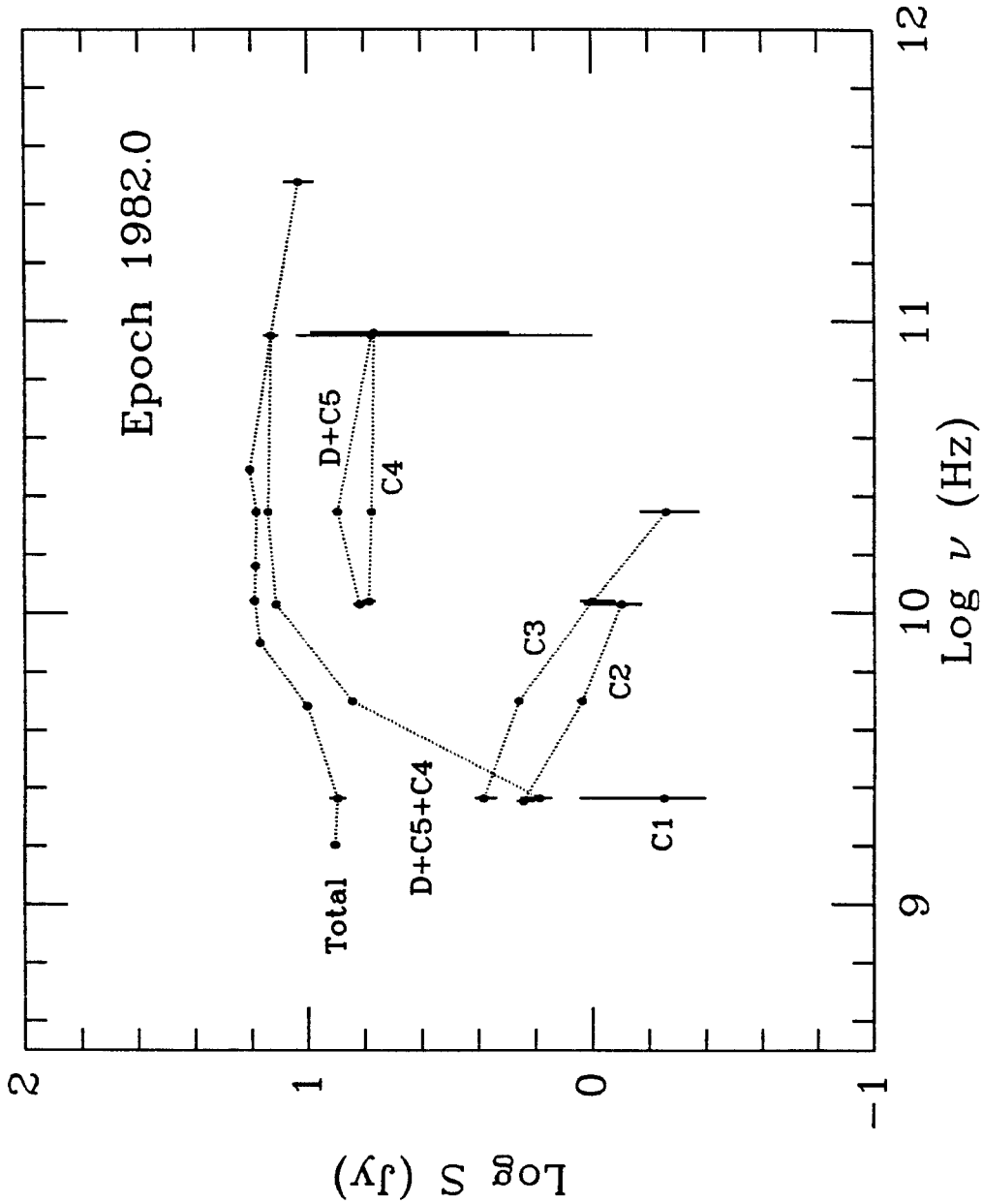
Epoch 1982.0
Log S (Jy)
Log ν (Hz)
2
1
0
−1
9
10
11
12
Total
D+C5+C4
D+C5
C4
C3
C2
C1

Figure 6.

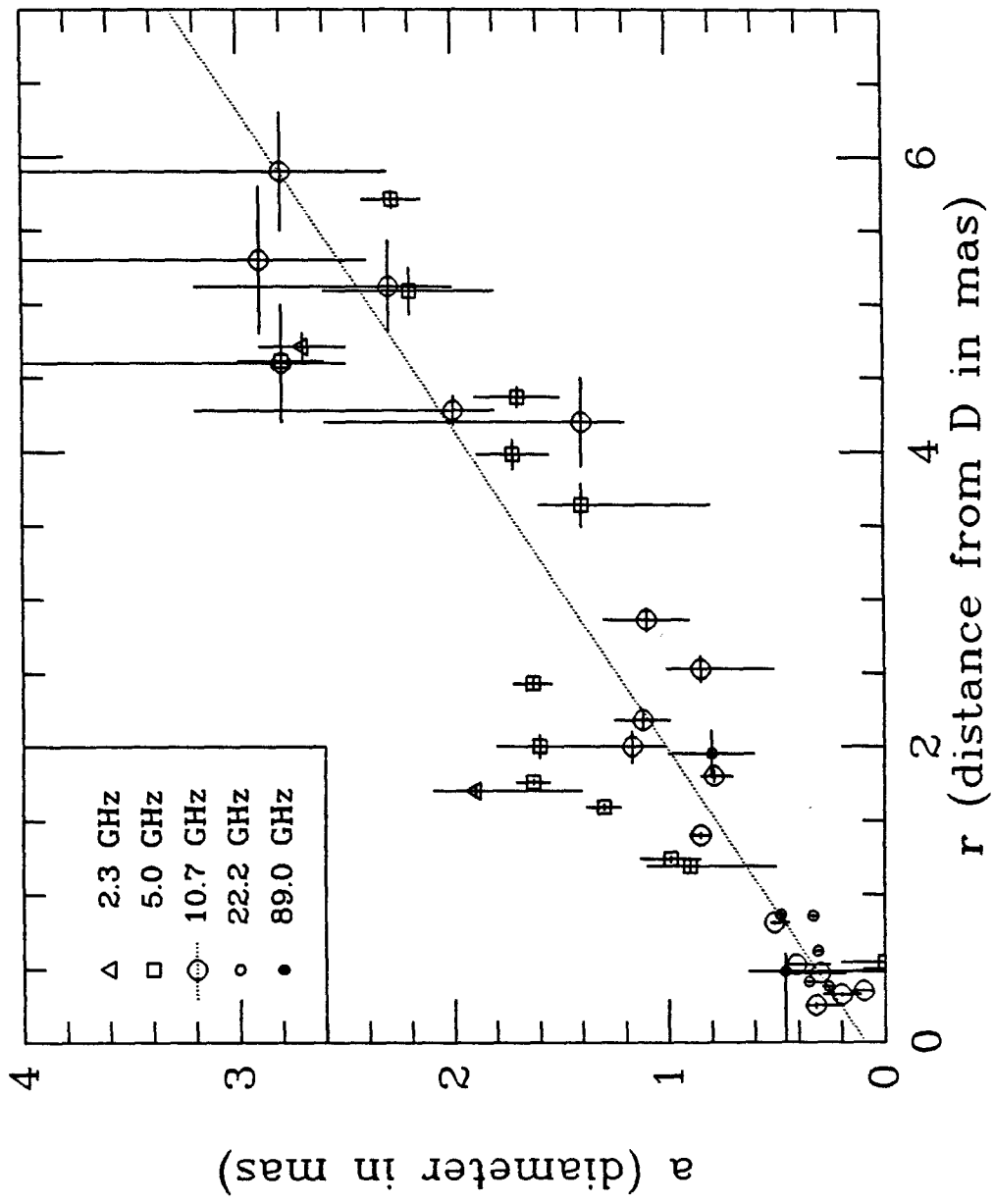
a (diameter in mas)
r (distance from D in mas)
0
1
2
3
4
0
2
4
6
2.3 GHz
5.0 GHz
10.7 GHz
22.2 GHz
89.0 GHz

Figure 7.

CHAPTER V

The Evolution of the Compact Radio Source in 3C345: Interpretation

To be submitted to The Astrophysical Journal

The Evolution of the Compact Radio Source in 3C345: Interpretation

J. A. Biretta

California Institute of Technology

Received _____

Abstract

We present physical interpretations for the VLBI observations of Biretta and Moore (1985). Simple models involving spherical knots or shocks in a relativistic jet are considered.

All of the emission regions show evidence for bulk relativistic motion with $\delta > 3$. The particle energies and pressures dominate those of the magnetic fields, unless $\delta \geq 20$. If the emission regions consist of an electron - proton plasma, then the density of thermal electrons is much less than the density of relativistic electrons. The fluxes decay with time much more rapidly than the synchrotron half-life, but much more slowly than predicted by adiabatic expansion. An attractive model for the observed kinematics identifies the emitting regions as shocks in an apparently broad and curved jet; a curvature of $\geq 3°$ and $\gamma \geq 10$ is required.

I. Introduction

We present physical interpretations for the VLBI observations of 3C345 by Biretta and Moore (1985, herein after Paper I). Simple models involving spherical components or shocks in a relativistic jet are considered (Ozernoy and Sazonov 1969, Blandford and Königl 1979). The advantages of relativistic models are described by Unwin *et al.* (1983). The physical conditions in the emission regions are described in Section II of this paper, while Section III examins their evolution with time. Section IV considers the kinematics of the emission regions.

Throughout this paper we will use a redshift $z=0.595$ (Burbidge 1965) and assume $H_0=100\ h$ km sec^{-1} Mpc^{-1} and $q_0=0.5$. For a standard Friedmann cosmology 1.00 mas corresponds to $3.79\ h^{-1}$ pc. A proper motion of 1.00 mas yr^{-1} corresponds to $v/c=19.7\ h^{-1}$. Spectral indices are defined as $\alpha=d(\ln S)/d(\ln \nu)$. Quoted uncertainties are 1.0 sigma.

II. Physical Conditions

A. Homogeneous Sphere Models

For the purpose of deriving physical properties of the emission regions, we have modeled them as homogeneous spheres (Gould 1979) containing a well-tangled magnetic field and a power law energy distribution of relativistic electrons. The observations do give some evidence for inhomogeneity, such as the distance between the "core" component (D) and the "outer" components (C3 and C4) being larger at higher frequencies, and C3 being larger at 5.0 GHz than at 10.7 GHz. Still, we will consider these models because of their simplicity.

The models are defined by six parameters: α_{thin}, ν_n, F_n, ϕ, ν_1, and ν_2. The optically thin spectral index α_{thin}, and the intersection point of the extrapolated optically thin and thick spectra (ν_n, F_n) were determined by fitting model spectra (Gould 1979) to the observed VLBI spectra. We also used the constraint that the component flux cannot exceed the total source flux. For components C4 and D there were insufficient VLBI data to determine all three parameters, so we considered two cases: (a) $\alpha_{thin}=-0.70$ which is similar to the values for C2 and C3, and (b) $\alpha_{thin}=0.0$. There is strong evidence for an observed $\alpha\sim0$ at high frequencies. This evidence is from VLBI data at 5, 11, and 22 GHz and from the

similarity of light curves at 8, 11, 15, 31, 89, and 300 GHz (see Section III. B. below). A simple explanation is that the intrinsic spectral index $\alpha_{thin}=0$. Marscher et al. (1977) have applied such a model to another source, PKS 0735+178. They find that the extremely flat observed spectrum requires a high upper cutoff frequency, and that this causes the model synchrotron spectrum to exceed the observed infrared flux. The same situation occurs in 3C345. None the less we will consider the $\alpha_{thin}=0$ case since it is the best possible homogeneous model.

The component diameters ϕ were measured by fitting homogeneous spheres to the VLBI visibility data. The last two parameters are the low and high frequency cutoffs for the synchrotron spectrum ν_1 and ν_2. We assume $\nu_1=100$ MHz; constraints from VLBI polarization observations will be discussed later. The upper limit is taken as $\nu_2=300$ GHz since there is no evidence for a turnover in the total flux up to this frequency, and because the light curve at this frequency resembles that at 11 GHz. Observed values of α_{thin}, ν_n, F_n, and ϕ are given in Table 1.

Values of magnetic field strength B, relativistic electron energy density U_e, ratio of magnetic to electron energy U_B/U_e, density and total mass in relativistic electrons n_e and M_e are all derived from the results of Burbidge, Jones, and O'Dell (1974)

with suitable modifications for spherical geometry (Unwin et al. 1983; Gould 1979). The values we give in Table 1 are in the proper frame of the source, with dependences on the relativistic Doppler factor δ and on $h=H_0/100$ km s^{-1} Mpc^{-1} given explicitly. Values of the observed synchrotron half-life τ at an observed frequency of 10.7 GHz are also given.

Magnetic fields are in the range 10^{-5} to 10^{-2} Gauss. The highest field strengths are obtained for the smallest components D and C4. The largest component C2 has the lowest field strength. The ratios U_B/U_e show that the relativistic electrons dominate the energetics, unless the Doppler factor δ is as large as 20 or 30. Values for M_e, the total mass of the relativistic electrons, are in the range 10^{31} to 10^{34}g and are larger for the more extended components. These values include only the electrons; for an electron - proton jet with no thermal plasma the total component mass would be $1837M_e$. Synchrotron half-lives are in the range 300 to 3×10^6 years.

It is of interest to compare the internal pressure of the emission regions with the external pressure. The internal pressure is given by $P=B^2/8\pi+U_e/3$. Since $B\sim\delta$ and $U_e\sim\delta^{-5}$ a minimum in the derived pressure occurs for some value of δ. For C4, which is the component closest to the "core" component D, this minimum pressure occurs at $\delta\sim20$ where $P_{min}=7\times10^{-5}$ dynes cm^{-2}. The

distance of this component from the "core" is at least 3pc. Since the maximum projection angle to the line of sight is $\theta_{max} \sim 8^{o}$ (see Section IV. A. below), the physical distance from the "core" must be at least 24 pc; smaller angles will give larger distances. This corresponds roughly to the radius of the narrow emission line region. For typical narrow line region conditions, such as a density $n \sim 10^{3}$ to 10^{6} cm^{-3} and temperature $T \sim 10^{4}$ ^{o}K, the external pressure is $P_{ext} \sim 10^{-9}$ to 10^{-6} dynes cm^{-2}. Thus the minimum internal pressures are much greater than the external pressures. It is unlikely that the jet could be collimated or confined by the external medium, and this is consistent with the observed expansion of components (Section III. A.). It may still be possible for ram pressure forces to bend the jet by small angles and hence produce the curvature needed for some kinematic models.

B. Limits on δ from Inverse Compton X-Rays

A lower limit for the Doppler factor (δ_{min}) may be derived by comparing the observed x-ray flux with that expected from inverse Compton scattering of the synchrotron photons off the relativistic electrons. Details of this calculation are described by Burbidge, Jones, and O'Dell (1974) and Unwin et al. (1983). X-ray observations of 3C345 have been made by Ku, Helfand, and Lucy

(1980). We have re-analyzed their data to obtain spectral indices across the 0.5 to 4.5 KeV band along with improved fluxes (Biretta et al., in preparation). Since the interstellar absorption varies strongly with frequency across the 0.5 to 4.5 KeV band, the derived spectral indices depend strongly on the assumed HI column density. High column densities yield lower spectral indices. We have used the value $N(HI)=2\times10^{20}$ cm^{-2} from the HI survey of Heiles (1975); the lack of HI absorption in the radio continuum of 3C345 (Hughes, Thompson, and Colvin 1971) gives a consistent limit of $N(HI)<4\times10^{20}$ cm^{-2}. Hence it is unlikely that the x-ray spectral indices could be much larger than the values we derive (Table 2). We obtain a spectral index of $\alpha_x=-0.9$, and there is no evidence for variability in the fluxes.

The calculation of δ_{min} requires simultaneous x-ray and three frequency VLBI observations to solve for α_{thin}, ν_n, F_n, and ϕ. The only epoch with $\geq$three frequencies is 1982, which is two years after the x-ray data. Hence for components C2, C3, and C4 we use the 1982 radio spectrum, and assume that the inverse Compton x-ray flux from these components remains constant or decreases between 1980 and 1982. This seems to be a safe assumption, since these components are observed to expand with time, and the since the x-ray flux is expected to drop rapidly as components expand. However, for the "core" component D there is

no clear evidence for expansion, so this assumption may not be valid. Instead, we have interpolated between 22 GHz VLBI data at 1978.8 and 1981.25 to obtain a third frequency for component D at epoch 1980.

Values of δ_{min} are given in Table 1. The lower limits are between 3 and 7 so that there is evidence for relativistic beaming in all the components. Component C4 shows the largest δ_{min}, and total flux monitoring suggests that $\alpha_{thin} \sim 0.0$ for this component. If the observed x-rays were from C4, we would expect $\alpha_{thin} \sim \alpha_x$, which is not the case. It appears that the observed x-rays are not from C4, and that the Doppler factor for this component may be somewhat larger than the limit we derive.

Our values for δ_{min} tend to be lower than those derived by Unwin *et al.* (1983) for 3C345. For component C3 this is due to their assuming $\alpha=-0.5$ while we fit for and obtain $\alpha=-0.81$. For component D they use the combined fluxes of D and C4, but only the diameter for D, and hence they obtain a larger δ_{min} value than ours. We note that a jet model with a fixed patten and a moving fluid (Königl 1981) may be more appropriate for the "core" component D.

C. Limits on Thermal and Low Energy Electron Density

The lack of Faraday depolarization may be used to place limits on the density of thermal and low energy electrons in the plasma. This calculation assumes that the emission region is homogeneous and that there are equal numbers of electrons and protons. Wardle and Roberts (1985) have made 5.0 GHz VLBI polarization observations which show that the radio emission from C3 is 21 percent polarized. Hence the fractional depolarization cannot be much greater than a factor ~2. Following Burn (1966) we obtain an upper limit for $n_{th} \leq 2\delta^{-3} h$ cm^{-3} for the density of thermal electrons. The factor δ^{-3} arises from the dependence of n_{th} on both the magnetic field ($B \sim \delta$) and on the frequency squared in the co-moving frame ($\nu \sim \nu_{observed} \delta^{-1}$).

The density of relativistic electrons n_e depends on both the Lorentz factor γ_1 at the low energy cutoff of the electron spectrum, and on δ. Allowed combinations of γ_1 and δ are given by the shaded region in Figure 1. The lower limit on γ_1 comes from the lack of Faraday depolarization by low energy relativistic electrons. This can be written in terms of a restriction on the equivalent density of cold electrons (Jones and O'Dell 1977; Wardle 1977) as

$$2 \delta^{-3} h \geq -2\alpha(3/2-\alpha) n_e \ln(\gamma_1) / (1-\alpha) \gamma_1^2$$

where α is the optically thin spectral index. The upper limit on

γ_1 comes from the requirement that the cutoff in the synchrotron spectrum occur below ~2 GHz, and the lower limit on δ is from the inverse Compton x-ray calculation. For the minimum allowed value of $\delta \sim 3$ we find $71 < \gamma_1 < 650$, a relativistic electron density $2h < n_e < 49h$ cm^{-3}, a lower cutoff in the synchrotron spectrum $.04 < \nu_1 < 2$ GHz, and $n_{th} \leq .07h$ cm^{-3}. Hence the relativistic electron density is much greater than the thermal electron density; only if $\delta > 35$ can the thermal electron density exceed the relativistic electron density. In the homogeneous sphere calculations above, we assumed $\nu_1 = .1$ GHz, since this value is allowed by the polarization data for a wide range of Doppler factor $3 \leq \delta \leq 31$.

These calculations all depend on the assumption that the plasma contains equal numbers of electrons and protons. For an electron - positron plasma there would be no depolarization.

III. Evolution of Components

The components are observed to both expand and fade with time. We will first consider the observed expansions.

A. Component Expansions

The components define an apparent opening angle of ~27° on the sky, so that their diameters must expand rapidly as they move away from the "core." This expansion is in fact seen directly for C2, C3, and C4. For example, component C3 at 5.0 GHz has an expansion rate $d\phi/dt = .15 \pm .03$ mas/year where ϕ is the component diameter. This corresponds to an expansion rate of $3.0\ h^{-1}\ \delta^{-1}$ c in the coordinate system of the source, where δ is the Doppler factor and c is the velocity of light.

B. Component Fluxes

We will first consider the new component C4. The 22 GHz flux of this component increases from ~1 Jy in 1978 to a peak of ~8 Jy in 1982 at 22 GHz (Paper I, Figure 5c). Comparison of the 11 and 22 GHz fluxes (Paper I, Figure 6) shows that the spectral index varied by only a small amount, $\alpha = -.30$ to $-.14$, while the flux increased from ~4 to ~8 Jy.

Additional evidence may be inferred from total flux measurements. Comparison of the fluxes for individual components (Paper I, Figure 5), with the 11 GHz total fluxes (Figure 2), shows that the new component is responsible for a large outburst in the total fluxes. This outburst in the total fluxes begins in

1978 and peaks at 1981.6. C4 contributes ~8 Jy to this outburst, while variations in D contribute ~2 Jy; variations in the other components are less than 0.5 Jy.

This outburst also is seen simultaneously and with similar amplitude at frequencies between 8 and 300 GHz (Biretta et al., in preparation). Table 3 gives epochs when peaks have occured in the total flux. Between 8 and 90 GHz the peak occured at 1981.6±.1. At 300 GHz the peak could not have occured much earlier than this. The amplitudes also are similar at the different frequencies. At 11 GHz the amplitude is ~9 Jy, while at 300 GHz it is $\geq$6 Jy. (Ennis, Neugebauer, and Werner 1982; Landau et al. 1983). It is possible that the wide frequency range is caused by chance coincidence of unrelated events; but this seems unlikely, since the previous peak in the total flux at ~1973.6 also was seen over a wide range of frequencies. Another possibility is that the high frequency outburst occured in some volume other than C4, such as the "core." But this would require a complex model to explain the simultaneity of events separated by $>4h^{-1}$pc, and so is rejected.

There is direct evidence for expansion of C4 when we consider all the data through 1984. When we consider only the size measurements prior to 1983, when the flux of C4 is increasing, the evidence for expansion is poorer; this is because the size is smaller relative to the resolution. However, given the ratio of

internal to external pressures discussed above, it seems certain that C4 must expand prior to 1983.

Hence the observed evidence on the initial outburst of C4 may be summarized as follows:

a) Its flux peaked simultaneously at 8 to 300 GHz;

b) Its spectrum is approximately flat from 8 to 300 GHz;

c) The flux peak occured when at a separation r~.4 mas from the "core" (Paper I, Figure 4c)

d) The diameter of C4 expands.

We will briefly consider several models for the evolution of this component. In priciple, the observed evolution can be affected by both internal effects and changes in the relativistic Doppler factor δ.

We first consider models with purely internal evolution and a constant Doppler factor δ. For homogeneous, adiabatically expanding models the optically thin flux decays rapidly with expansion (Kardashev 1962; van der Laan 1966). Since we observe an increasing flux with $\alpha \sim 0$, this model fails. Inhomogeneous

expanding models will have the same problem, since the peak flux contributed by each region will decay as its size expands.

Models with no internal evolution, where only the Doppler factor changes, can be excluded for two reasons: First the components are observed to expand so that internal evolution is expected. Secondly, in this model the fluxes must all peak at the same epoch. But this is inconsistent with the fact the 5 GHz flux peaks after the other frequencies (Table 3).

We now consider models with both kinematic (Doppler factor) and internal evolution. For a homogeneous model with simple adiabatic expansion, the intersection of the optically thin and thick spectra (ν_n, F_n) evolves according to

$$\nu_{nf}/\nu_{ni}=(\phi_f/\phi_i)^{-2}\ (\delta_f/\delta_i)$$
$$F_{nf}/F_{ni}=(\phi_f/\phi_i)^{-2}\ (\delta_f/\delta_i)^3$$

where the subscripts i and f denote the initial and final values. The variable ϕ represents the component diameter. At 22 GHz the flux of C4 increases by a factor of ~8 so that $F_{nf}/F_{ni}\sim 8$. From Figure 5e of Paper I it is apparent that C4 contributes about half as much flux at 5 GHz as at 11 GHz, and that the ratio of the 5 GHz to 11 GHz contribution is roughly constant in time. This requires $\nu_{nf}/\nu_{ni}\sim 1$. Solving the above equations gives $\phi_f/\phi_i\sim 1.7$ and $\delta_f/\delta_i\sim 2.8$. Similar results are obtained for adiabatic expansion with continuous reacceleration by the Fermi process

(Kardashev 1962); for this case $\phi_f/\phi_i \sim 1.7$ and $\delta_f/\delta_i \sim 2.4$. Hence this model can explain the observed flux increase only if the Doppler factor increases by a factor of 2 or 3. The required kinematic evolution for this model is plotted in the (β_{app},δ) plane in Figure 3. At early epochs $\beta_{app} \sim 1.3$ (Table 4) and $\delta \sim 4$. By 1982 $\beta_{app} \sim 6.5$ and the Doppler factor has increased to $\delta \sim 11$. Later, between 1982 and 1984, the diameter of C4 doubles while the flux decays by a factor ~0.7. From the above equations, this requires another increase in δ by a factor of 1.4 to $\delta \sim 15$. During this time β_{app} was approximately constant (Paper I, Figure 4c).

There are problems with this model. First, this model requires that either C4 will begin to fade rapidly, or the Doppler factor will continue to increase until it is unacceptibly large. The fact that we see components at larger radii such as C2 suggests that the former will not occur and that a huge Doppler factor would be needed. Secondly, the components at larger radii have steeper spectra ($\alpha \sim -.7$), so it seems likely that the spectrum of C4 will also steepen; but simple adiabatic models cannot account for this behavior. Another problem is that it requires Θ, the angle between the jet velocity and the line of sight, to decrease as the jet moves away from the "core," so that the strongest projection effects would occur away from the "core." Hence, this model would make it more difficult to explain why the

jet has a large apparent curvature near the "core," and a smaller curvature farther out.

Another possible model for the evolution involves particle acceleration at a shock (Blandford and McKee 1977). Such a model has the advantage that the radiating relativistic electrons and magnetic fields can be generated locally, and need not be ejected from the "core" component. Hence it is possible to have the observed flux increase without requiring that δ increase by a large amount.

The observed fluxes for component C3 decay with a time scale of 3 to 5 years. The derived time scales τ for energy loss by synchrotron emission (Table 1) are much longer than this for any reasonable value of δ. Other possible internal mechanisms involve expansion losses which give a powerlaw decay $S/S_0 \sim (\phi/\phi_0)^{\eta}$ where fluxes are given by S and diameters are given by ϕ. Such a power law gives a good fit to the observed fluxes and diameters assuming an opening angle of ~27° for the structure, with a resulting exponent of $\eta = -1.01 \pm .08$. For component C3 an adiabatic expansion model predicts $\eta = 4\alpha - 2 = -5.2 \pm .3$ (van der Laan 1966) while adiabatic expansion with continuous reacceleration gives $\eta = 2\alpha - 1 = -2.6 \pm .1$ (Kardashev 1962). Both of these models predict a decay which is much too rapid.

IV. Kinematics

A. Constraints on γ and Θ

The strongest constraints on γ and Θ (the bulk Lorentz factor of the jet and the angle between the jet velocity and the line of sight, respectively) generally come from the observed proper motion of the components. Values of β_{app}, γ_{min}, and Θ_{max} are given in Table 4. Component C4 accelerates from β_{app}=1.3 to 6.5. Component C3 has β_{app}=6.0. Component C2 has β_{app}=9.5 which requires $\gamma \geq 9$, the largest value seen in a superluminal source.

Minimum values of the Doppler factor, δ_{min} also provide constraints on the kinematics and these are given in Table 4. For component C4, these constraints are stronger than those from the proper motion.

The ratio between the counter jet and jet flux is R=-.007$\pm$.007. This is consistent with the values of γ_{min} and Θ_{max} in Table 4 which require $R=5\times10^{-5}$, assuming the ratio contains the Doppler factors as $\delta^{2-\alpha}$ (Linfield 1982).

B. Evidence on the Kinematics of C2 and C3.

As we have seen, there is direct evidence that the apparent speed of C4 increases as it moves away from the "core." It is interesting to ask whether C2 and C3 might have similar behavior.

The VLBI data presented in Paper I permit either acceleration or constant velocity. Evidence from early VLBI data, when C2 and C3 were closer to the "core," has been discussed by Cohen et al. (1983). They find evidence for an acceleration of C2. This is based on data from Shaffer et al. (1977) and Wittels et al. (1976) which give an apparent spped of ~.1 mas/yr for C2 when at r~1 mas from the "core." However, this early data must be viewed with caution since it is from two component models with no maps to compare against. These two component models do give a good fit to the data, but they may not be unique. For example, a three component model might also give a good fit with a different picture of the kinematics. A third component could have been present since C3 was ejected near those epochs.

Another source of evidence on the kinematics of C2 and C3 is the total flux history of the source. Component C4 caused a large total flux outburst which peaked when it was at a distance r~.34 mas from component D. If we assume that C2 and C3 had similar evolutions, we may ask what kinematic model gives the best

agreement with the observed light curves.

At 11 GHz four major peaks are seen between 1966 and 1984. These occur at epochs 1968.2±.1, 1970.2±.2, 1973.6±.2, and 1981.6±.1 (Biretta et al., in preparation; Figure 2; Table 3). The 1970.2 peak is seen only at ν<11 GHz while both the 1973.6 and 1981.6 peaks are seen to at least 90 GHz. There is no data at 31 or 90 GHz for the 1968.2 peak.

Comparison of the 11 GHz total fluxes and the 11 GHz fluxes of C4 show that C4 is clearly responsible for the 1981.6 outburst, and that the total flux peaked when C4 was at r=.34 mas. (The flux of C4 actually peaks after 1981.6, when C4 is at .45 mas, but the same conclusions are obtained regardless of which of these two radii we use.) We will test two models for the kinematics of C2 and C3 by seeing whether total flux outbursts are observed when the model predicts the components to be at r~.34 mas.

Model 1 assumes that C2 and C3 have constant velocity. The predicted epochs, when these components have r=.34 mas and when peaks in the total flux should be seen, are given in Table 5. This model gives a very poor fit to the epochs where peaks in the total flux were observed. It predicts that C3 should have caused a peak in the total flux at 1976.0±.3, but the closest observed peak was in 1973.6±.2. The difference cannot be due to minor

differences in the flux evolution of C3 and C4, since in this model C3 would not appear until 1979.4, which is more than a year after the observed flux peak.

Model 2 assumes that there is a single dr/dt(r) function for all components in which they accelerate as they move away from component D. For r>.64 mas this function was defined by linear interpolation between values of dr/dt given in Table 3 of Paper I. At r<.64 we used the curve obtained by linear interpolation in Figure 4c of Paper I. This model gives a much better fit than Model 1. In this model the 1968.2 peak is caused by C2, and the 1973.6 peak is caused by C3. The 1970.2 peak is not explained, but this peak appears to be of a different nature than the others in that it is not seen at 31 and 90 GHz. The reduced chi-square for this model is larger than unity, so the evolution of C2 and C3 may differ slightly from that of C4. For example, a perfect fit would be obtained if C2 and C3 caused flux peaks when at r=.38 and .28 mas, respectively, instead of r=.34 mas as we assumed.

In summary, there is evidence from both early VLBI data, and from the total flux history, that the apparent speeds of C2 and C3 have increase as they moved away from the "core."

C. Simple Models for Component Trajectories

The apparent positions of the components on the sky can be used to immediately rule out two models. In the model suggested by Cohen et al. (1983) the components would move along straight ballistic trajectories. This is inconsistent with the path of C4, which is clearly curved and non-radial.

The other model which can be ruled out involves simple homogeneous components moving on a fixed, curved path such as a bent jet (Moore et al. 1983). This is consistent with most of the observations except the position angle of the "core" extension C5. This extension is at position angle -90°, whereas C4 first appeared at -135°, so it appears that there is no simple fixed path.

A more attractive model is a modification of the fixed path model with constant γ where components are internal shocks in a jet. The kinematic evolution of one such model is shown in Figure 4. The value $\gamma \geq 10$ is required by the proper motion of C2. The apparent acceleration in the observed proper motion is explained as curvature of the path away from the line of sight. Such a curvature increases θ, the angle between the velocity vector and the line of sight, and thus increases the observed proper motion. The change in θ must be $\geq 3°$ to produce the observed

acceleration. This model also explains the strong curvature observed near the "core," since that is where projection effects would be greatest. Also, different components could appear to have different paths, since the brightness centroid of the shock need not be coincident with the path centroid. This effect would be especially strong near the "core" where Θ is small, and would explain why C4 and C5 had different position angles.

V. Summary

Our results may be summarized as follows:

a) All emissions regions show evidence for bulk relativistic motion with $\delta > 3$.

b) Unless $\delta \geq 20$ the particle energies and pressures are much greater than those due to magnetic fields.

c) If the emission regions consist of an electron - proton plasma, then the density of thermal electrons is much less than the density of relativistic electrons.

d) The component fluxes decay with time much more rapidly than the synchrotron half-life, but much more slowly than predicted by adiabatic expansion models. A model which combines adaibatic expansion and kinematic evolution requires variations in γ and Θ which are difficult to explain.

e) An attractive model identifies the emitting components as shocks in an apparently broad and curved jet. A fixed path which curves by $\geq 3^{\circ}$ and has $\gamma \geq 10$ is able to explain the observed kinematics.

VI. References.

Andrew, B. H. *et al.* 1978, A.J. **83**, 868.

Biretta, J. A. and Moore, R. L. 1985 (Paper I,
to be submitted to Ap.J.).

Blandford, R. D. and McKee, C. F. 1977, M.N.R.A.S. **180**, 343.

Blandford, R. D. and Königl, A. 1979, Ap.J. **232**, 34.

Burbidge, E. M. 1965, Ap.J.Lett. **142** 1674.

Burbidge, G. R., Jones, T. W., and O'Dell, S. L. 1974,
Ap.J. **193**, 43.

Burn, B. J. 1966, M.N.R.A.S. **133**, 67.

Cohen, M. H. *et al.* 1983, Ap.J. **269**, 1.

Ennis, D. J., Neugebauer, G., and Werner, M. 1982,
Ap.J. **263**, 451.

Feldman, P. A., MacLeod, J. M. and Andrew, B. H.
1981, IAU Circular **3637**.

Gould, R. J. 1979, A.A. **76**, 306.

Heiles, C. 1975, A.A.Supp. **20**, 37.

Hughes, M. P., Thompson, A. R., and Colvin, R. S. 1971,
Ap.J.Supp. **23**, 323.

Jones, T. W. and O'Dell, S. L. 1977, Ap.J. **214**, 522.

Kardashev, N. S. 1962, Sov.A.J. **6**, 317.

Konigl, A. 1981, Ap.J. **243**, 700.

Ku, W. H.-M., Helfand, D. J., and Lucy, L. B. 1980,
Nature 288, 323.

Landau, R., et al. 1983, Ap.J. 268, 68.

Linfield, R., 1982, Ap.J. 254, 465.

Marscher, A. P. et al. 1977, A.J. 82, 781.

Medd, W. J., et al. 1972, Mem.R.A.S. 77, 109.

Moore, R. L. et al. 1983, Nature 306, 44.

Ozernoy, L. M. and Sazonov, V. N. 1969, Ap.Sp.Sci. 3, 395.

Pearson, T. J. and Seielstad, G. A. 1984,
Private Communication.

Seielstad, G. A. et al. 1979, Ap.J. 229, 53.

Seielstad, G. A., Pearson, T. J. and Readhead, A. C. S.
1983, Pub.A.S.P. 95, 842.

Shaffer, D. B. et al. 1977, Ap.J. 218, 353.

Unwin, S. C. et al. 1983, Ap.J. 271, 536.

van der Laan, H. 1966, Nature 211, 1131.

Wardle, J. F. C. 1977, Nature 269, 563.

Wardle, J. F. C. and Roberts, D. H. 1985, in
The Physics of Energy Transport in Extragalactic
Radio Sources (eds. A. H. Bridle and J. A. Eilek), p.99.

Wittels, J. J. et al. 1976, A.J. 81, 933.

Table 1. Physical parameters for homogeneous sphere models. Observed parameters are in observer reference frame. Derived parameters are in source frame. The range of values allowed by the uncertainties in the observables is given.

Component		C2	C3	C4	C4	D	D	D
Epoch		1982.	1982.	1982.	1982.	1982.	1982.	1980.
Observed Parameters:								
α_{thin}		$-.59\pm.07$	$-.81\pm.07$	0.0	-.7	0.0	-.7	0.0
ν_n (GHz)		.8-.06	$2.2\pm.2$	$5.6\pm.8$	10.7 ± 1.0	$6.0\pm.8$	12.0 ± 1.0	$5.6\pm.2$
F_n (Jy)		3.2-15	$3.9\pm.1$	$6.2\pm.2$	$10.2\pm.8$	$8.2\pm.3$	13.0 ± 1.0	$5.0\pm.2$
ϕ (mas)		$2.15\pm.08$	$.97\pm.07$	$.29\pm.02$	$.29\pm.02$	$.36\pm.14$	$.36\pm.14$	$.52\pm.07$
Derived Parameters:	Dependence on δ and h (1):							
B (Gauss)	δ	$<3\times10^{-5}$	2×10^{-4} 7×10^{-4}	8×10^{-4} 4×10^{-3}	8×10^{-4} 3×10^{-3}	6×10^{-4} 2×10^{-2}	7×10^{-4} 2×10^{-2}	2×10^{-2} 5×10^{-2}
U_e (erg cm^{-3})	δ^{-5} h	>2	0.5 4	7 90	17 160	.3 260	.5 300	2×10^{-2} .2
U_B/U_e	δ^{+7} h^{-1}	$<2\times10^{-11}$	5×10^{-10} 3×10^{-8}	3×10^{-10} 9×10^{-8}	2×10^{-10} 2×10^{-8}	5×10^{-11} 3×10^{-5}	7×10^{-11} 2×10^{-5}	6×10^{-5} 6×10^{-3}
n_e (cm^{-3})	δ^{-4} h	$>5\times10^{+2}$	$1\times10^{+3}$ $4\times10^{+3}$	$5\times10^{+3}$ $3\times10^{+4}$	$5\times10^{+4}$ $3\times10^{+5}$	$5\times10^{+2}$ $8\times10^{+4}$	$4\times10^{+3}$ $5\times10^{+5}$	50 300
M_e (g)	δ^{-4} h^{-2}	$>4\times10^{+33}$	$8\times10^{+32}$ $2\times10^{+33}$	$1\times10^{+32}$ $5\times10^{+32}$	$1\times10^{+33}$ $5\times10^{+33}$	$4\times10^{+31}$ $1\times10^{+33}$	$3\times10^{+32}$ $7\times10^{+33}$	$7\times10^{+30}$ $2\times10^{+31}$
τ (yrs.,2)	$\delta^{-1/2}$	$>2\times10^{+6}$	$2\times10^{+4}$ $1\times10^{+5}$	$2\times10^{+3}$ $2\times10^{+4}$	$2\times10^{+3}$ $2\times10^{+4}$	$2\times10^{+2}$ $3\times10^{+4}$	$2\times10^{+2}$ $2\times10^{+4}$	30 180
δ_{min}		>5	2.9 4.2	11 17	7 10	(7) (22)	(4) (12)	4 6

---

1) Derived parameters should be multiplied by these factors.
2) Synchrotron half-life measured in observer frame at observed frequency of 10.7 GHz.

Table 2. Derived X-ray fluxes and spectral indices for data of Ku, Helfand, and Lucy (1980).

Epoch	Flux (erg cm^{-2} sec^{-1})	α_x
1979.65	3.3±0.5x10-12	0.9±0.2
1980.07	4.0±0.9x10-12	0.9±0.4
1980.15	4.4±0.5x10-12	1.0±0.2

Table 3. Epochs when peaks have occured in the total flux of 3C345.

ν (GHz)	~1968	~1970	1973.6	1981.6
1.6	-----	-----	1974.8±.4	ns
2.7	-----	-----	1974.5±.3	-----
5.0	-----	-----	<1974.4	>1984.0
8	1968.5±.2	1970.9±.5	1973.7±.2	1981.5±.1
11	1968.2±.1	1970.2±.2	1973.6±.2	1981.6±.1
15	1967.9±.2	1970.1±.2	1973.6±.2	1981.6±.1
31	-----	ns	1973.7±.3	1981.6±.3
90	-----	ns	1973.4±.3	1981.5±.2
300	-----	-----	-----	>1981.0

ns = No event seen
--- = No data

Table 4. Constraints on γ and θ.

			From Proper Motion			From X-rays		
Component	ν (GHz)	Epoch	β_{app}	γ_{min}	θ_{max}	δ_{min}	γ_{min}	θ_{max}
C2	5.0	1982	$9.5\pm.4$	$9.6\pm.4$	$12.0\pm.5^{o}$	5	2.6	11.5^{o}
C3	5.0,10.7	1982	$6.0\pm.2$	$6.0\pm.2$	19 ± 1	3	1.7	20
C4	22.2	1983.5	$6.5\pm.3$	$6.6\pm.3$	18 ± 1	---	---	---
	22.2	1982	$1.3\pm.2$	$1.6\pm.2$	75 ± 10	7	2.1	14.5
Dependence on H_0:			h^{-1}	h^{-1}	h			

Table 5. Comparison of two kinematic models for C2 and C3 with the 11 GHz light curve.

Model	Component	Epoch of Predicted Outburst	Epoch of Nearest Observed Outburst	Predicted Epoch–Nearest Epoch (years)	Reduced Chi-square
1	C2	1972.4±.5	1973.6±.2	-1.2±.5	23.3
	C3	1976.0±.3	1973.6±.2	2.4±.4	
2	C2	1967.5±.5	1968.2±.1	-.7±.5	7.7
	C3	1974.7±.2	1973.6±.2	1.1±.3	

Figure Captions.

Figure 1. Allow combinations of γ_1 and δ for component C3 are indicated by the shaded region. The upper and lower limits on γ_1 are respectively from the lack of an observed cutoff in the synchrotron spectrum above 2 GHz and from the lack of Faraday depolarization. The lower limit on δ is from the weakness of the inverse Compton x-rays.

Figure 2. Light curve of 3C345 at 11 GHz. Data are from Medd et al. (1972), Andrew et al. (1978), Seielstad et al. (1979), Feldman, MacLeod, and Andrew (1981), Seielstad, Pearson, and Readhead (1983), and Pearson and Seielstad (1984).

Figure 3. Kinematic evolution of C4 required by adiabatic expansion model for the fluxes. The original figure is from Unwin et al. (1983).

Figure 4. Kinematic evolution for components in a fixed path model with γ=10.

Running title: Evolution of 3C345.

Author's address:
J. A. Biretta
105-24 Caltech
Pasadena, CA 91125

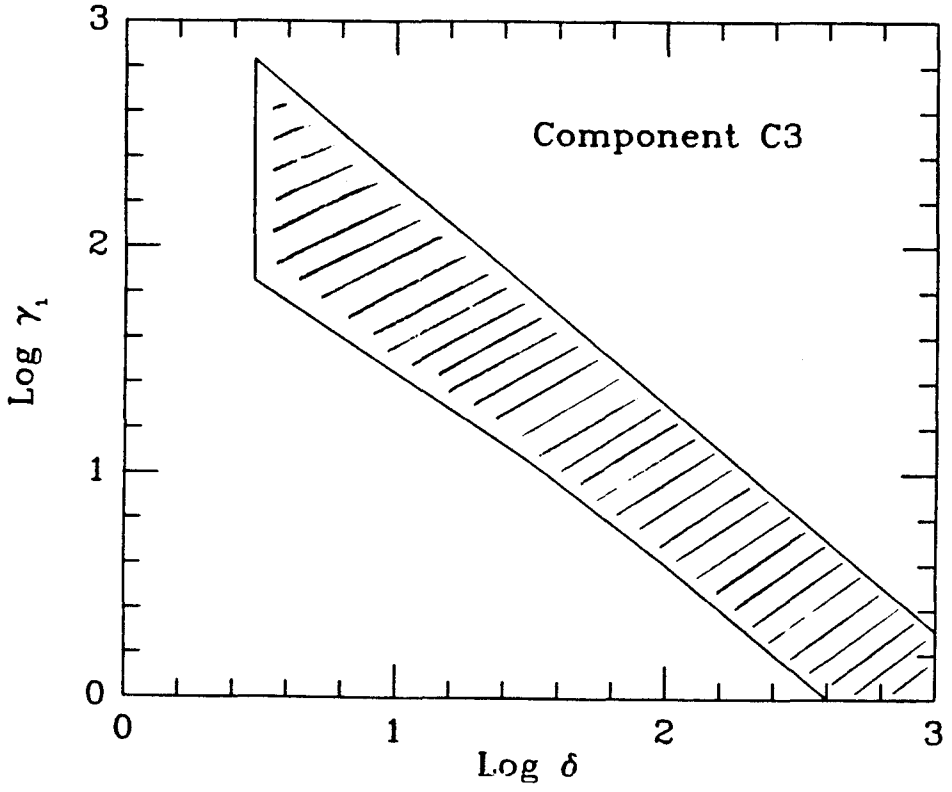

Figure 1.

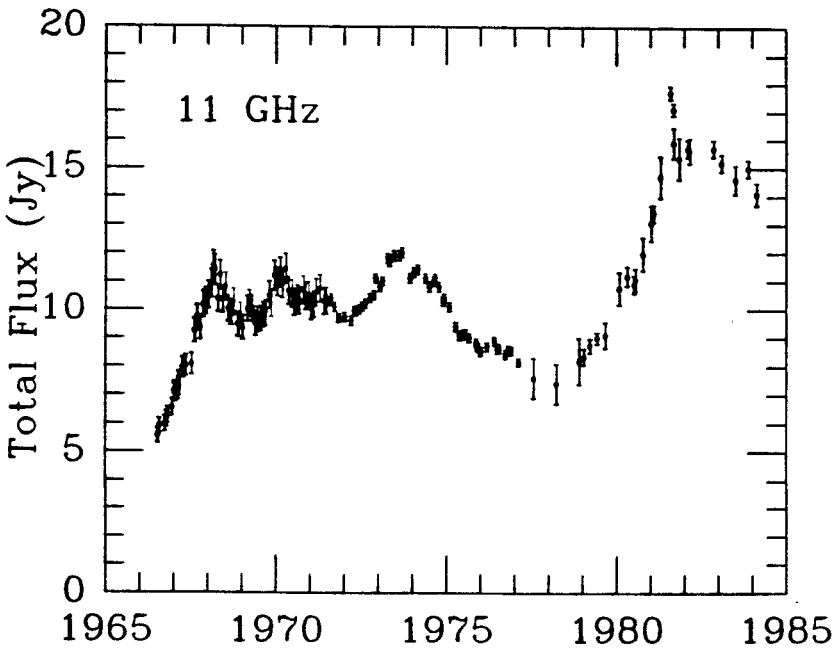

Figure 2.

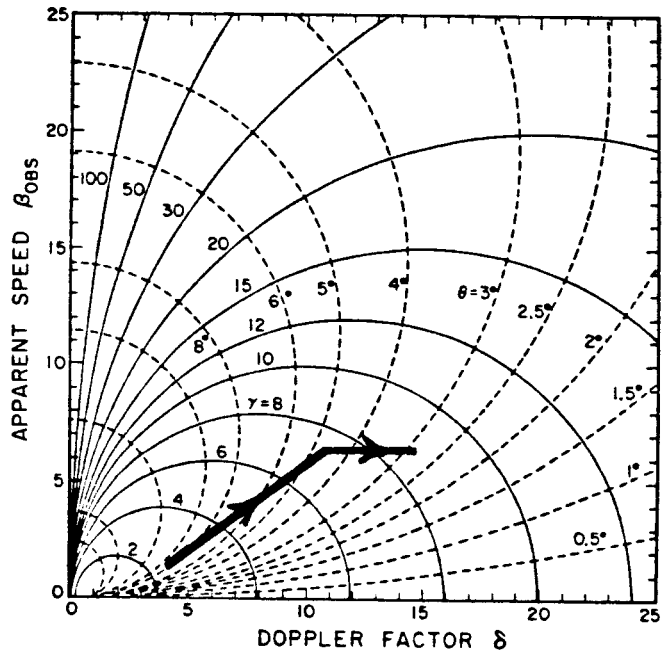
APPARENT SPEED β_{OBS}
DOPPLER FACTOR δ
0
5
10
15
20
25
100
50
30
20
15
12
10
8
6
4
2
$\gamma=8$
$\theta=3°$
2.5°
2°
1.5°
1°
0.5°
6°
5°
4°

Figure 3.

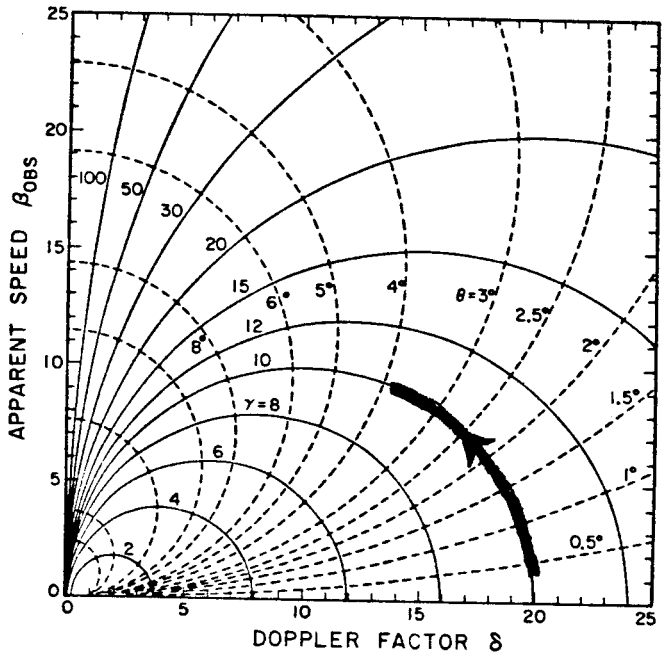
APPARENT SPEED β_{OBS}
DOPPLER FACTOR δ
0
5
10
15
20
25
100
50
30
20
15
12
10
8
6
4
2
$\gamma=8$
$\theta=3°$
6°
5°
4°
2.5°
2°
1.5°
1°
0.5°

Figure 4.